NASA CR-165309
EDR 10600

ABRADABLE DUAL-DENSITY CERAMIC TURBINE SEAL SYSTEM

FINAL REPORT

By

D.L. Clingman, B. Schechter, K.R. Cross, J.R. Cavanagh

DETROIT DIESEL ALLISON DIVISION
GENERAL MOTORS CORPORATION
INDIANAPOLIS, INDIANA 46206

Prepared For
NATIONAL AERONAUTICS AND SPACE ADMINISTRATION

FEBRUARY 1981

NASA LEWIS RESEARCH CENTER
CONTRACT NAS 3-22012

1. Report No.	2. Government Accession No.	3. Recipient's Catalog No.
CR 165309		

4. Title and Subtitle	5. Report Date
Abradable Dual-Density Ceramic Turbine Seal System	February, 1981
	6. Performing Organization Code

7. Author(s)	8. Performing Organization Report No.
D. L. Clingman, B. Schechter, K. R. Cross, J. R. Cavanagh	EDR 10600
	10. Work Unit No.

9. Performing Organization Name and Address	11. Contract or Grant No.
Detroit Diesel Allison Division General Motors Corporation Indianapolis, Indiana 46206	NAS3-22012
	13. Type of Report and Period Covered
12. Sponsoring Agency Name and Address	Contract Report, Final
Propulsion Laboratory U.S. Army R&T Lab (AVRADCOM) Lewis Research Center Cleveland, OH 44135	14. Sponsoring Agency Code

15. Supplementary Notes

Final Report. Project Manager, R. C. Bill
Structures and Mechanical Technology Division, NASA Lewis Research Center
Cleveland, Ohio

16. Abstract

This effort has expanded on previous work conducted under Contract NAS3-21263. The primary objective in each case has been to develop a plasma-sprayed dual density ceramic abradable seal system for direct application to the HPT seal shroud of small gas turbine engines.

The system concept is based on the NASA-developed thermal barrier coating and depends upon an additional layer of modified density ceramic material adjacent to the gas flow path to provide the desired abradability. This is achieved by co-deposition of inert fillers with yttria-stabilized zirconia (YSZ) to interrrupt the continuity of the zirconia structure.

The investigation of a variety of candidate fillers, with hardness values as low as 2 on Moh's scale, has led to the conclusion that solid filler materials in combination with a YSZ matrix, regardless of their hardness values, have a propensity for compacting rather than shearing as originally expected. The observed compaction is accompanied by high energy dissipation in the rub interaction, usually resulting in the adhesive transfer of blade material to the stationary seal member.

Two YSZ-based coating systems which incorporated hollow alumino-silicate spheres as density-reducing agents were surveyed over the entire range of compositions from 100% filler to 100% YSZ. Abradability and erosion characteristics were determined, hardness and permeability characterized, and engine experience acquired with several system configurations.

17. Key Words (Suggested by Author(s))	18. Distribution Statement
Abradable Seals High Temperature Ceramic Zirconia Plasma-Sprayed Porous	Unclassified Unlimited

19. Security Classif. (of this report)	20. Security Classif. (of this page)	21. No. of Pages	22. Price*
Unclassified	Unclassified		

* For sale by the National Technical Information Service, Springfield, Virginia 22161

FOREWORD

This Final Technical Report covers the work performed by the Materials Research and Engineering Department, Detroit Diesel Allison Division, General Motors Corporation under NASA Contract NAS 3-22012. The NASA Project Manager was Dr. R. C. Bill of the NASA Lewis Research Center.

TABLE OF CONTENTS

LIST OF ILLUSTRATIONS

LIST OF TABLES

SUMMARY

This effort has expanded on previous work conducted under Contract NAS3-21263. The primary objective in each case has been to develop a plasma-sprayed dual density ceramic abradable seal system for direct application to the HPT seal shroud of small gas turbine engines.

The system concept is based on the NASA-developed thermal barrier coating and depends upon an additional layer of modified density ceramic material adjacent to the gas flow path to provide the desired abradability. This is achieved by co-deposition of inert fillers with yttria-stabilized zirconia (YSZ) to interrupt the continuity of the zirconia structure.

The investigation of a variety of candidate fillers, with hardness values as low as 2 on Moh's scale, has led to the conclusion that solid filler materials in combination with a YSZ matrix, regardless of their hardness values, have a propensity for compacting rather than shearing as originally expected. The observed compaction is accompanied by high energy dissipation in the rub interaction, usually resulting in the adhesive transfer of blade material to the stationary seal member.

Two YSZ-based coating systems which incorporated hollow alumino-silicate spheres as density-reducing agents were surveyed over the entire range of compositions from 100% filler to 100% YSZ. Abradability and erosion characteristics were determined, hardness and permeability characterized, and engine experience acquired with several system configurations.

INTRODUCTION

The search for acceptable abradable seal materials for small gas turbine engines in the size class of the Army's 800 shp Advanced Technology Demonstrator Engine (ATDE) has gained increasing importance in the present climate of rapidly escalating fuel costs. The efficiency of these engines is extremely sensitive to operating clearances between compressor and turbine blade tips and the stationary seal components. From the standpoint of specific fuel consumption (SFC) the single most significant blade tip clearance location is the high pressure turbine (HPT). The plasma-sprayed ceramic seal system investigated in this program was inspired by the continuing lack of satisfactory available seal systems adaptable to the HPT application.

This program follows the approach used in Contract NAS 3-21263 which was completed in October 1979. Inert fillers are co-deposited with yttria-stabilized zirconia (YSZ) to interrupt the continuity of the zirconia structure in the outermost layer. The resulting system is deposited over an intermediate layer of moderately high density ceramic (approximately 12% porosity) adjacent to the metallic bond coat and metal substrate to mitigate the mismatch in thermal expansion characteristics between the metallic and low density ceramic components of the system. The filled layer provides a zone of modified density adjacent to the gas stream to provide abradability.

Disappointing results obtained from attempts to incorporate "soft" solid fillers in the YSZ matrix caused a major revision in the program scope during the course of the investigation. When it became apparent that the solid filler materials, regardless of their hardness value, invariably tended to compact rather than shear as originally expected, effort was redirected to concentrate on systems in which density reduction was achieved through incorporation of porosity.

Commercially supplied alumino-silicate hollow spheres were subsequently used exclusively as the filler to provide "closed pore" porosity in two different types of YSZ matricies. Pre-stabilized YSZ in the form of ZrO_2• 8 w/o Y_2O_3 as supplied by ZIRCOA Division of Corning Glass Works and YSZ that achieves stabilization during the spray process as supplied in the form of a composite designated as Metco 202NS by Metco, Inc. were investigated. Compositional variations ranging from 100% filler to 100% YSZ were evaluated for each system.

SEAL SYSTEM DEVELOPMENT

The seal systems developed during this program have continued to build upon the ever-increasing background of success obtained with the NASA-developed yttria-stabilized zirconia thermal barrier coating systems. The basic philosophy guiding the program has been to start with a proven high temperature material, preferably one with significant engine experience, and to modify the coating structure toward the end of improving the abradability of the material while retaining the desirable high temperature charactertistics of the original coating system. The end result becomes an "abradable thermal barrier".

Coating Configuration

Typically, the NASA coating successes have been achieved with "thin" coating systems - i.e., bond coats 0.013-0.018 cm (0.005-0.007 in.) and oxide layers 0.038-0.051 cm (0.015-0.020 in.) thick, as shown in Figure 1a. Further, the coatings have been "duplex" in that only two discrete layers are present, with no "graded" or mixed-composition layers.

From the structure of the dual-density coating system, shown in Figure 1b, it is readily apparent that the concept involves essentally the addition of a 0.046-0.051 cm (0.018-.020 in.) reduced-density abradable layer superposed on top of the basic NASA thermal barrier coating. An incursion of turbine blades into a rub track particularly in small engines such as the GMA 500/ATDE, is unlikely to exceed 0.025-0.038 cm (0.010-0.015 in.) without considerable damage being incurred by the rotor system. The coating system geometry selected has provided for this margin in the abradable outer layer.

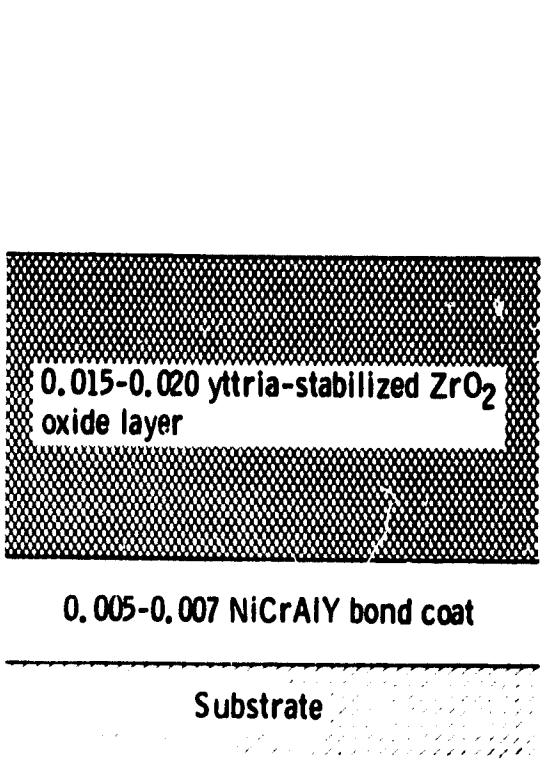

(a) Typical NASA duplex thermal barrier coating

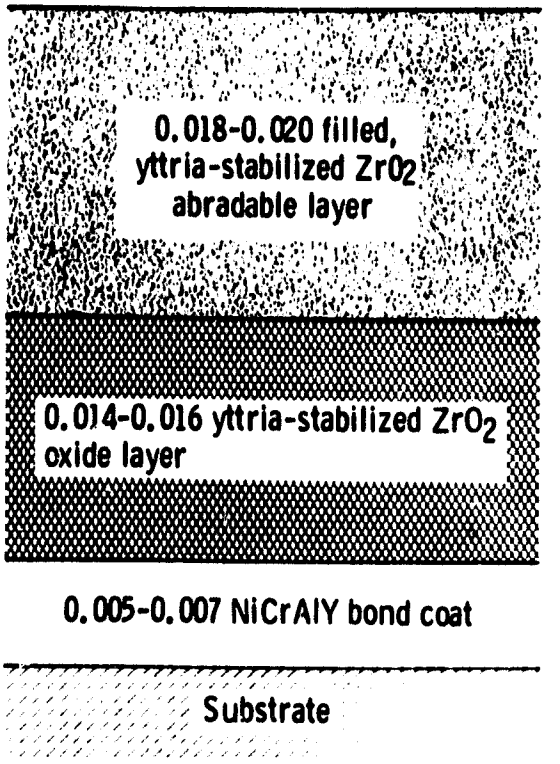

(b) Dual-density/composition abradable thermal barrier coating

Figure 1 Cross sections of thermal barrier coating configurations

Specimen Fabrication

The basic concept of an abradable thermal barrier depends on devising a method whereby the density in the blade track region of the seal is reduced below that normally obtained in the plasma-spray process. One attractive method for accomplishing the desired density reduction is to "co-spray" an inert "filler" concurrently with the YSZ of the thermal barrier. This procedure interrupts the continuity of the YSZ and produces a controlled structure. A major difficulty in using this technique arises from the significantly different temperature capabilities (melting points) of YSZ and candidate fillers. It is this feature that prevents the constitutent powders from being bound together and sprayed as a single composite material, since particle temperature adequate for softening YSZ (required for good deposition) would surely result in premature melting or softening and subsequent collapse of the hollow spheres comprising the filler material used exclusively during the latter stages of the program. This consideration is less significant for the case of solid, "soft" filler particles; however, the same general procedure was used for fabricating all specimens.

A workable solution to the problem of spraying materials with such vastly different characteristics has resulted from providing different residence times in the plasma stream for each constituent powder according to its particular requirements. This is accomplished by introducing the high-temperature component (YSZ) through a powder feed port directly into the plasma-spray gun body. The low-temperature component (filler) is fed by a separate powder feeder into the plasma stream external to the gun body at a point downstream from the nozzle. With the fillers employed throughout this program, no subsequent thermal treatment (e.g., for decomposition and volatilization to generate residual porosity) was required or provided, the filler remaining *in situ*.

Fabrication Equipment

The plasma spray equipment used in constructing the various coating specimens was identical to that used by NASA in developing the yttria-stabilized zirconia thermal barrier coating system. The Plasmadyne Model SG-1B plasma spray gun used exclusively for deposition of all layers of the coatings has powder feed ports located both internal and external to the gun body. Normally, only one of these ports is used at a time. However, because of the peculiar requirements of the filled coating layer, separate powder feeders are used to supply both ports simultaneously - the YSZ being introduced within the gun body and the filler powder injected into the plasma stream through the external downstream port. With this arrangement the optimum parameter ranges for the multiple component system reflect a compromise of the requirements of the individual component powders.

Processing Procedures

All substrate materials used in this investigation are Hastelloy X. This is the same material as that used for the shroud segments of the GMA 500/ATDE and ensures that a fully developed coating system will be compatible with engine hardware.

The elasped time between plasma spray processing steps was held to the minimum possible consistent with exercising care and good technique and in no case was allowed to exceed 2 hours. This condition thus required that all specimens be completed the same day that they were started.

Prior to deposition of each particular coating system, the substrates were prepared by vapor degreasing, followed by grit blasting with 60 grit aluminum oxide.

Powder flow rates were precisely determined by collecting and weighing timed specimens of material delivered by the powder feeder. Spray distances were the same as those established by NASA for the several discrete layers of the coatings, with the same distance maintained for both the standard density layers and the filled layers, regardless of the filler employed. All spraying was done with hand-held equipment, specimens oriented vertically, and cooling air supplied to the rear face of the specimen coupons.

Bond Coat Powder

The bond coat employed in all instances was NiCrAlY obtained from Alloy Metals, Inc., Troy, Michigan, with the following chemical composition:

Cr	25.7%
Al	5.6%
Y	0.32%
Ni	Balance

Mesh specification was -200 +325. Although this composition differs from the 16.2% Cr-5.5% Al-0.6% Y-Bal Ni material originally developed for the NASA thermal barrier coating, it is representative of a later, improved NASA technology. The source of supply is identical to that used by NASA.

Oxide Layer Powder

The yttria-stabilized powder employed in the early phases of this investigation marked a potentially significant departure from the NASA-developed thermal barrier materials. Because the material used in the NASA-developed coatings was quite expensive and had a history of lengthy delivery times, Metco 202-NS was selected for the oxide layer component in the interest of controlling costs and expediting the execution of the program. A principal difference between the two powders is in the method of stabilization. Metco 202-NS achieves stabilization during the spray process instead of by pre-alloying and is available off the shelf at a fraction of the cost of the pre-stabilized material.

Recent, and as yet unpublished, investigations at DDA on various combinations of bond coat and yttria-stabilized zirconia materials indicates that the NASA-developed material possesses superior thermal shock/fatigue resistance compared to other materials tested. This fact, together with the unexpected availability of an improved pre-stabilized YSZ containing 8 w/o Y_2O_3 (again, representative of later, improved NASA technology) resulted in the use and comparison of both Metco 202-NS and pre-stabilized YSZ during the latter stages of the program.

Standard Density Layers

Techniques identical to those used by NASA were employed in depositing the standard density intermediate layer for each coating configuration. As previously mentioned, however, in some cases Metco 202-NS was substituted for the pre-alloyed yttria-stabilized zirconia used in the NASA -developed thermal barrier coatings.

Abradable Layers

Preparation of the abradable layers for most of the coating system investigated was predicated on minor modifications to the spray parameters developed by NASA. Earlier work showed that modest reductions in both arc current and operating voltage (arc power level) were beneficial for depositing filled (abradable) layers without overheating the filler particles. Since adequate melting of the zirconia particles was exhibited when using the modified parameters, these values were retained for the process baseline.

Surface Machining

The surface of each specimen was prepared by machining with a single-point cutting tool of the replaceable carbide insert variety prior to any further conditioning. The specific machining parameters were determined as part of an earlier effort by trial and error using both single-point machining and wet grinding techniques. The coatings were found to machine easily with either method, and as expected, the smoother surfaces were obtained by grinding. Specimens subjected to grinding operations were flushed with clear water and

dried in vacuum to remove any contamination from the grinding coolant. The parameters established for single-point machining were used for the preparation of all subsequent coating systems. These parameters were:

- Cutting tool carbide insert -TPG 431 -KG 8
- Work Speed 118.9 m/min. (390 ft./min.)
- Cross Feed 0.015 cm/min. (0.006 in/min.)
- Material removed per pass 0.025 cm (0.010 inches)

Hardness of each of the coating systems was measured after machining by using the R15Y superficial hardness scale (15 kg load, 1.27 cm (1/2 inch) diameter ball indenter).

Abradable Layer "Fillers"

The materials used as fillers in the outermost or "abradable" layer, fall into two separate and distinct categories:

- Soft, solid particles with low shear strength to reduce overall coating strength and enhance abradability while retaining a more or less continuous structure
- Hollow spherical particles to act as density-reducing agents within the zirconia matrix.

Materials in the former classification that were obtained and analyzed for particle size distribution in the as-received powder form included:

Bentonite	Pyrophyllite
Dolomite	Silica
Kaolin, GEO	Wollastonite
Mullite, KMC	Zinc-Zirconium Silicate
Mullite, Metco XP 1146	Zircon, H & G
Mullite, Plasmadyne 314M	Zircon, Plasmadyne 360F
Nickel Oxide, Metco XP 1145	

A primary criterion for the selection of these materials was reasonable compatibility of the thermal coefficient of expansion with the YSZ matrix material. In most cases, however, it was impossible to locate a commercial source for plasma spray-grade powders, with the as-received materials containing an exceptionally large percentage of "fines". These powders tended to clog the plasma spray unit powder feeders and made it impossible to produce coatings with the desired composition and structure.

Particle sizes, both distributed and cumulative, for a typical material, e.g., wollastonite ($CaO \cdot SiO_2$) are shown by the solid lines in Figure 2. This powder, in addition to several other potential fillers, was modified by a proprietary agglomeration technique to produce the particle size distribution shown by the dashed lines in Figure 2. The agglomerated powder was found to feed and deposit satisfactorily when co-sprayed with YSZ.

Materials Ranking Methodology

With materials systems that possess the wide variety of performance-related characteristics found in abradable seals, it becomes desirable to establish a formalized basis for ranking and, ultimately, selection.

In order to establish a ranking methodology that would be as objective and unbiased as possible, rather than the product of exclusive opinion and conjecture by the investigators, the assistance of a wide variety of technical personnel closely associated with small gas turbine technology was recruited. Participants were requested to assign a value between one and five (five being highest) to the relative importance of listed evaluation criteria. Identification of the respondent was optional. Twenty seven requests were issued, with nineteen responses received, only one of which was submitted anonymously.

Because of the generally subjective nature of abradable seal studies and the fact that no universally accepted evaluation criteria exist, the personal opinion of the respondents appears to have been heavily influenced by their individual areas of responsibility. In most cases, it is a simple matter to identify the technical discipline of the respondent, if not the identity of the individual himself by analyzing the content of the response.

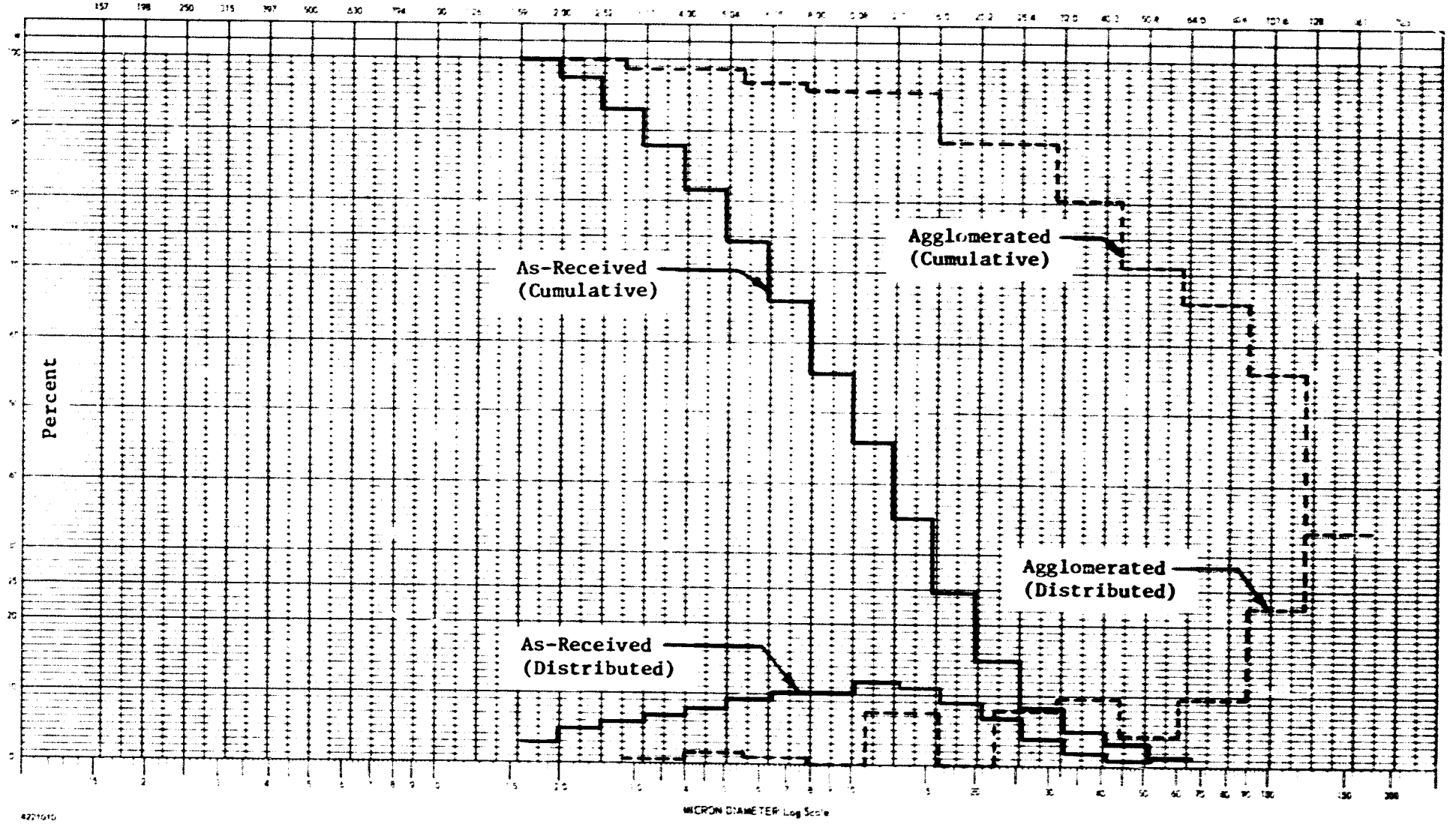

Figure 2 Particle size distributions for as-received and agglomerated wollastonite

In spite of the unavoidable bias inherent in an evaluation methodology that must be established without the benefit of absolutes, the procedure is nevertheless useful in establishing the criteria deemed most important and, conversely, least significant by the concensus. The criteria considered were:

- Abradability
- Permeability (internal leakage)
- Surface roughness
- Thermal shock resistance
- Stability with time (at temperature)
- Erosion resistance
- Chemical stability (with respect to turbine environment)
- Fabrication repeatability
- Cost
- Chemical and metallurgical compatibility with downstream components
- Risk of mechanical damage to downstream components in event of spalling

In addition, the following were suggested by one or more of the respondents:

- Simplicity in application
- Tolerance for thermal distortion without spalling
- Machinability (related to cost)
- Thermal insulation effects (cooling air reduction)
- Adaptability to complex geometry

The final rankings and average weighting factors compiled from the survey are presented in Table I.

It is not surprising to note that there was nearly unanimous agreement in establishing abradability as the most important criterion for evaluation. Lacking this important characteristic, all other considerations become inconsequential. The nearly equivalence in estimated importance of thermal shock resistance and erosion resistance should probably be expected since both of these features are related to durability.

Stability with time at temperature and fabrication repeatability were judged to be nearly equal in importance, followed closely by chemical stability with respect to the turbine environment, cost and permeability.

Ranked lowest in importance were risk of mechanical damage to downstream components, chemical and metallurgical compatibility with downstream components and surface roughness. Exception to this low ranking of the importance of surface roughness was taken by the aerodynamicist charged with maximizing turbine performance and serves to illustrate the difficulty of removing the subjectivity from the task.

Selection of the best seal material system from the candidates evaluated can be accomplished by scoring the relative performance of all materials for each test on a scale of 1 to 10 (10 being highest), then multiplying the performance score by the appropriate weighting factor and finally summing the resulting products for each material candidate. In spite of the recognized imperfect nature of this methodology, the highest total weighted score should result in the systematic election of the "best" overall system based on the predetermined evaluation criteria.

Table I

Evaluation Criteria Average Weighting Factors

Criterion	Rank	Average Weighting Factor
Abradability	1	4.8
Thermal Shock Resistance	2	4.3
Erosion Resistance	3	4.2
Stability with Time (at Temperature)	4	3.9
Fabrication Repeatability	5	3.8
Chemical Stability (wrt Turbine Envir.)	6	3.5
Cost	7	3.3
Permeability	8	3.2
Risk of Mechanical Damage to Downstream Components	9	2.9
Chemical and Metallurgical Compatibility Components	10	2.8
Surface Roughness	11	2.6

Simplicity in Application	*	*
Tolerance for Thermal Distortion without Spalling	*	*
Machinability	*	*
Thermal Insulation Effects	*	*
Adaptability to Complex Geometry	*	*

*Isolated or insufficient response to warrant inclusion

TEST APPARATUS

High Speed Abradability Rig

Abradability evaluations were conducted on both a low speed, room temperature screening rig and on the high speed, high temperature test rig shown in Figure 3. This rig consists of a steam turbine-driven spindle with replaceable test disks.

The mechanism used to provide the rub incursion motion is designed around a rigid frame system which supports the test coupon above the rotating IN 792 test disc in the quartz lamp heated cavity. The vertical incursion drive is fixed to the frame above the test coupon through a thin flexure which essentially isolates the normal and tangential forces produced by the rub. The rub interaction rates of 0.0025 cm/sec (0.001 in/sec) and 0.025 cm/sec (0.010 in/sec) are achieved by controlling the pulse rate of a stepping motor which drives a lead screw. Normal forces are sensed by a load cell positioned between the lead screw and the flexure leaf. The tangential forces are transmitted by a rigid load frame through swivel couplings to two load cells mounted outside the heated cavity. These signals are then summed electrically to provide the total instantaneous tangential force signal.

When large numbers of specimens must be screened for abradability as is the case in this program it is expedient to conduct at least the initial tests on the low speed, room temperature test rig shown in Figure 4. Tactile feedback is an important feature of these tests since any "chatter" or similar distress is immediately apparent to the test operator.

Although intuitively suspect, testing at low speeds has the decided advantages of:

- Rapid turn-around time
- Relative insensitivity to minor imbalance
- Minimal cost
- Reduced risk to rig or operators in the event of blade loss

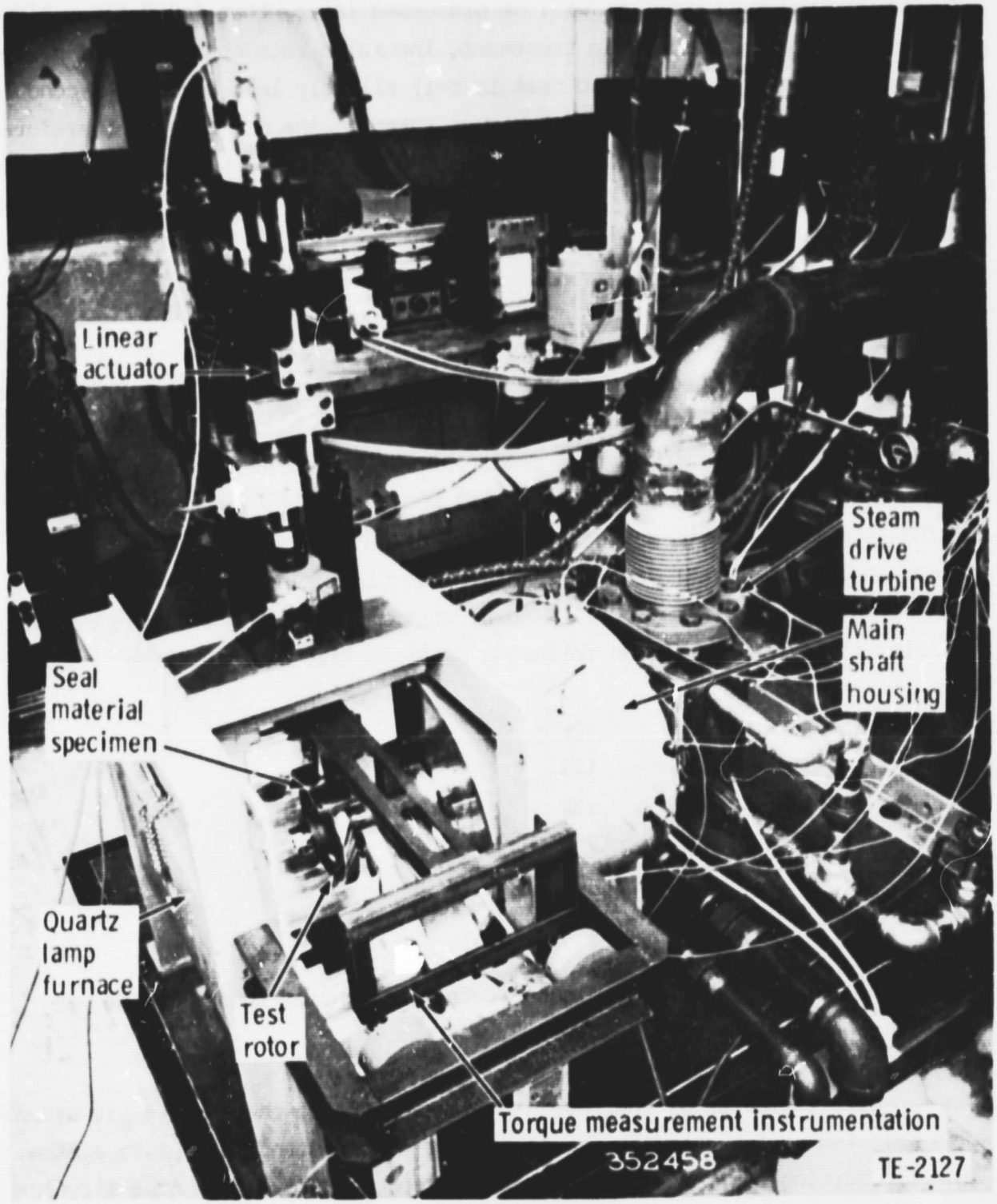

Figure 3 High-speed/high-temperature abradable seal materials test rig

Numerical arguments show, as will be discussed later, that for a given blade geometry without abrasive tip treatment, incursion rate and number of blades on the test rotor, a low speed test is only slightly less severe and conducive to smearing than one conducted at higher speeds. The net effect, therefore, is that at least for screening purposes, the validity of testing at low and high speeds is comparable. This conclusion has generally been supported by laboratory observation.

Erosion Test Rig

Erosion tests were conducted on the appartus shown in Figure 5. The specimen is mounted at the prescribed angle to the impinging air/particulate stream. The tests were performed at room temperature with the particulate flow rate set at a nominal 30 gms/hr (0.066 lb/hr) and the air flow nominally at 11.2 m^3/hr (400 ft^3/hr) with a supply pressure of 482.3 KPag (70 psig). A timer shuts the rig off at the predetermined time. The erosive medium used was AC Coarse Air Cleaner Dust (Natural Arizona Road Dust) which is primarily calcium silicate and has the following particle size distribution:

0.5 microns	12%
5-10 microns	12%
10-20 microns	14%
20-40 microns	23%
40-80 microns	30%
80-200 microns	9%

Specimen and dust reservoir weights are recorded prior to and at the conclusion of each test.

The angular incidence of the specimen with respect to the erosive air stream was selected as 15^o based on previous tests of the standard density system. The 15^o setting was considered to be most representative of engine air flow conditions and would not unduly penalize candidate coating systems.

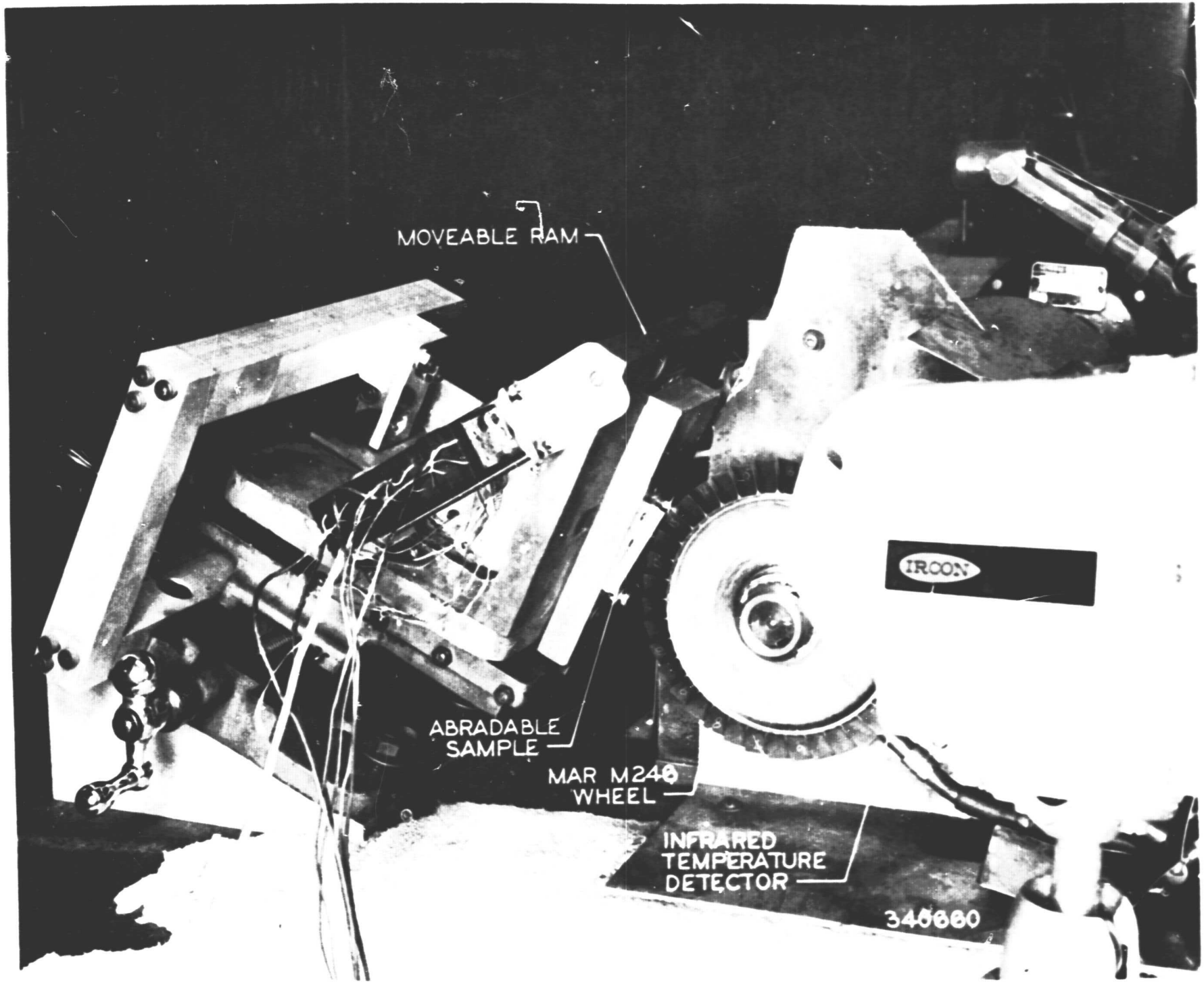

Figure 4 Low-speed abradable seal materials screening test rig

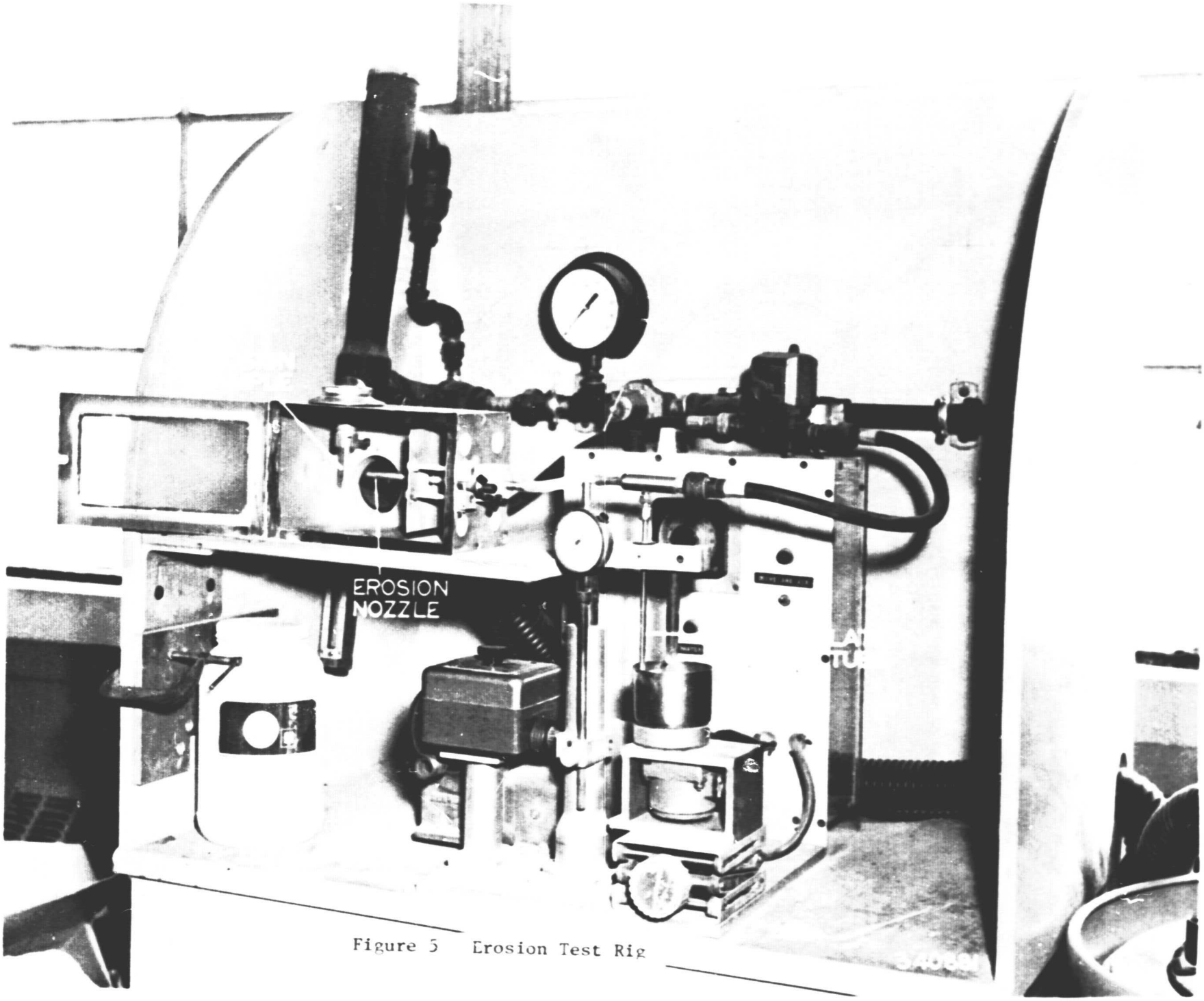

Figure 5 Erosion Test Rig

Permeability Rig

Through-leakage as a result of interconnected porosity was evaluated on the rig schematically shown in Figure 6. This simple fixture consists essentially of inlet and exhaust ports which are formed in a polyurethane insert in the cover. When the cover is clamped in place over the sample, polyurethane acts as a seal preventing leakage across the abradable surface to the exhaust port or to the atmosphere. The incoming argon is thereby forced to pass through the abradable material in order to reach the exhaust port. The feed port is connected to a pressure gage, flowmeter and argon tank and the exhaust port is open to the atmosphere. Pressure is set at the argon tank by means of a regulator, and through-flow in the coating is monitored at the flowmeter. The area used for the flow calculation is the actual cross sectional area of the specimen.

Engine Tests

It is generally agreed that the most realistic test conditions are found in actual engine tests. Dual density seal systems developed during the course of this program have been engine tested in two different engines.

The GMA 500 Advanced Technology Demonstrator Engine (ATDE) being developed by DDA for the U. S. Army provided an opportunity for testing early formulations in the 1st and 2nd stage (unshrouded) and in the 4th stage (shrouded) turbine seal locations. Later formulations were tested in the gas generator turbine (unshrouded) seal location of the CATE (Ceramic Applications in Turbine Engines) engine being developed by DDA for DOE under NASA management. The results of these tests will be discussed in more detail later in this report.

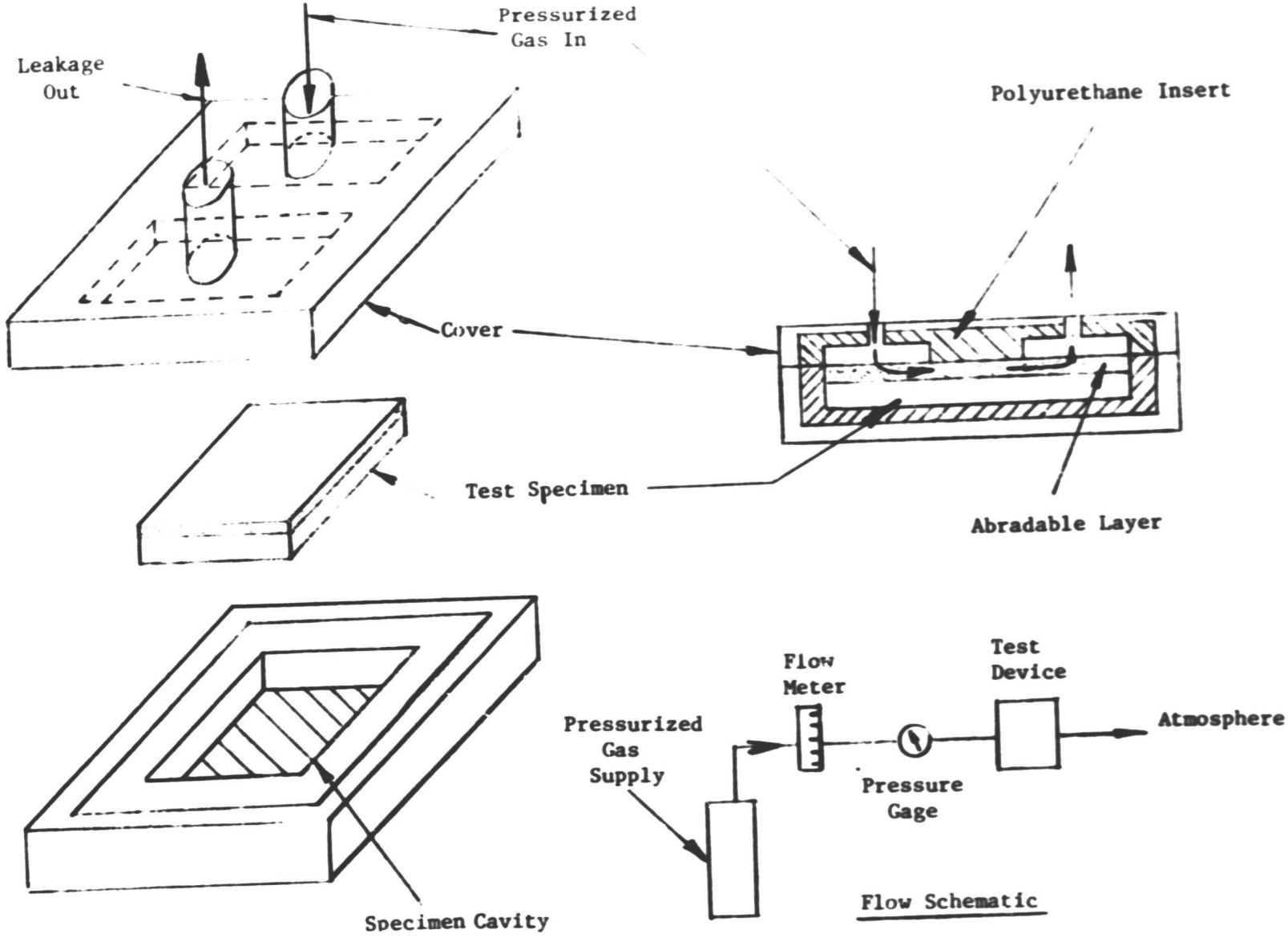

Figure 6 Permeability Test Device

All specimens, regardless of the test apparatus employed, were tested in a fully machined condition so that the exposed surface was representative of a finished part.

TEST RESULTS

Low-Strength Solid-Filled Systems

All results of tests with systems employing various low-strength solid fillers to interrupt the continuity of the YSZ matrix structure were obtained prior to the discovery of a powder feeder fill-dependency problem and its subsequent correction. Consequently, the structures prepared and tested were probably of non-optimized proportions. This is discussed in further detail in the Engine Test Results section.

The rub wear scar shown in Figure 7 was obtained in a low speed test of a system comprised of 50 v/o YSZ and 50 v/o pyrophyllite ($Al_2Si_4O_{10}(OH)_2$). This result was typical of all tests in which solid-filled YSZ structures were abraded by turbine wheels of cast MAR-M246 alloy. There are several features common to all of these solid-filled systems. Most pronounced was the tendency of each structure to compact or densify in the rub zone rather than shear as originally anticipated. Accompanying the observed densification were 1) adhesive transfer of blade tip material in varying degrees and 2) nearly total absence of seal structure penetration by the blade tip.

Although the filled structures tested were non-optimized, the rub wear scars produced were significantly more severe than those obtained with non-filled normal density YSZ structures. Since the latter are considered to be virtually "non-abradable", there appeared to be little potential for producing the desired abradability using the solid filler approach. These efforts were

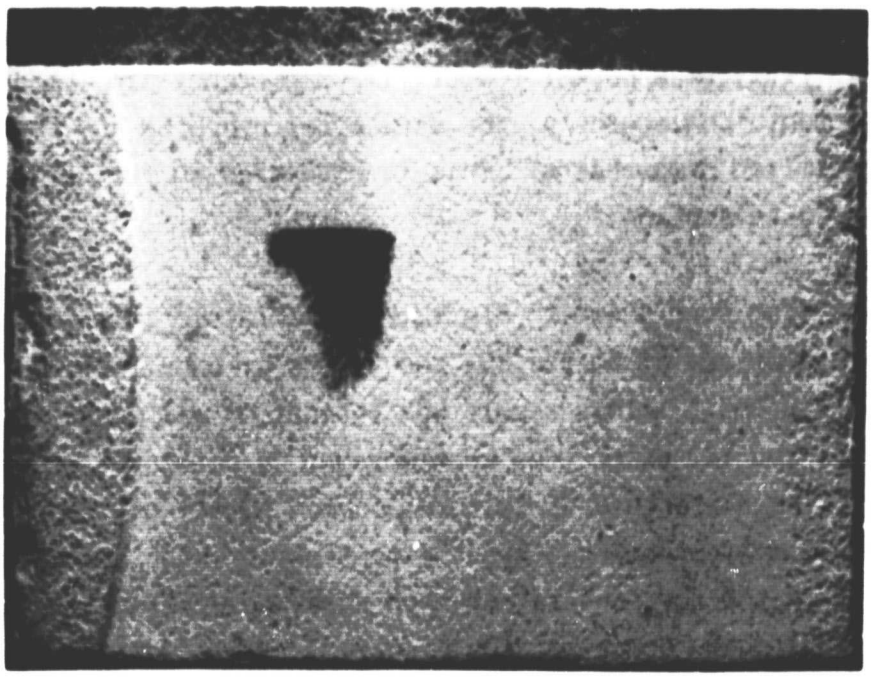

Magn: 3X

Rub Direction

Figure 7 Abradability Wear Scar 50 v/o YSZ/50 v/o Pyrophyllite

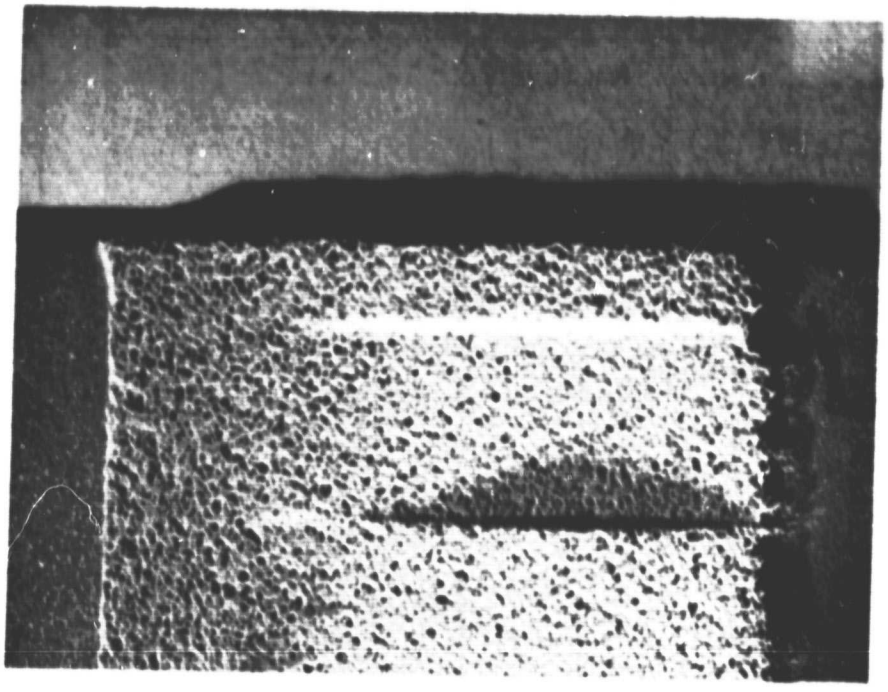

Figure 8 Abradability Wear Scar 80 v/o Eccosphere Filler/20 v/o YSZ

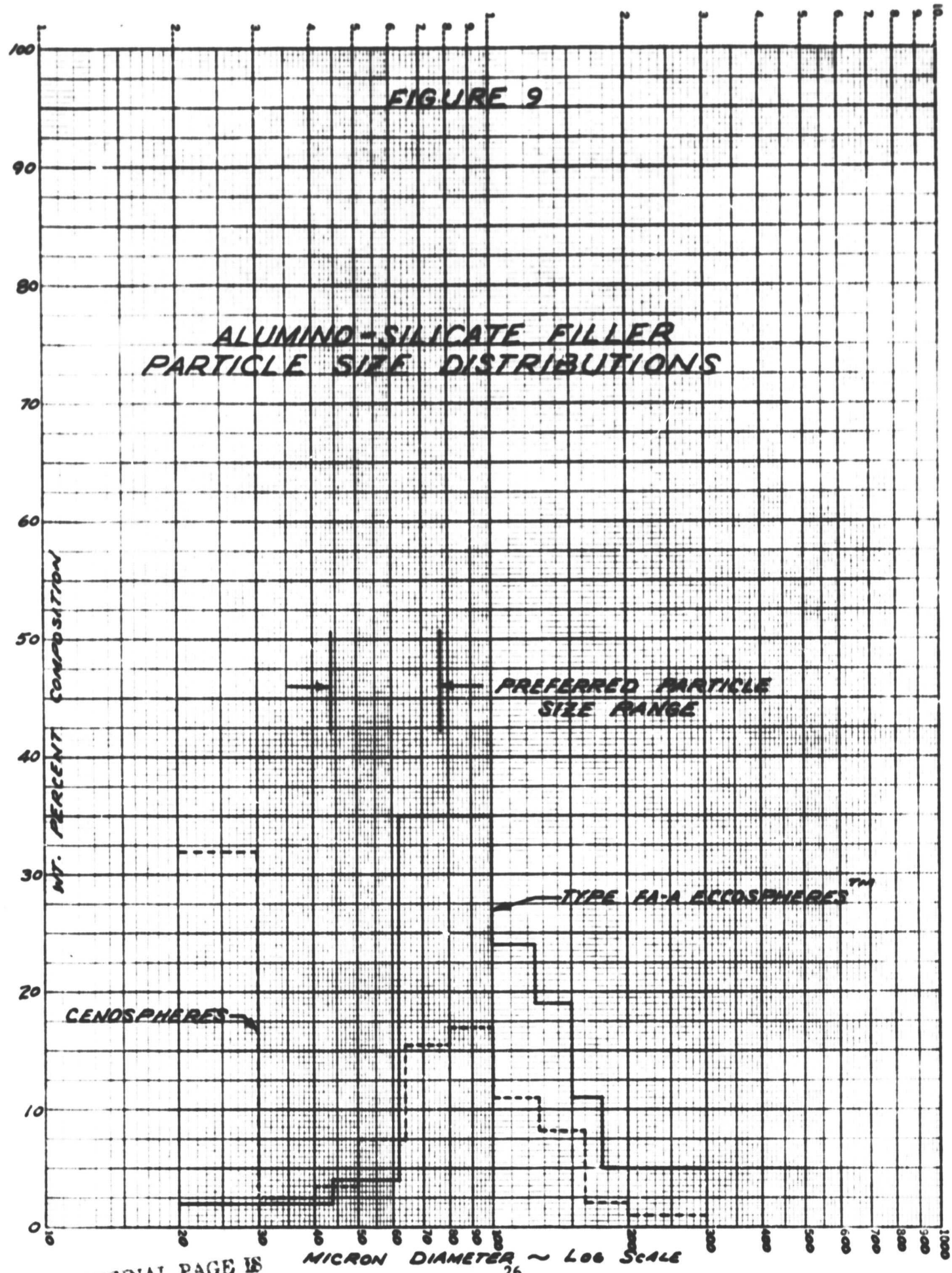

subsequently discontinued in favor of approaches which introduced porosity to interrupt the continuity of the YSZ structures. The resulting systems achieved abradability through the friability and crushing of the porous filled structures. A typical abradability wear scar for this type of structure is shown in Figure 8.

Alumino-Silicate Hollow Sphere Fillers for YSZ Matrix System

Hollow alumino-silicate spheres were used to provide closed-pore porosity in both pre-stabilized and flame-stabilized YSZ structures. These spheres were obtained commercially as Type FA-A Eccospheres ™ from Emerson and Cuming, Inc. This material is chemically identical to the Cenospheres used previously in Contract No. NAS 3-21263. However, as shown in Figure 9, the particle size distribution of the Eccospheres is much more heavily weighted in the larger sizes than the Cenospheres, which consist of more than 30 percent "fines". The larger particles, in addition to being more suitable for the plasma spray process, produce a more uniform, porous structure when combined with a YSZ matrix.

Pre-Stabilized YSZ Matrix Systems

The pre-stabilized YSZ selected for evaluation in combination with the previously described Type FA-A Eccosphere filler was supplied by ZIRCOA Division of Corning Glass Works. The composition was ZrO_2 • 8 w/o Y_2O_3 and was considered by NASA to rank among the best thermal barrier materials available at the time the tests were conducted.

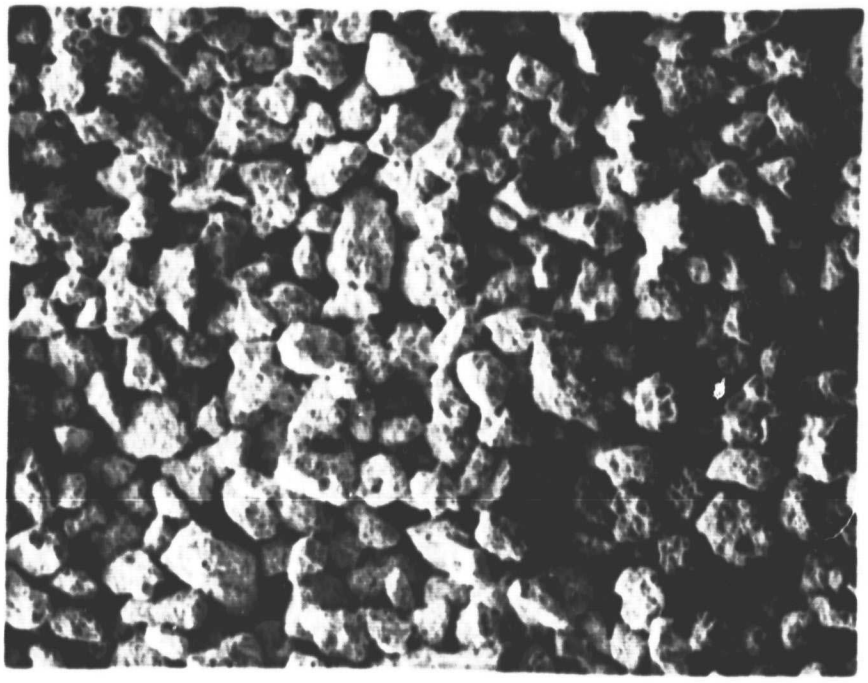

Magn: 100X

Figure 10 Particle shape for pre-stabilized YSZ plasma-spray grade powder ZrO_2· 8 w/o Y_2O_3

The granular form of the plasma-spray grade powder is shown in Figure 10. The particle size distribution of the powder as supplied is shown in Figure 11 where it can be seen that the majority of the material is within the preferred particle size range of 44-77 microns (-200 +325 mesh). It should be noted that the abscissa of Figure 11 differs from Figure 9 by one decade.

The array of composition and spray parameter variations investigated is shown in Table II. Three spray distances and three arc power variations were tested for each of 7 compositions within the material system. In addition, one composition consisting of 14 v/o matrix/86 v/o filler (designated as System III-G) was tested, which corresponded to 50/50 weight percent as shown in Figure 12. Typical photographs of the low speed abradability wear scars and time-dependent erosion signatures for 30, 60 and 120 minutes total exposure for some of the variations listed in Table II are presented in Figures 13 through 20.

In general, power levels and spray distances reduced from the median values resulted in softer coatings which exhibited increased erosion damage, as may be seen by comparing Figures 13 and 14. Significant improvements in abradability were observed for filler concentration levels of 50 v/o and higher as shown in Figures 13 and 15 through 20. Observe the deep, distinct grooving on the ceramic surface for compositions containing 50 v/o or more filler in contrast to the glazed wear scar and smeared layer of blade tip material shown in Figure 13.

Because only the 20/80 and 14/86 ratio systems, prepared by using the mid-range parameters (SD 1, PL 1), indicated a reasonable balance between abradability and erosion resistance, high speed rig testing was restricted to these systems. Results of these abradability tests, showing the rub wear scar and blade tip condition for the 20 v/o matrix/80 v/o filler system (System III-F) are presented in Figure 21.

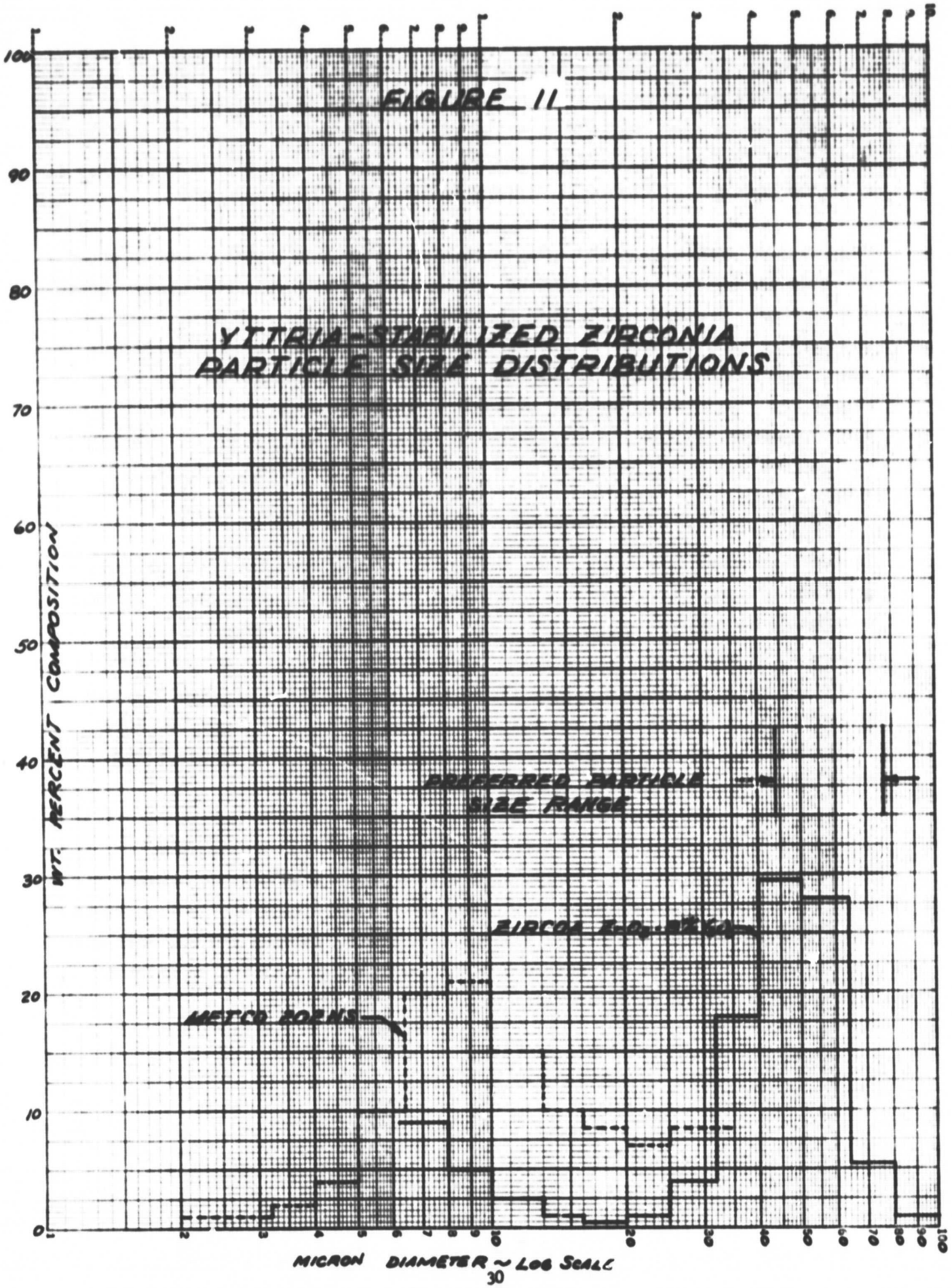
FIGURE II
YTTRIA-STABILIZED ZIRCONIA
PARTICLE SIZE DISTRIBUTIONS
WT. PERCENT COMPOSITION
PRESCRIBED PARTICLE SIZE RANGE
METCO 204 NS
MICRON DIAMETER ~ LOG SCALE

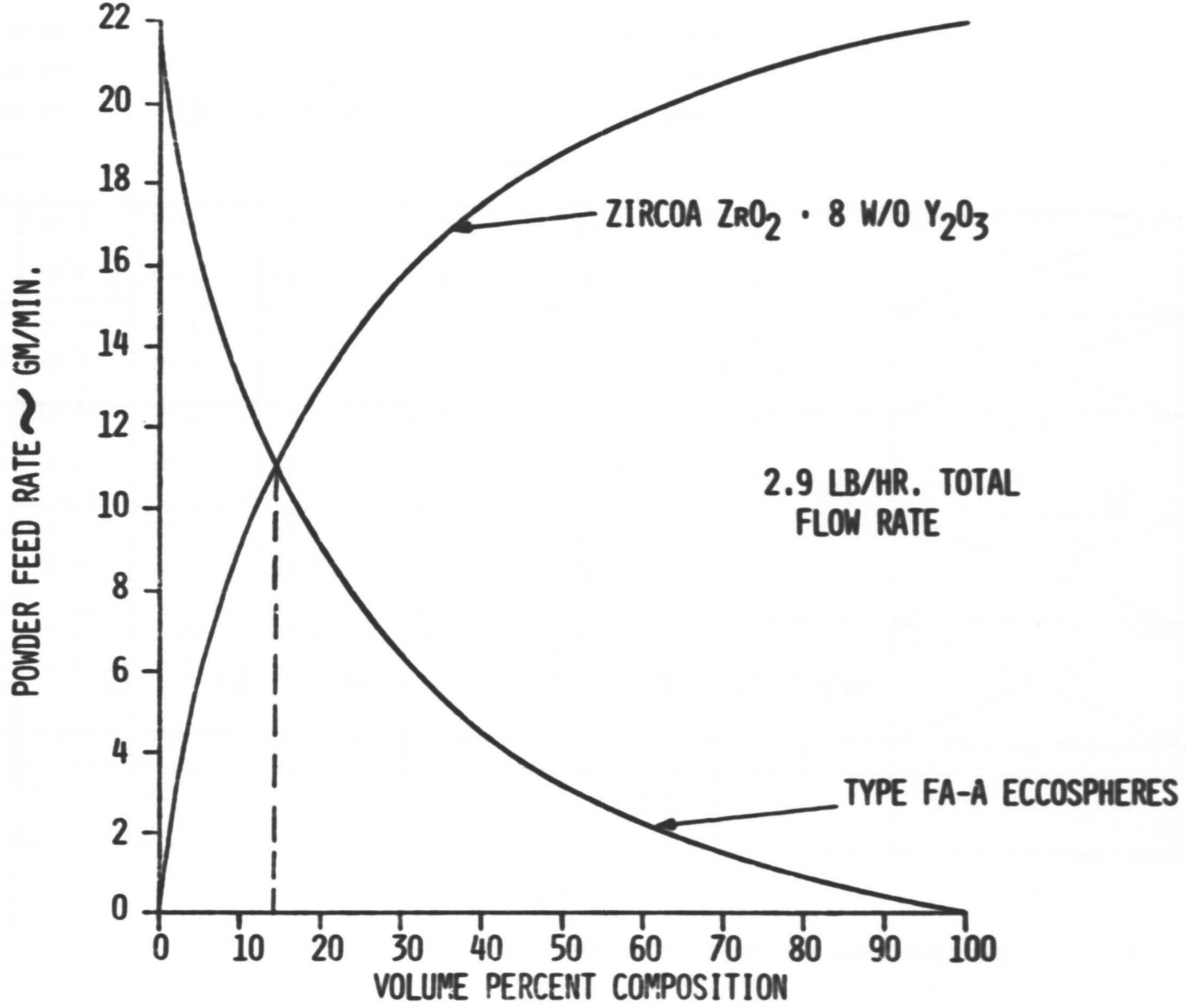

Figure 12 Effect of volume percent composition on powder feed rate for 8 w/o Y_2O_3 zirconia/type FA-A eccosphere coating system

Table II

Composition and Parameter Variations Investigated for Pre-Stabilized

YSZ Matrix

YSZ Matrix / Filler — Volume Percent Ratio		100/0	80/20	60/40	50/50	40/60	20/80	14/86 (50/50 w.o)	0/100
System		A	B	C	D	E	F	G	H
Spray Parameter Combinations	I	SD 1 (13) PL 2	SD 1 (15) PL 2	SD 1 (16) PL 2	SD 1 (17) PL 2	SD 1 (18) PL 2	SD 1 (19) PL 2		SD 1 (20) PL 2
	II	SD 2 PL 1	SD 2 PL 1	SD 2 PL 1	SD 2 PL 1	SD 2 PL 1	SD 2 PL 1		SD 2 PL 1
	III	SD 1 PL 1	SD 1 PL 1	SD 1 PL 1	SD 1 PL 1	SD 1 PL 1	SD 1 (21) PL 1	SD 1 (22) PL 1	SD 1 PL 1
	IV	SD 3 PL 1	SD 3 PL 1	SD 3 PL 1	SD 3 PL 1	SD 3 PL 1	SD 3 PL 1		SD 3 PL 1
YSZ Matrix: Zircoa $ZrO_2 \cdot 8$ w/o Y_2O_3	V	SD 1 (14) PL 3	SD 1 PL 3	SD 1 PL 3	SD 1 PL 3	SD 1 PL 3	SD 1 PL 3		SD 1 PL 3

Spray Distance:

SD 1 = 4.25 in.

SD 2 = 5.25 in.

SD 3 = 3.25 in.

(XX) Figure No. in text

Power Level:

PL 1 = 550 amps

PL 2 = 650 amps

PL 3 = 450 amps

Results obtained for the system comprised of 14 v/o matrix/86 v/o filler (System III-G) are shown in Figure 22, where the rub wear scar, blade tip condition and erosion signature following 30 minutes exposure are presented.

Hardness as measured on the R15Y scale as a function of composition is shown in Figure 23 for various spray distances and Figure 24 for various power levels.

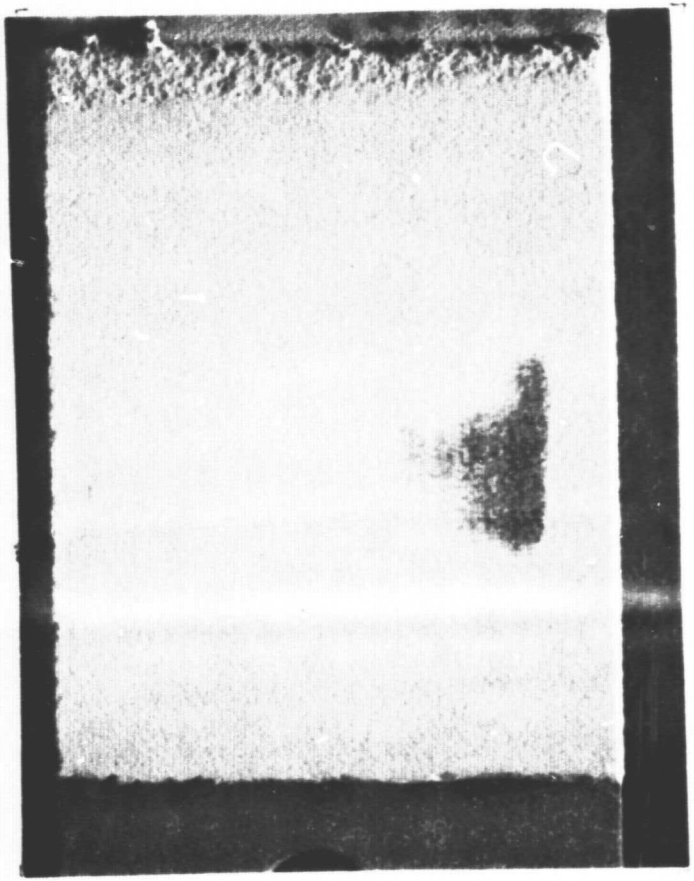

a. Abradability wear scar

(Rub direction ↓)

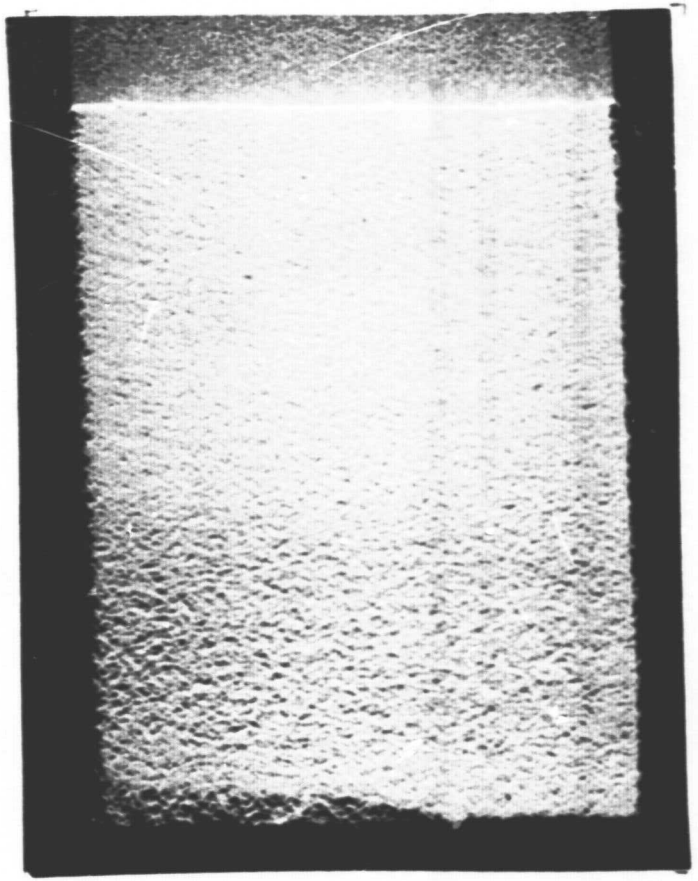

b. Erosion signature (30 min. exposure)

(Flow direction →)

Figure 13 Abradability and initial erosion results for System I-A

(Table II) Magn: 3X

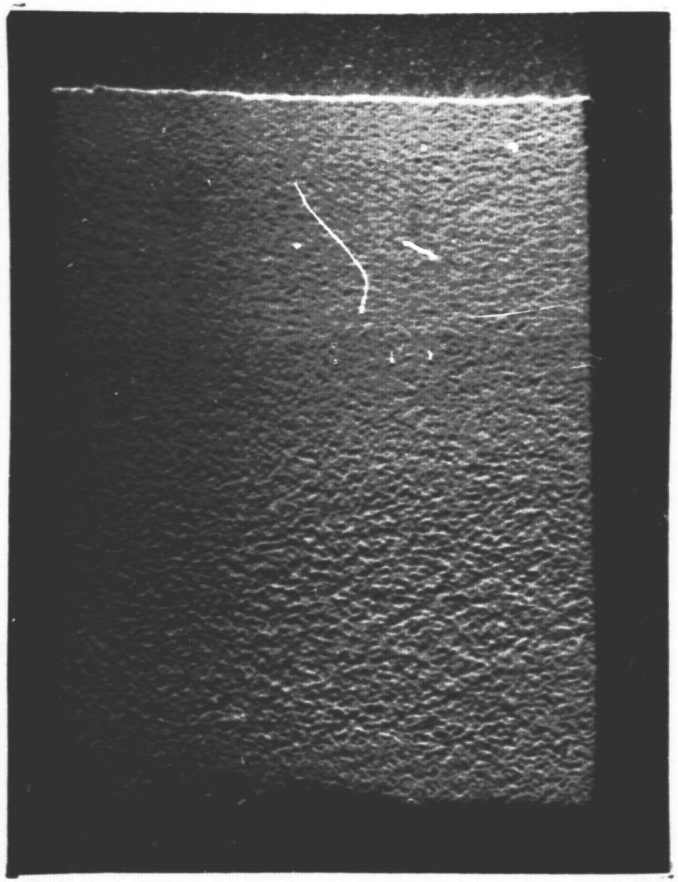

c. Erosion signature (60 min. exposure)

(Flow direction ➡)

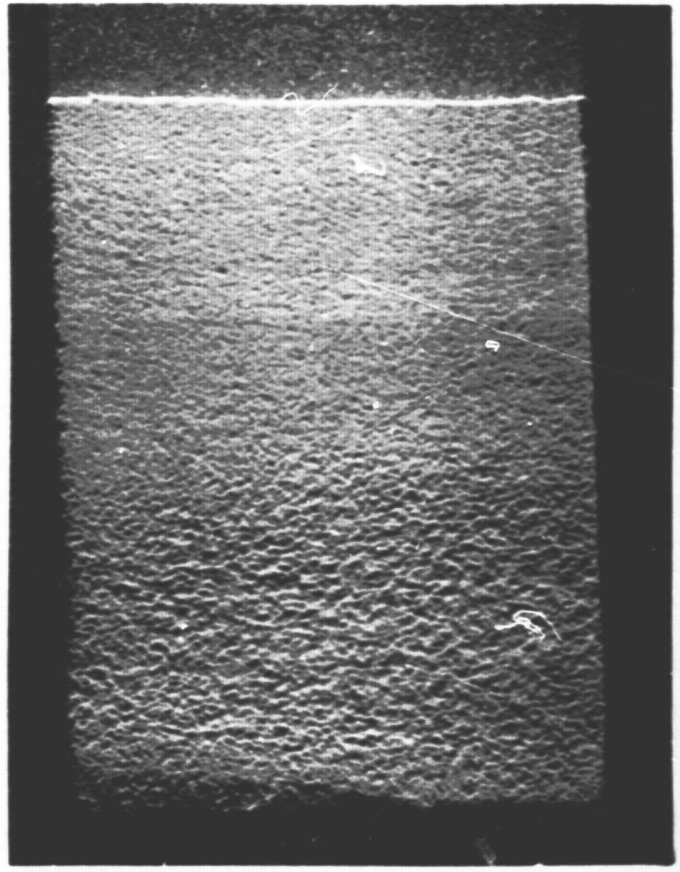

d. Erosion signature (120 min. exposure)

(Flow direction ➡)

Figure 13 Cont'd. Erosion results (continued) for System IA

(Table II) Magn: 3X

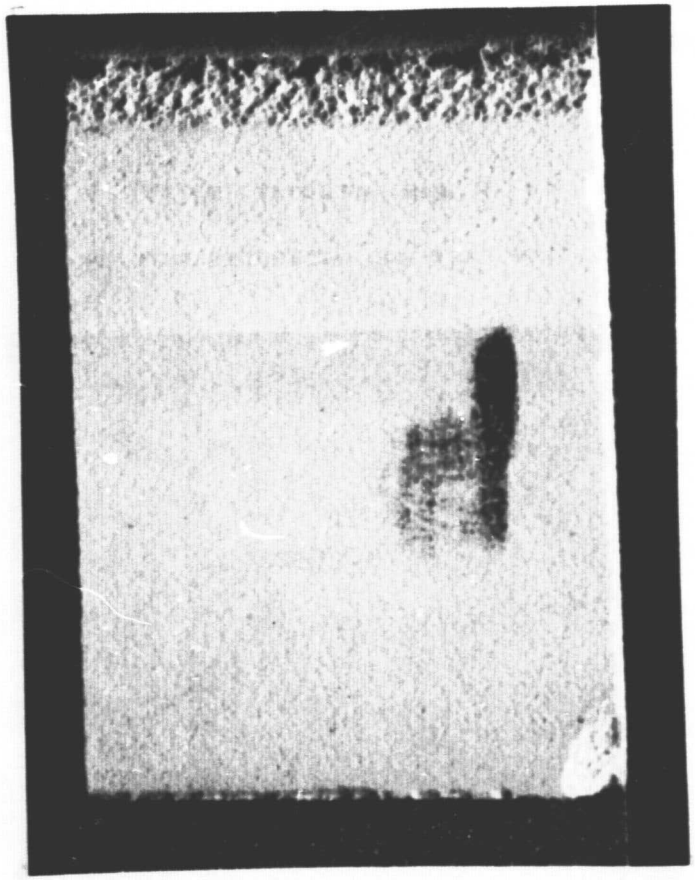

a. Abradability wear scar

(Rub direction ⬇)

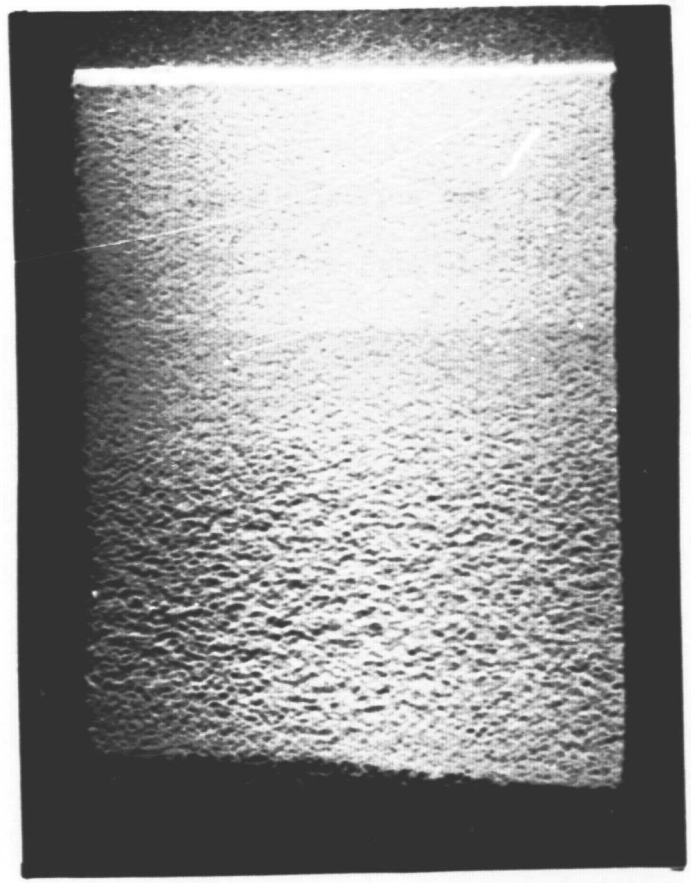

b. Erosion signature (30 min. exposure)

(Flow direction ➡)

Figure 14 Abradability and initial erosion results for System V-A

(Table II) Magn: 3X

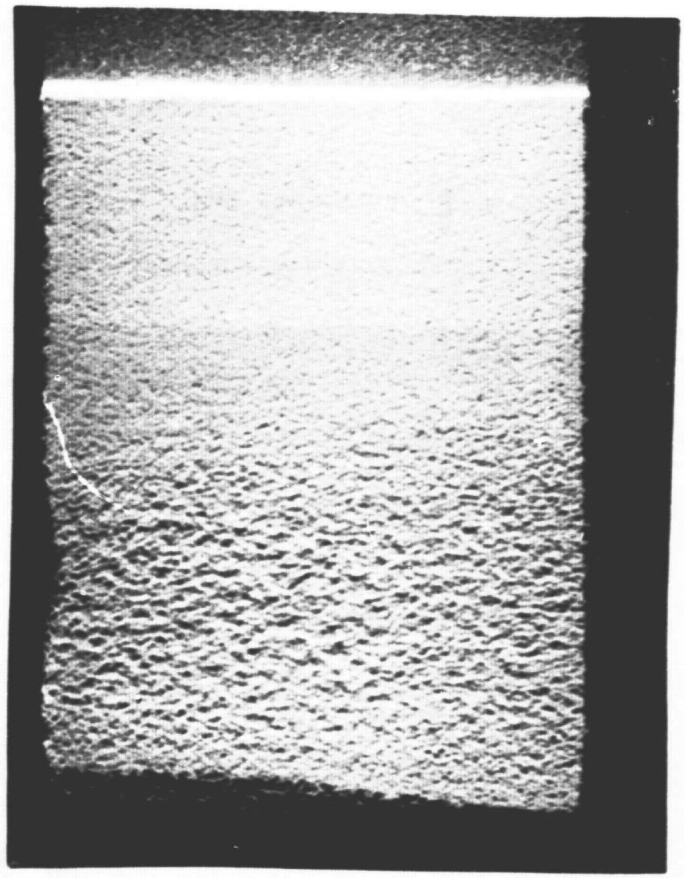

c. Erosion signature (60 min. exposure)

(Flow direction ➡)

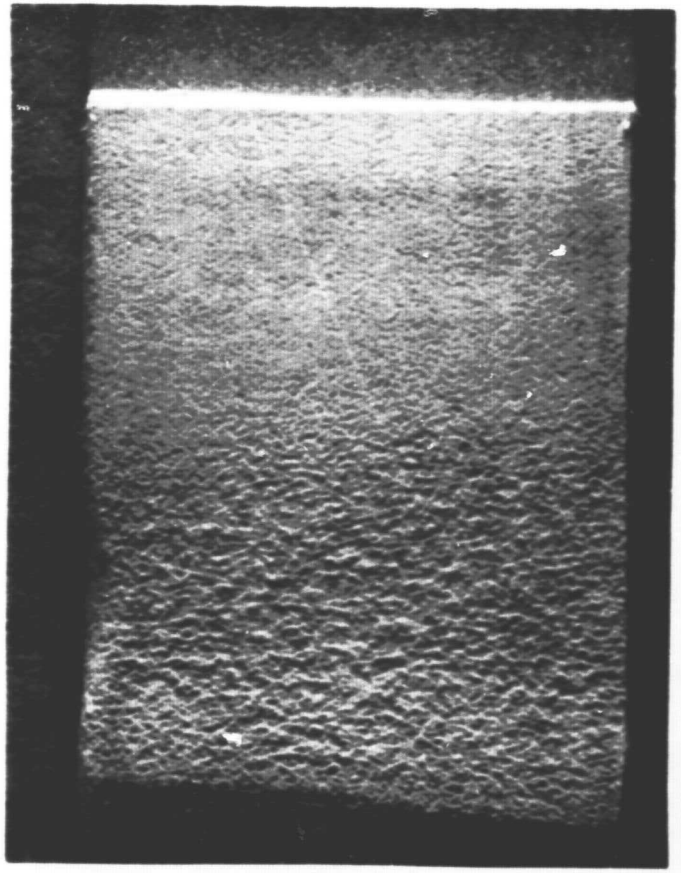

d. Erosion signature (120 min. exposure)

(Flow direction ➡)

Figure 14 Cont'd. Erosion results (continued) for System V-A

(Table II) Magn: 3X

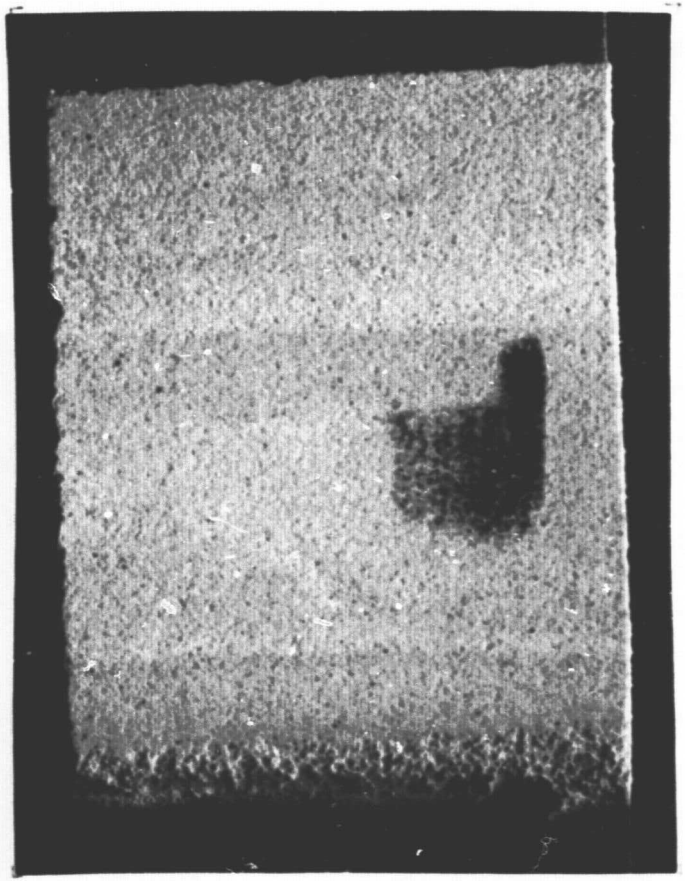

a. Abradability wear scar

(Rub direction ↓)

b. Erosion signature (30 min. exposure)

(Flow direction →)

Figure 15 Abradability and initial erosion results for System I-B (Table II) Magn: 3X

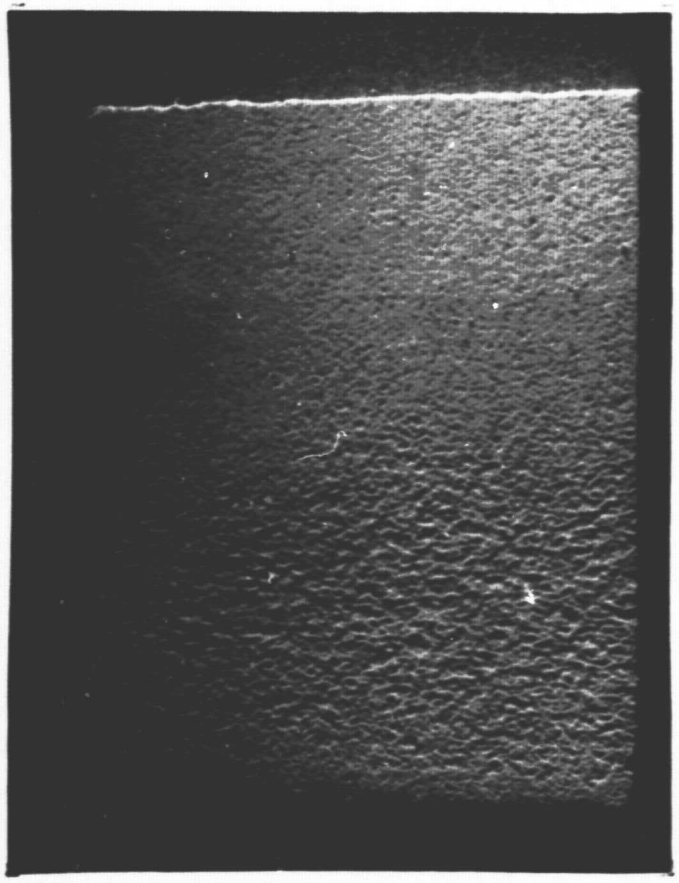

c. Erosion signature (60 min. exposure)

(Flow direction ➡)

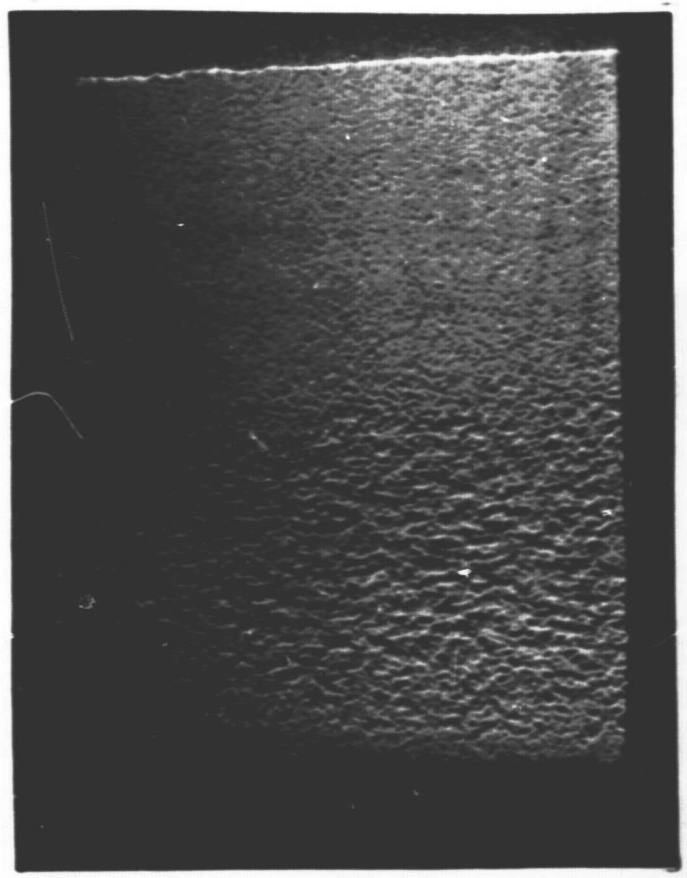

d. Erosion signature (120 min. exposure)

(Flow direction ➡)

Figure 15 Cont'd. Erosion results (continued) for System I-B

(Table II) Magn: 3X

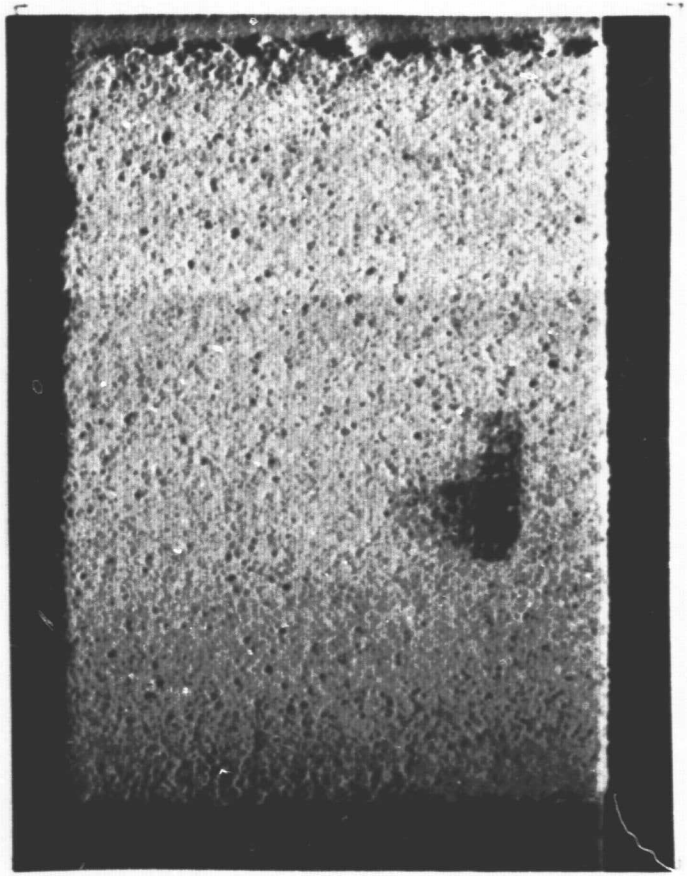

a. Abradability wear scar

(Rub direction ↓)

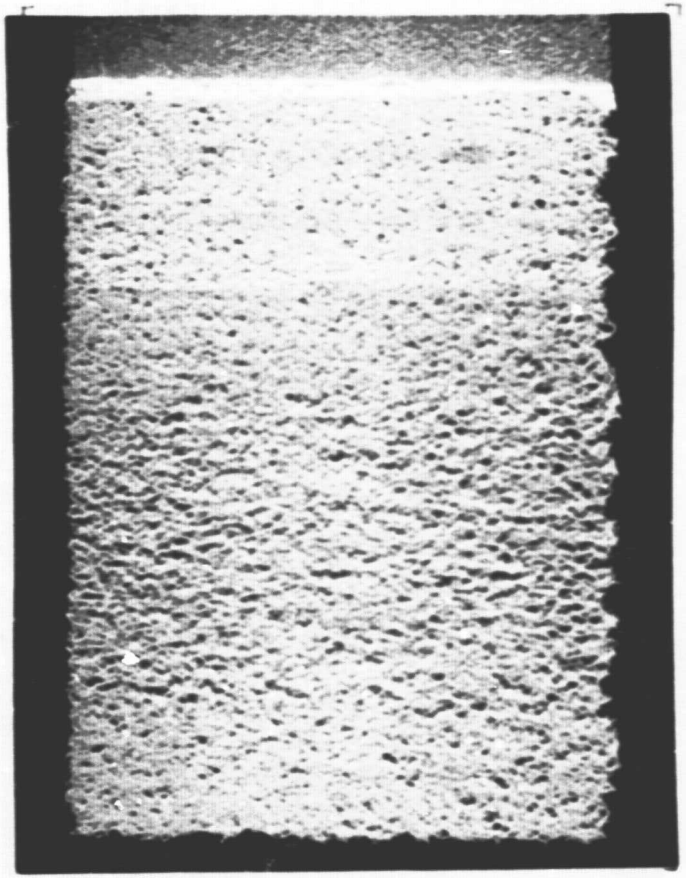

b. Erosion signature (30 min. exposure)

(Flow direction →)

Figure 16 Abradability and initial erosion results for System I-C

(Table II) Magn: 3X

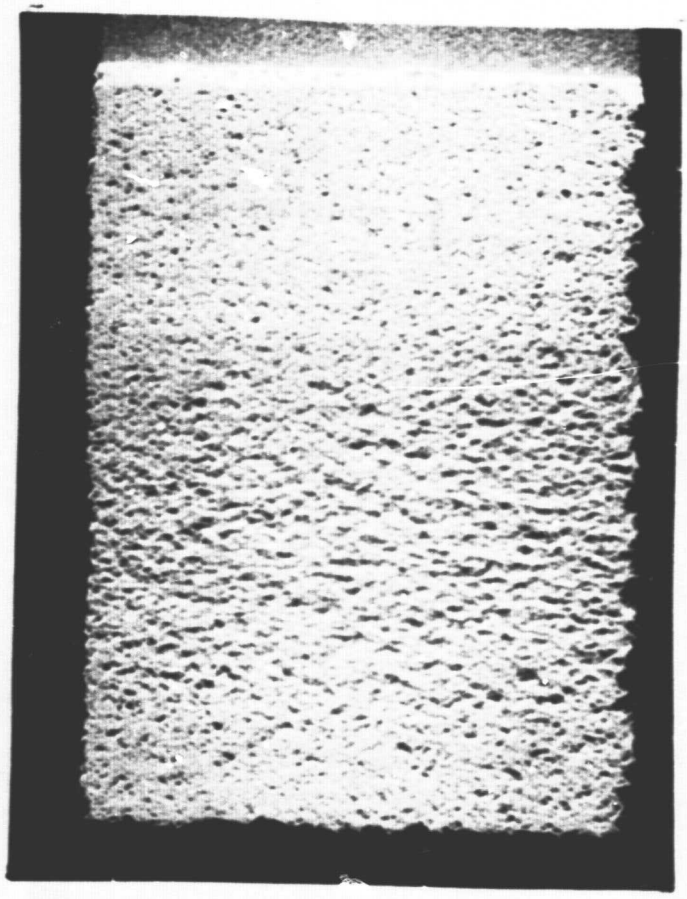

c. Erosion signature (60 min. exposure)

(Flow direction ➡)

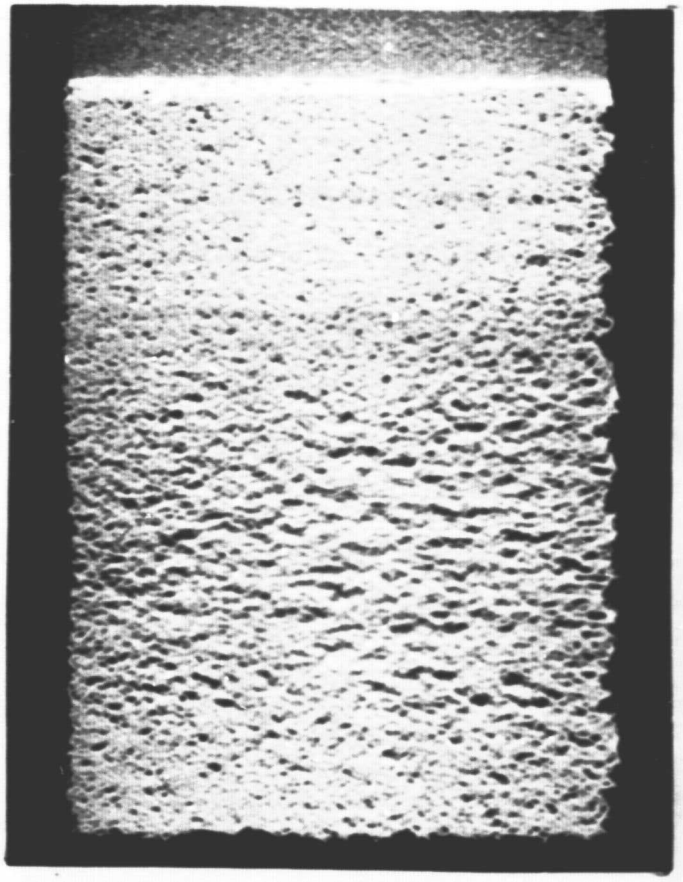

d. Erosion signature (120 min. exposure)

(Flow direction ➡)

Figure 16 Cont'd. Erosion results (continued) for System I-C

(Table II) Magn: 3X

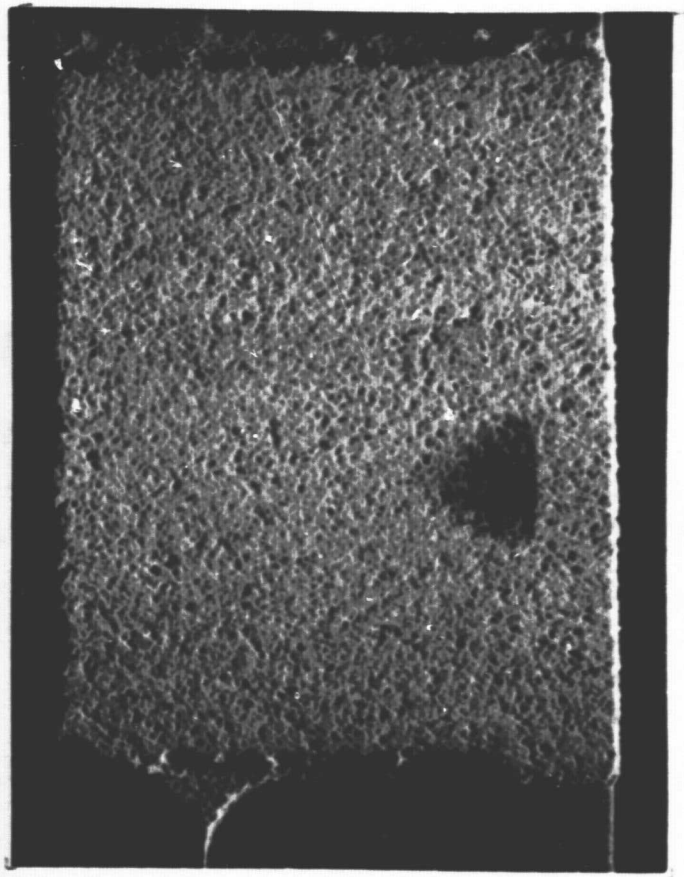

a. Abradability wear scar

(Rub direction ↓)

b. Erosion signature (30 min. exposure)

(Flow direction →)

Figure 17 Abradability and initial erosion results for System I-D

(Table II) Magn: 3X

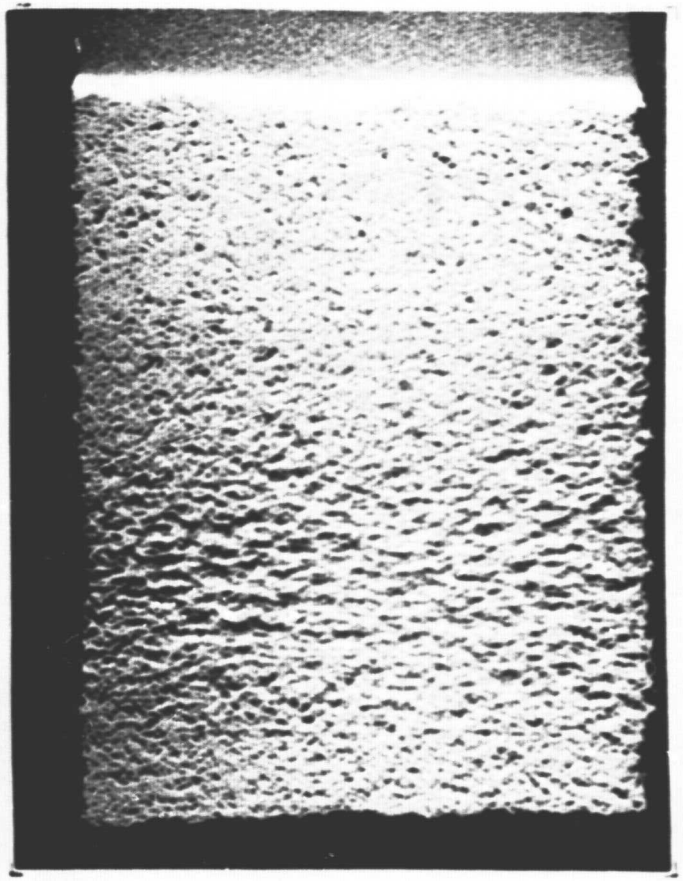

c. Erosion signature (60 min. exposure)

(Flow direction ➡)

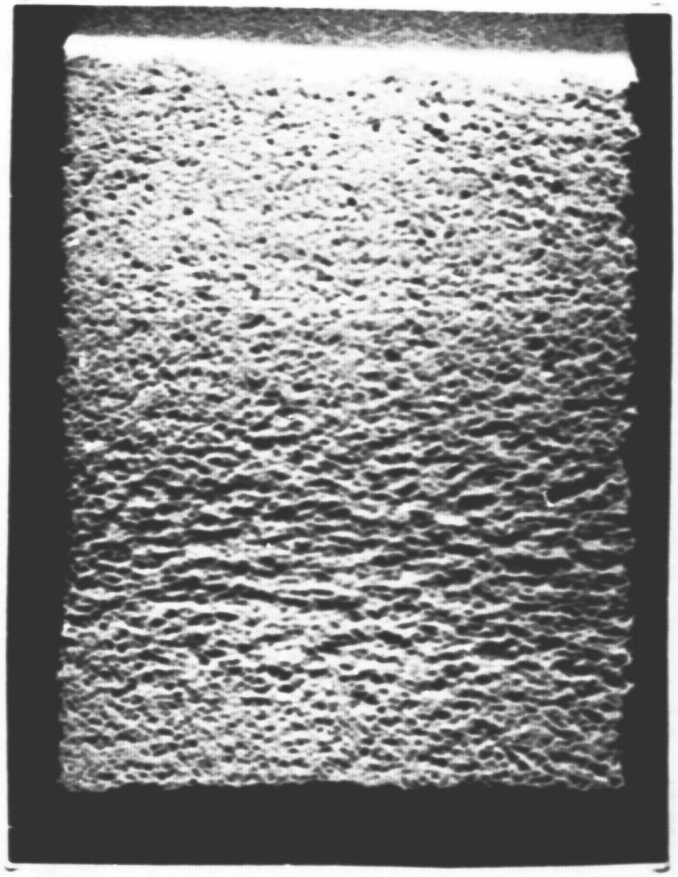

d. Erosion signature (120 min. exposure)

(Flow direction ➡)

Figure 17 Cont'd. Erosion results (continued) for System I-D

(Table II) Magn: 3X

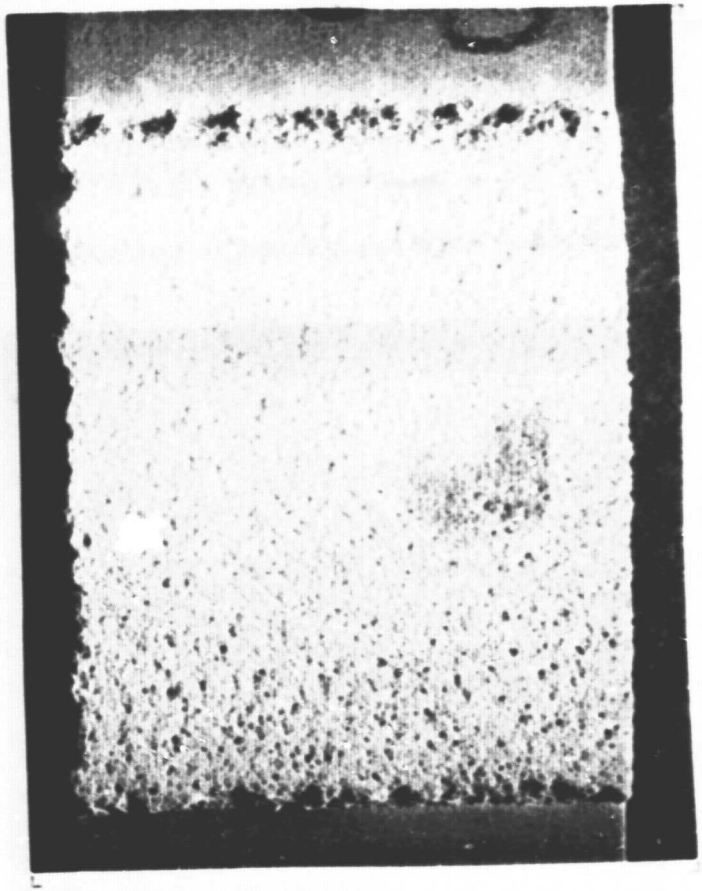

a. Abradability wear scar

(Rub direction ⬇)

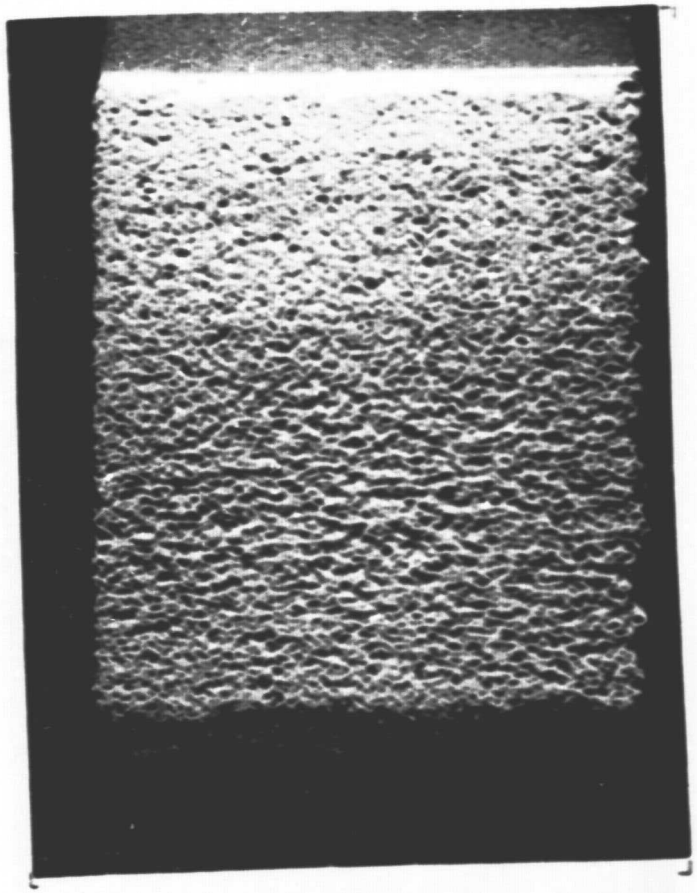

b. Erosion signature (30 min. exposure)

(Flow direction ➡)

Figure 18 Abradability and initial erosion results for System I-E

(Table II) Magn: 3X

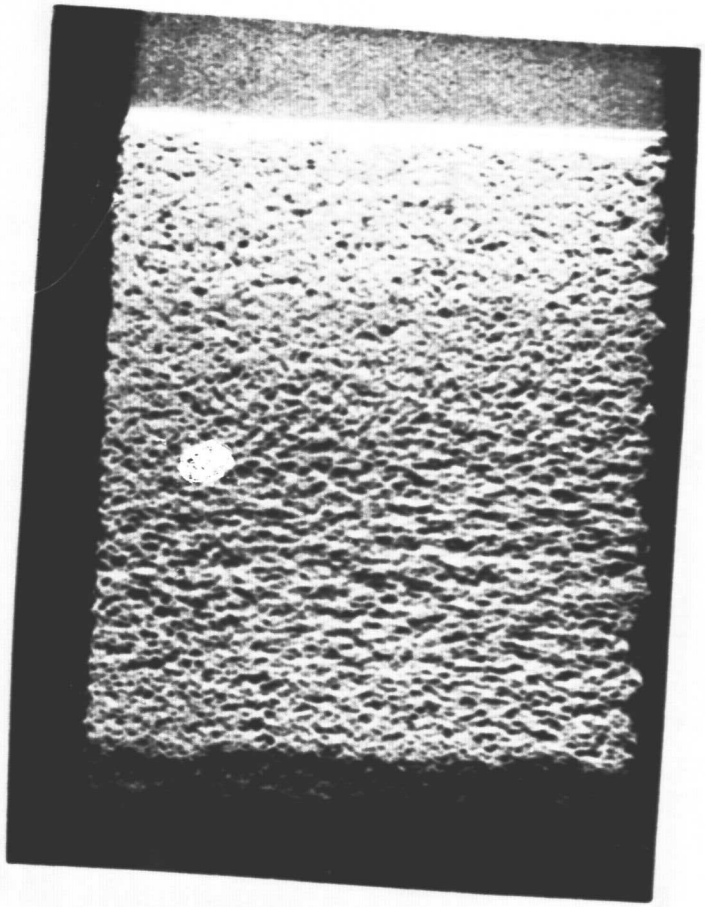

c. Erosion signature (60 min. exposure)

(Flow direction ➡)

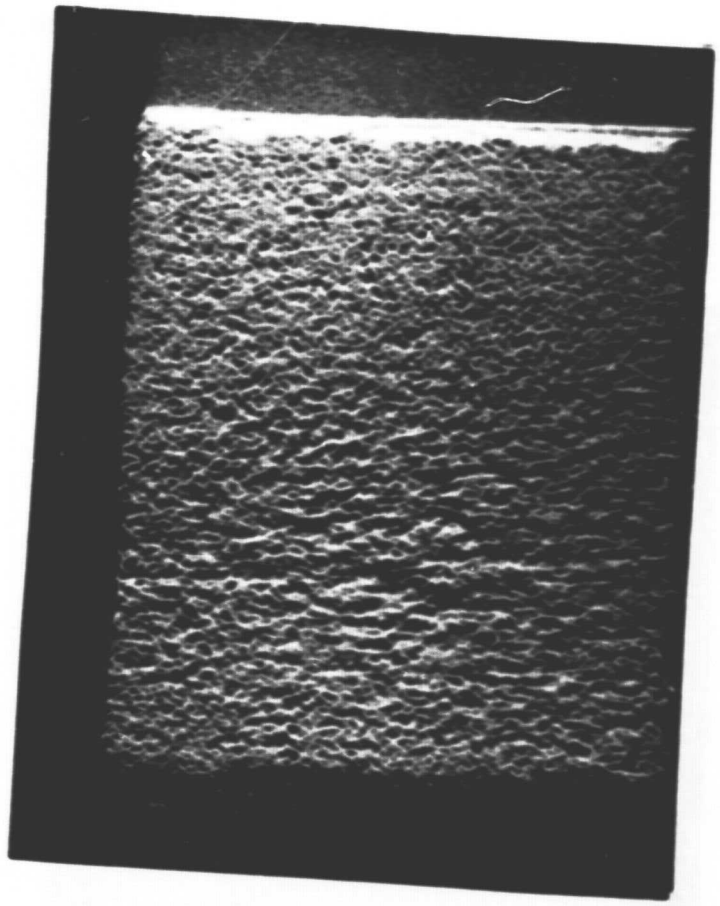

d. Erosion signature (120 min. exposure)

(Flow direction ➡)

Figure 18 Cont'd. Erosion results (continued) for System I-E
(Table II) Magn: 3X

a. Abradability wear scar

(Rub direction ⬇)

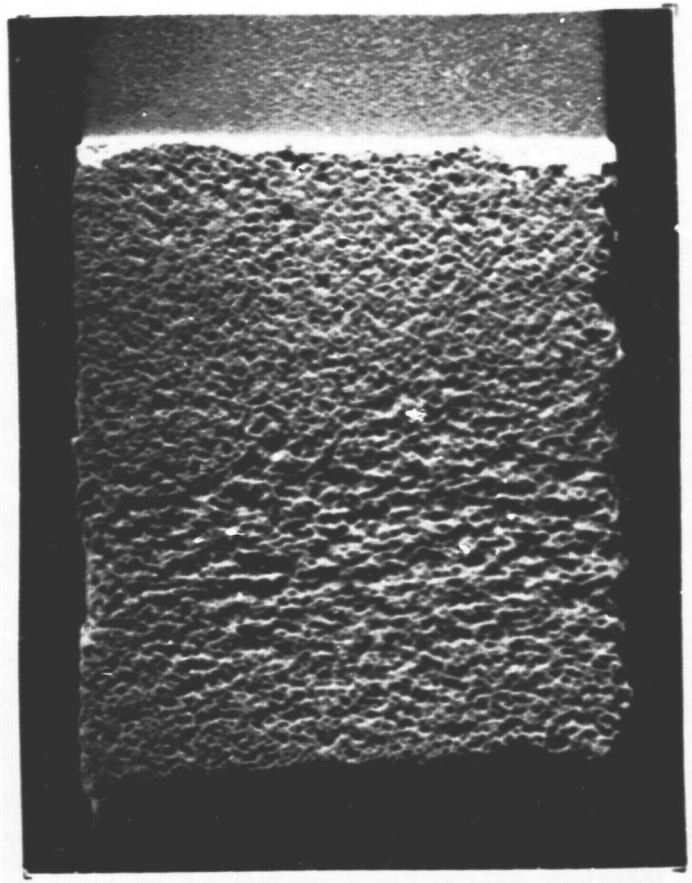

b. Erosion signature (30 min. exposure)

(Flow direction ➡)

Figure 19 Abradability and initial erosion results for System I-F

(Table II) Magn: 3X

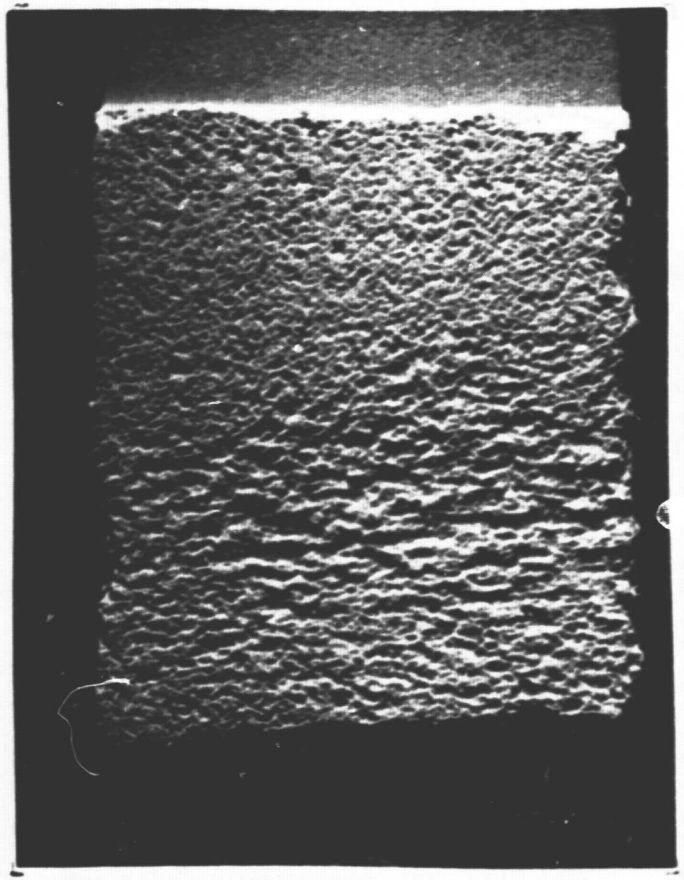

c. Erosion signature (60 min. exposure)

(Flow direction ➡)

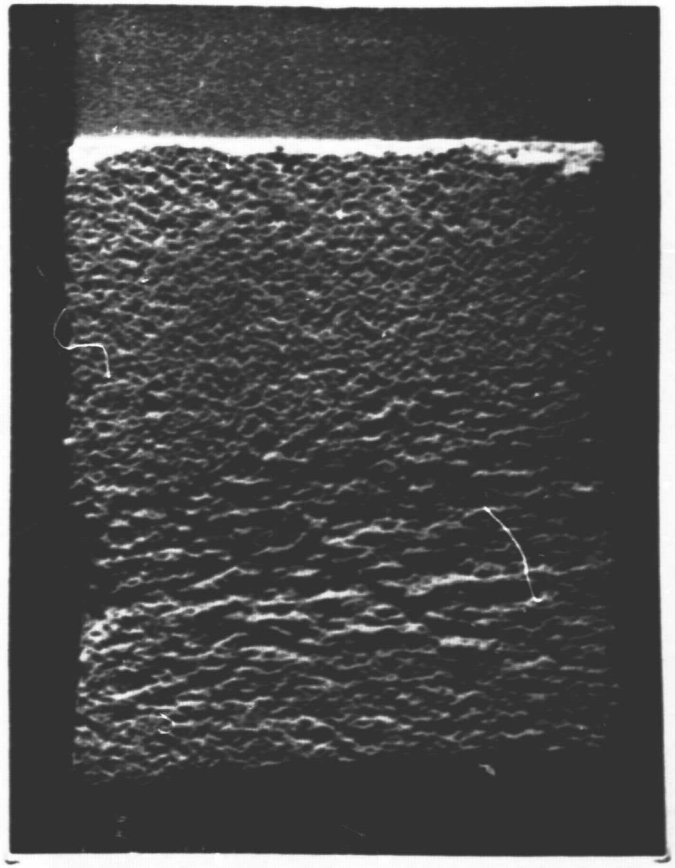

d. Erosion signature (120 min. exposure)

(Flow direction ➡)

Figure 19 Cont'd. Erosion results (continued) for System I-F

(Table II) Magn: 3X

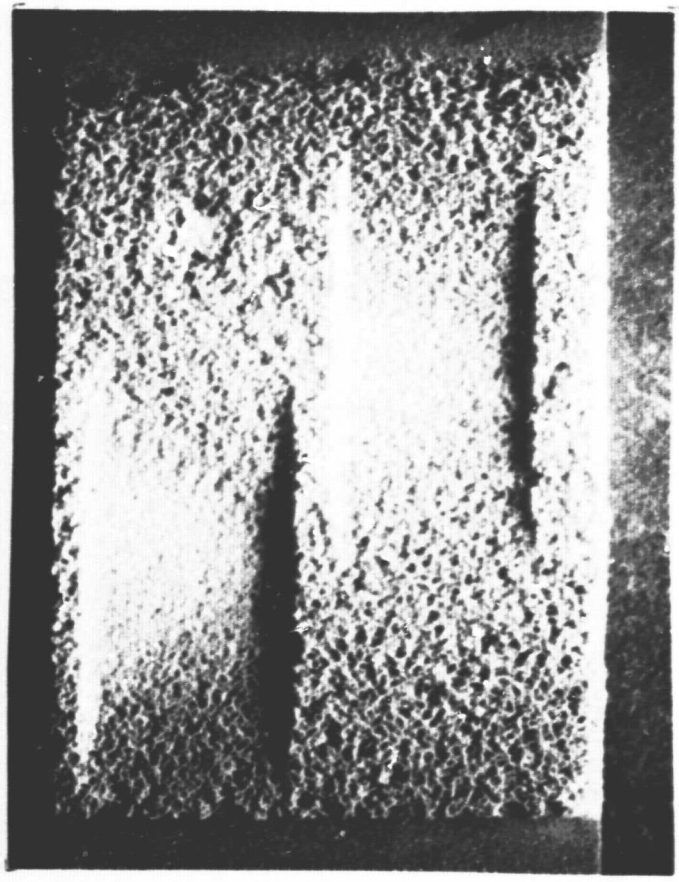

a. Abradability wear scar

(Rub direction ↓)

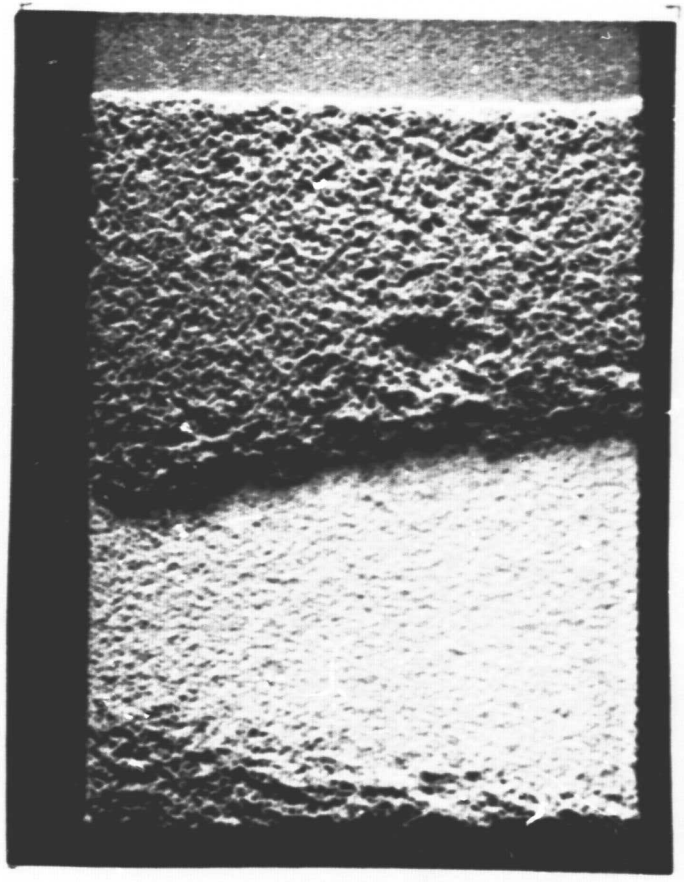

b. Erosion signature (30 min. exposure)

(Flow direction →)

Figure 20 Abradability and initial erosion results for System I-H

(Table II) Magn: 3X

Coating destroyed during test

Coating destroyed during test

c. Erosion signature (60 min. exposure)

(Flow direction ➡)

d. Erosion signature (120 min. exposure)

(Flow direction ➡)

Figure 20 Cont'd. Erosion results (continued) for System I-H
(Table II) Magn: 3X

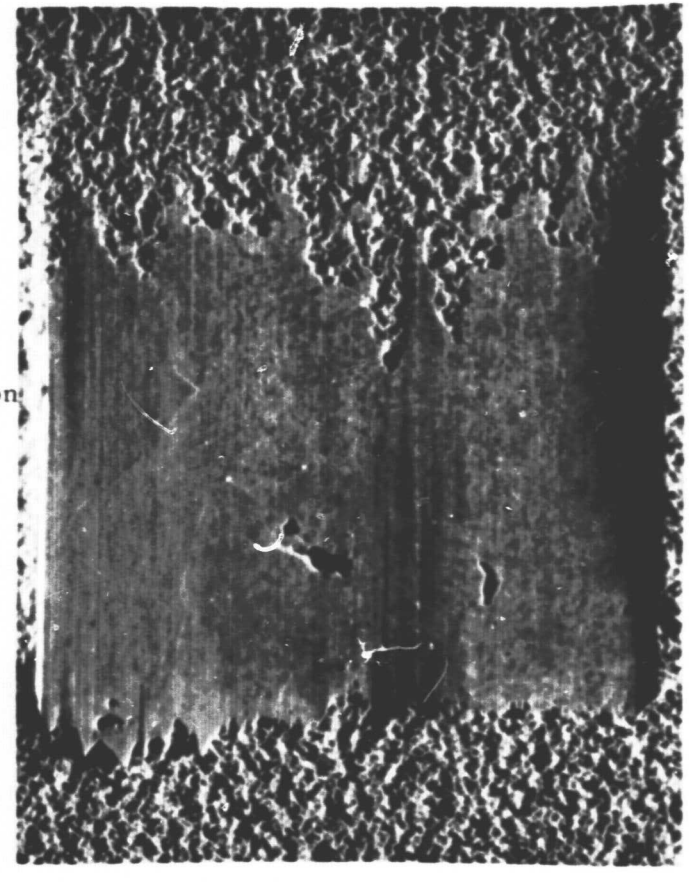

a) Blade Track Wear Scar

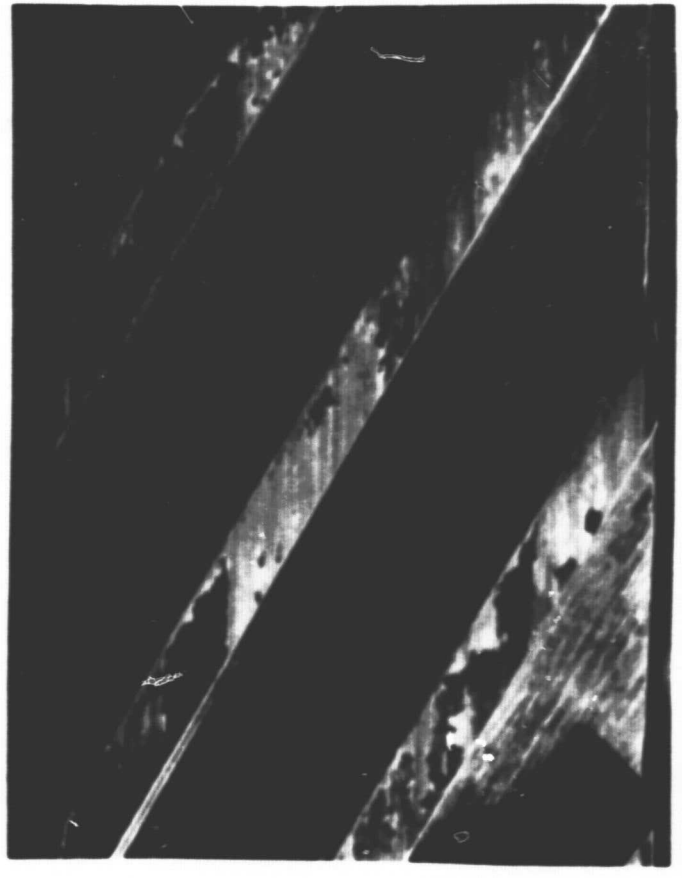

b) Blade tip condition

Incursion Rate	.0025 cm/sec (.001 in/sec)
Blade Tip Speed	229 m/sec (750 ft/sec)
Depth of Rub	.043 cm (.017 in)

Figure 21 Slow incursion rate high speed abradability test results for system III-F

Magn: 5X

Pub Direction

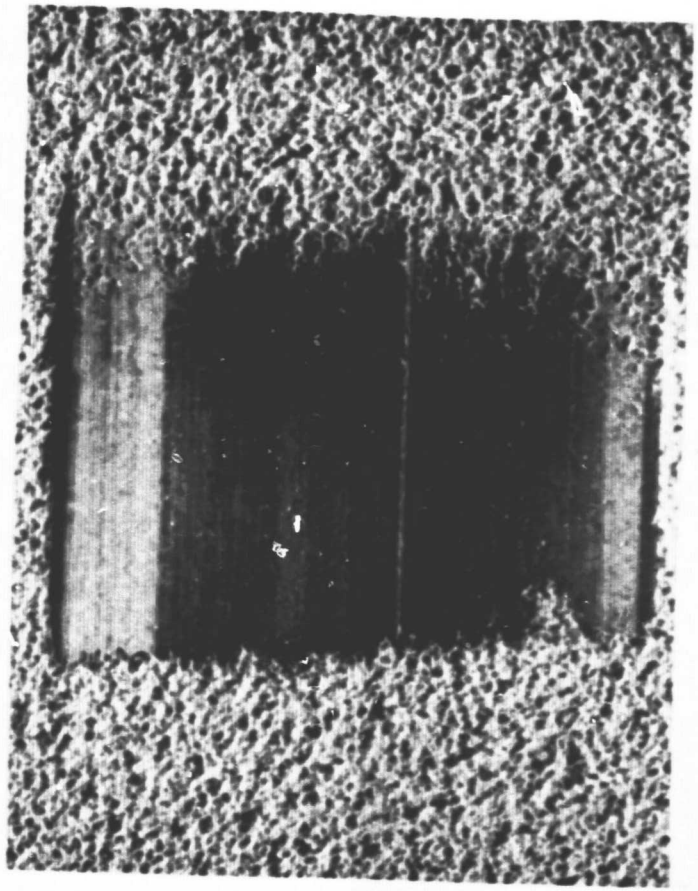

a) Blade track wear scar

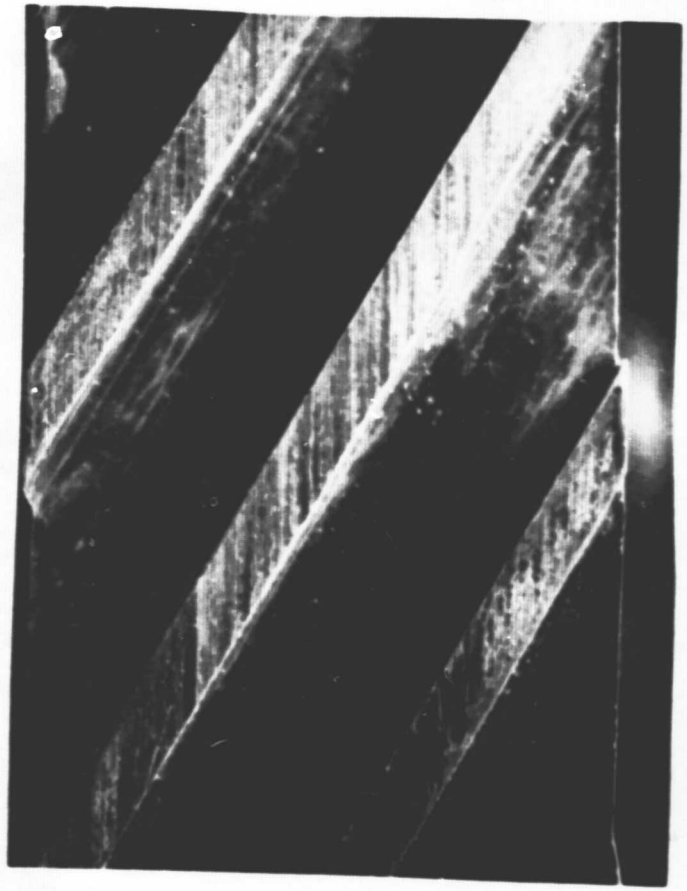

b) Blade tip condition

Incursion Rate	.0025 cm/sec (.001 in/sec)
Blade Tip Speed	229 m/sec (750 ft/sec)
Depth of Rub	.03 cm (.012 in)

Figure 22 Slow incursion rate high speed abradability test results for system III G

Magn: 5X

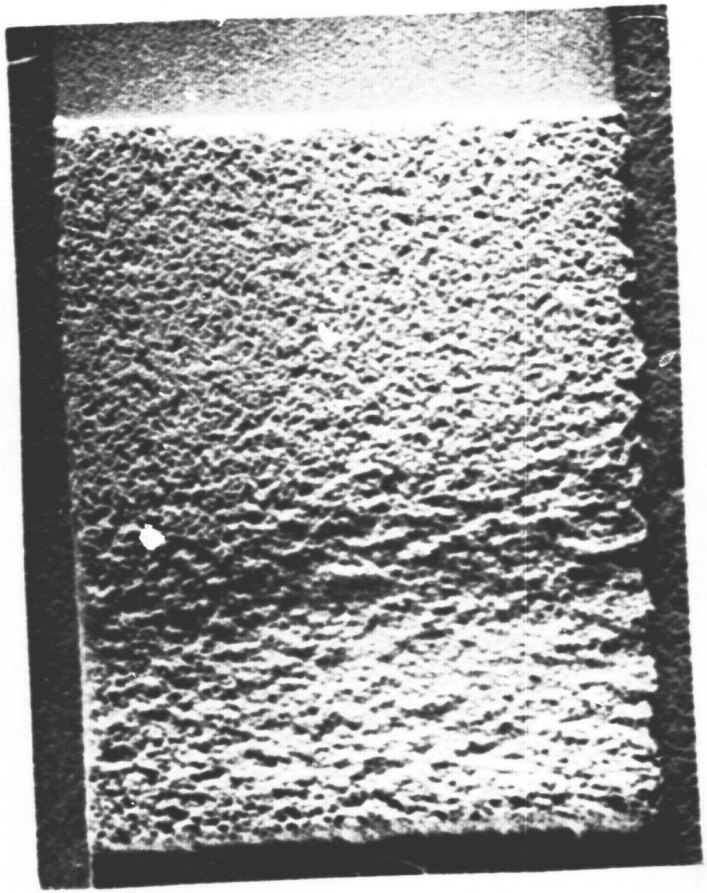

Flow Direction

Figure 22C Erosion test results for system IIIG (30 min exposure)

Magn: 3X

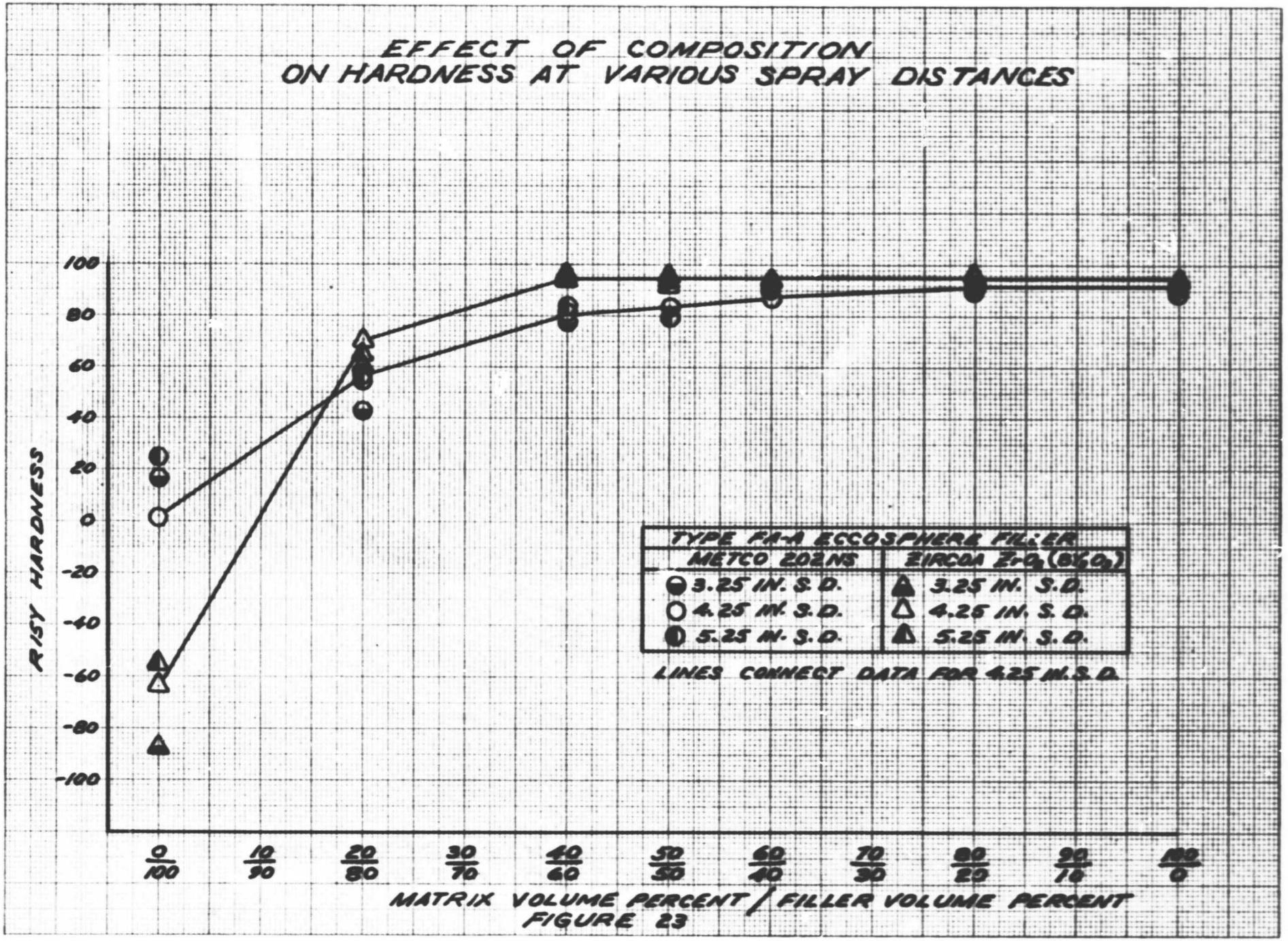
EFFECT OF COMPOSITION
ON HARDNESS AT VARIOUS SPRAY DISTANCES
RISY HARDNESS
100
80
60
40
20
0
-20
-40
-60
-80
-100
TYPE FA-A ECCOSPHERE FILLER
METCO 202 NS
ZIRCOA ZrO_2 ($85\%O_2$)
3.25 IN. S.D.
4.25 IN. S.D.
5.25 IN. S.D.
3.25 IN. S.D.
4.25 IN. S.D.
5.25 IN. S.D.
LINES CONNECT DATA FOR 4.25 IN. S.D.
0/100
10/90
20/80
30/70
40/60
50/50
60/40
70/30
80/20
90/10
100/0
MATRIX VOLUME PERCENT / FILLER VOLUME PERCENT
FIGURE 23

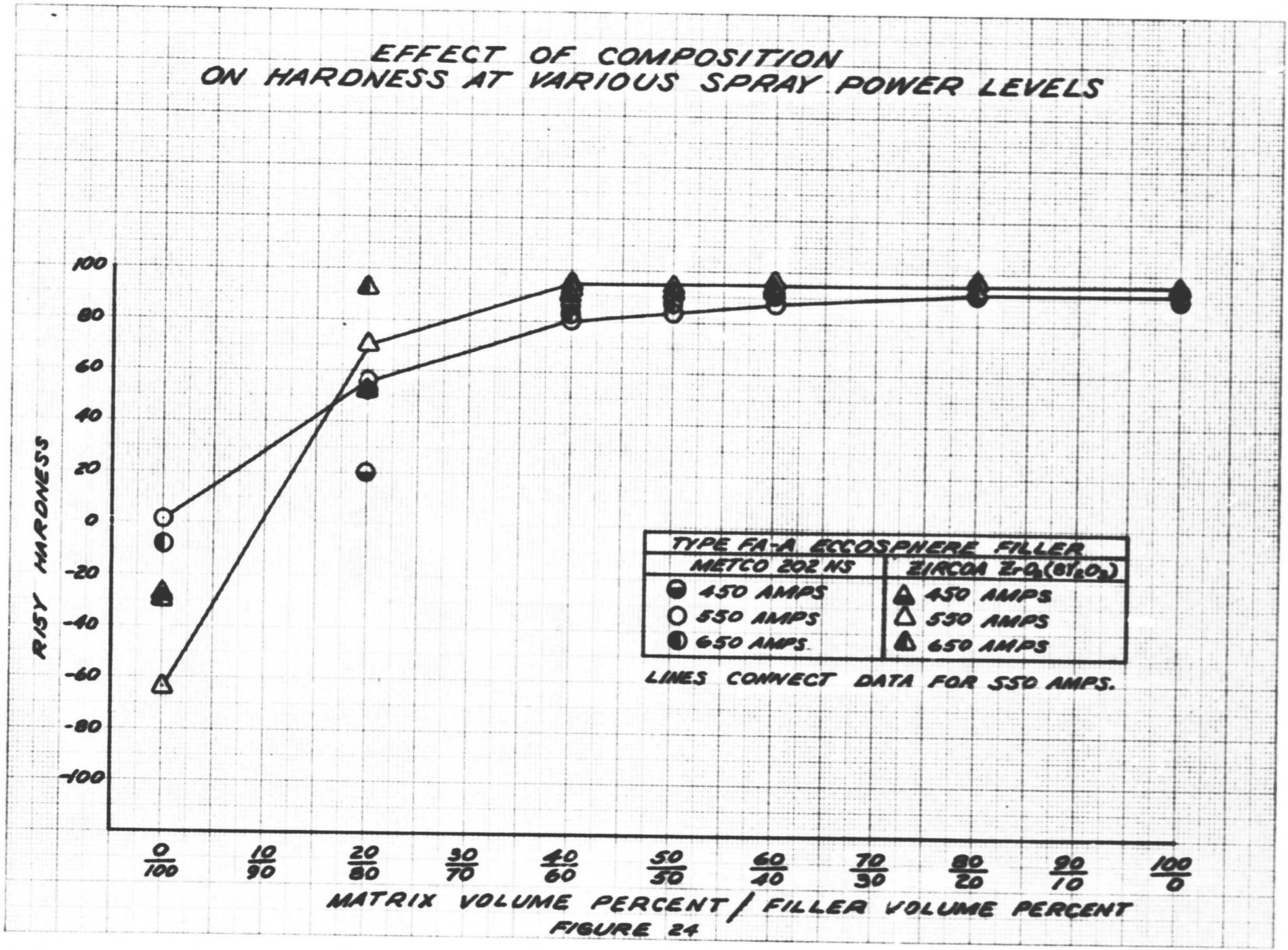
EFFECT OF COMPOSITION
ON HARDNESS AT VARIOUS SPRAY POWER LEVELS
RISY HARDNESS
100
80
60
40
20
0
-20
-40
-60
-80
-100
TYPE FA-A ECCOSPHERE FILLER
METCO 202 NS
450 AMPS
550 AMPS
650 AMPS
ZIRCOA Zr-O2 (SiO2)
450 AMPS
550 AMPS
650 AMPS
LINES CONNECT DATA FOR 550 AMPS.
0/100
10/90
20/80
30/70
40/60
50/50
60/40
70/30
80/20
90/10
100/0
MATRIX VOLUME PERCENT / FILLER VOLUME PERCENT
FIGURE 24

Photomicrographs of the microstructures corresponding to the spray distance and power level variations of the 80 v/o filler/20 v/o matrix composition are shown in Figure 25-29 inclusive. Both 100X and 1000X magnifications are presented for each of the microstructures. Reducing the spray distance and reducing the power level both resulted in coatings in which the FA-A filler particles retained their hollow sphere morphology. Baseline spray conditions as well as increased spray distance and power level resulted in some apparent softening and deformation ("splatting") of the hollow filler particles, thereby reducing the porosity.

Flame-Stabilized YSZ Matrix Systems

The flame-stabilized YSZ selected for evaluation in combination with the previously described Type FA-A Eccosphere filler was supplied by Metco, Inc. The initial composition of this composite material is described by Metco as ZrO_2 • 20 w/o Y_2O_3. The composition of the deposited coating is unknown.

The spherical form of the plasma-spray grade composite powder is shown in Figure 30. The particle size distribution of the powder as-supplied is shown in Figure 11 where it can be seen that virtually all of the material is below the preferred particle size range of 44-77 microns (-200 +325 mesh). It should be recalled that the abscissa of Figure 11 differs from Figure 9 by one decade, as noted previously. The large fraction of "fines" in this material undoubtedly contributed to the different performance exhibited by coatings within this system.

The array of compositions and spray parameter variations investigated is shown in Table III. Three spray distances and three arc power variations were tested for each of 7 compositions within the material system. In addition one composition consisting of 18 v/o matrix/82 v/o filler (designated as System III-0) was tested, which corresponded to 50/50 weight percent as shown in Figure 31. Typical photographs of the abradability wear scars and time-dependent erosion signatures for 30, 60 and 120 minutes total exposure for some of the variations listed in Table III are presented in Figures 32 through 41.

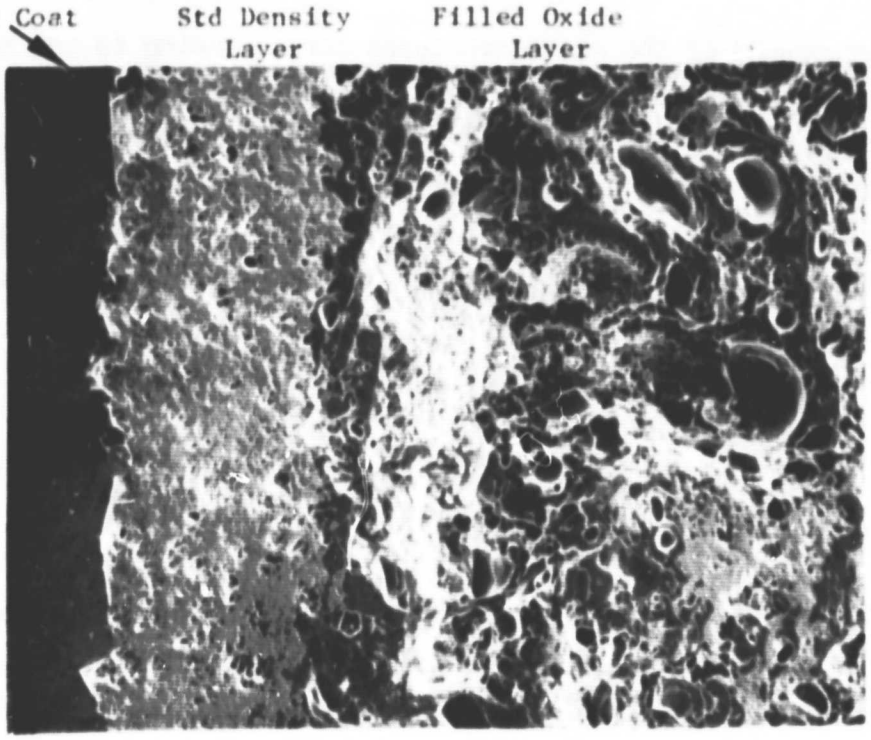

Magn: 100X

a) Porosity Characteristics

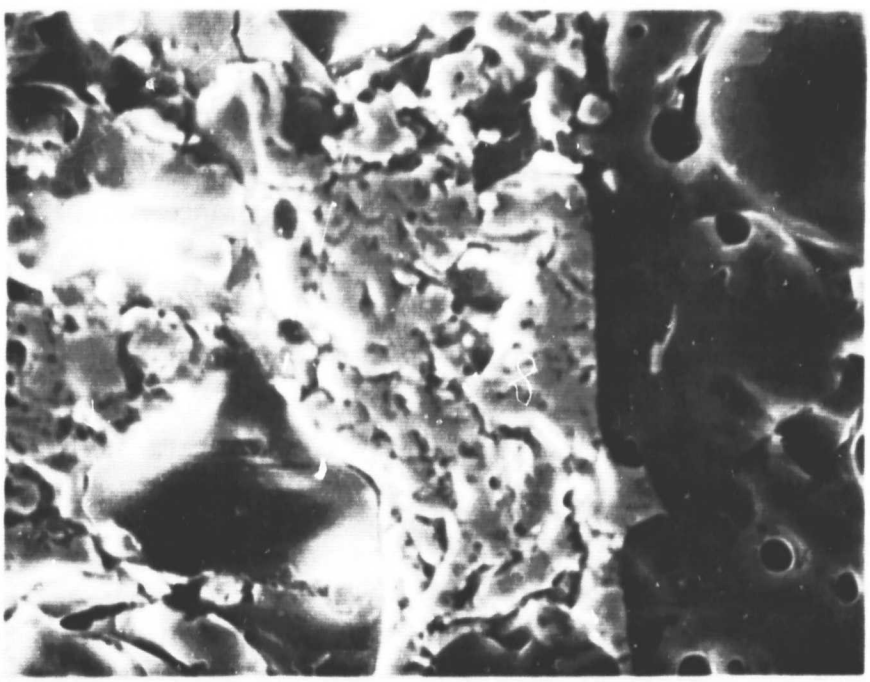

Magn: 1000X

b) Ceramic Particle Morphology (outer layer)

Figure 25 Porosity characteristics and ceramic particle morphology of coating system I-F

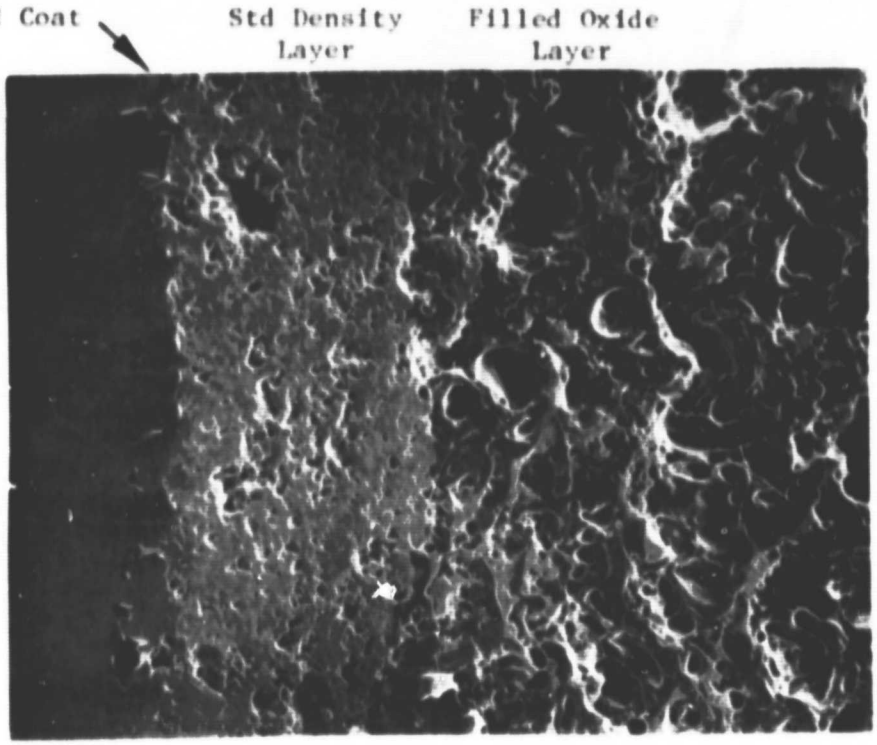

Magn: 100X

a) Porosity Characteristics

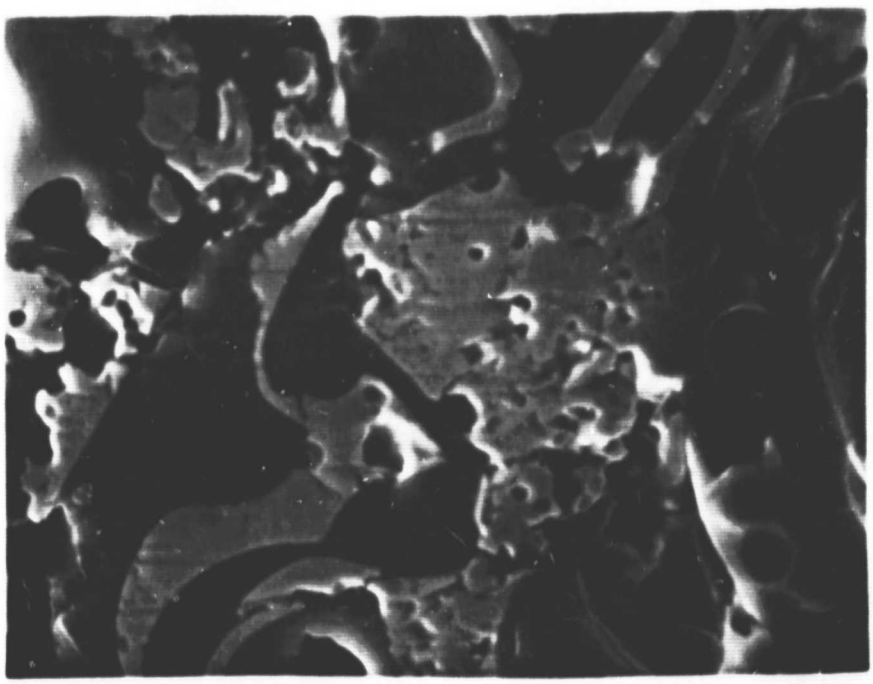

Magn: 1000X

b) Ceramic Particle Morphology (outer layer)

Figure 26 Porosity characteristics and ceramic particle morphology of coating II-F

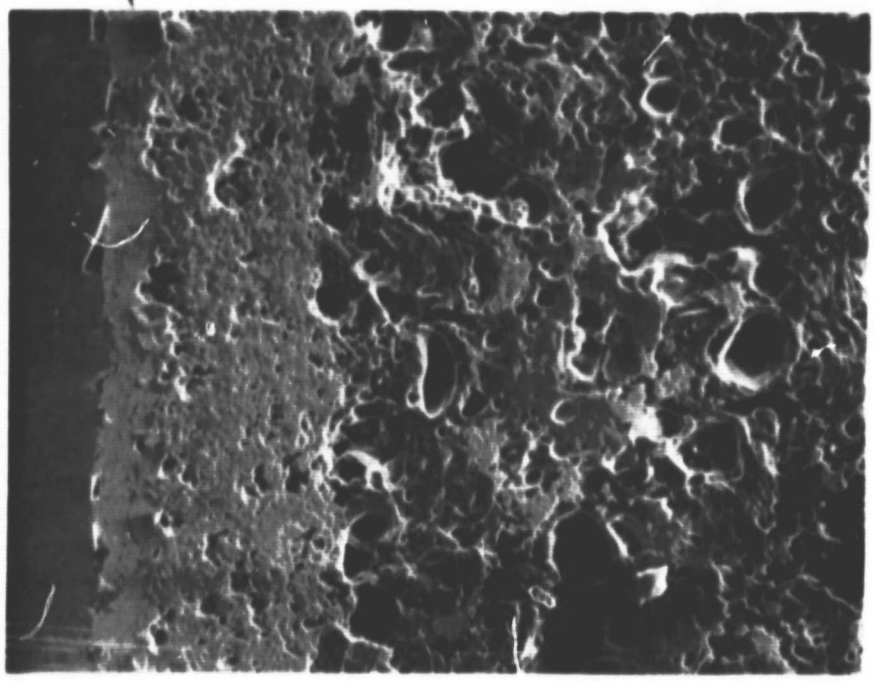

Magn: 100X

a) Porosity Characteristics

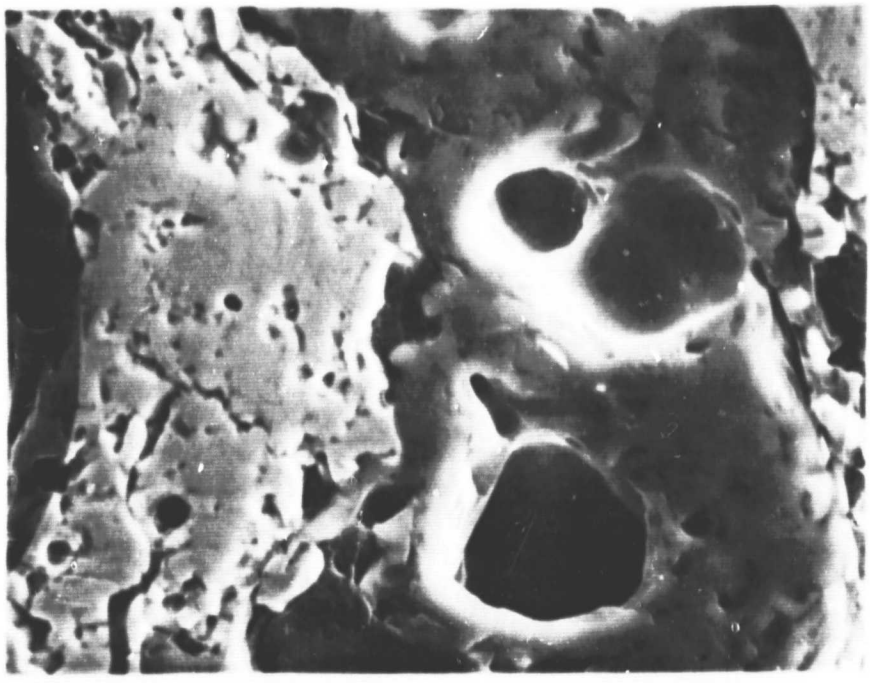

Magn: 1000X

b) Ceramic Particle Morphology (outer layer)

Figure 27 Porosity characteristics and ceramic particle morphology of coating system III-F

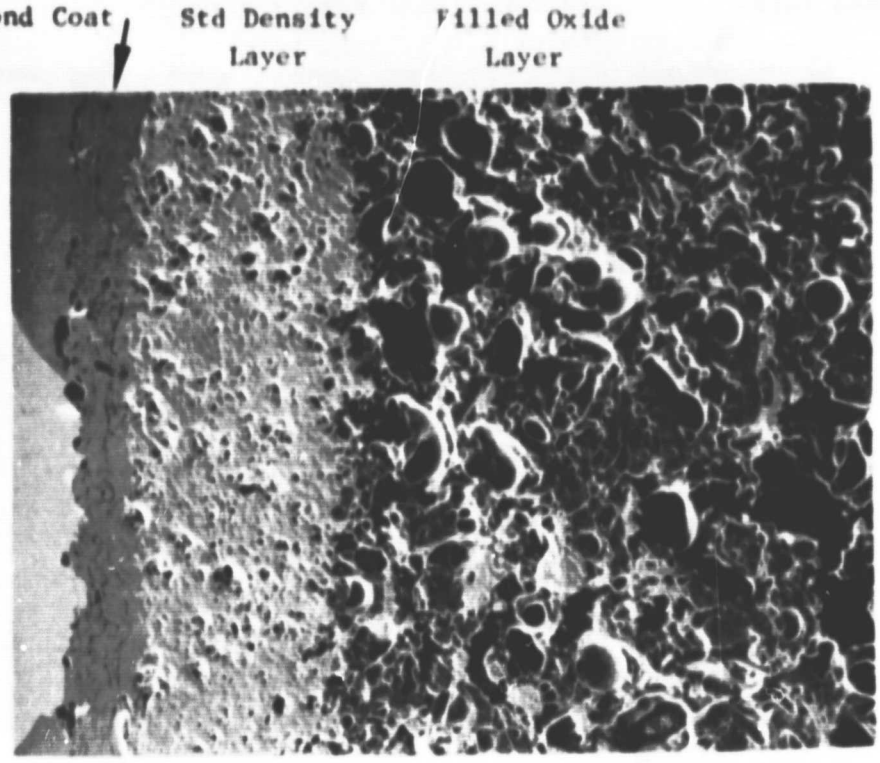

Magn: 100X

a) Porosity Characteristics

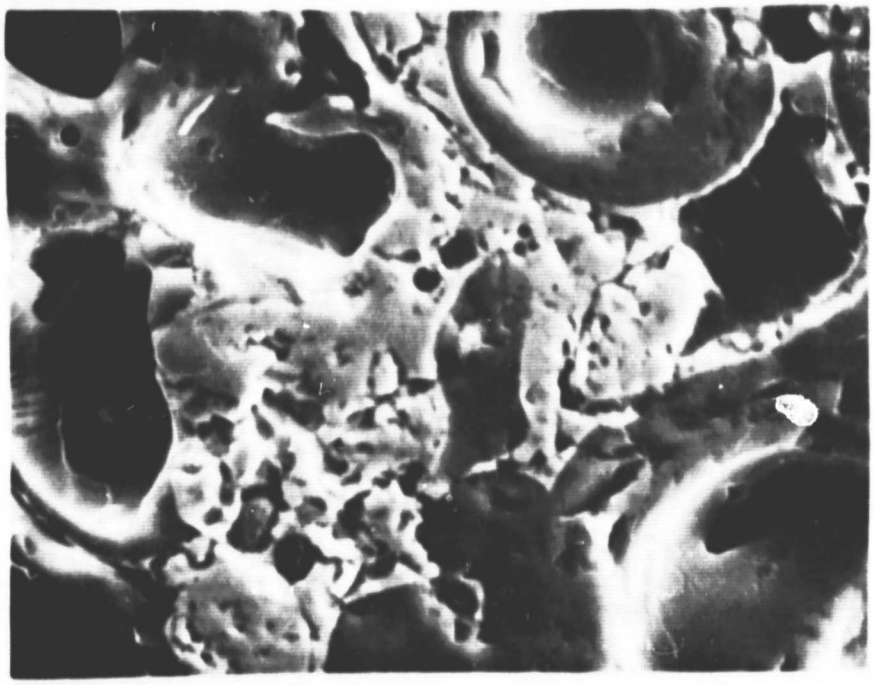

Magn: 1000X

b) Ceramic Particle Morphology (outer layer)

Figure 28 Porosity characteristics and ceramic particle morphology of coating IV-F

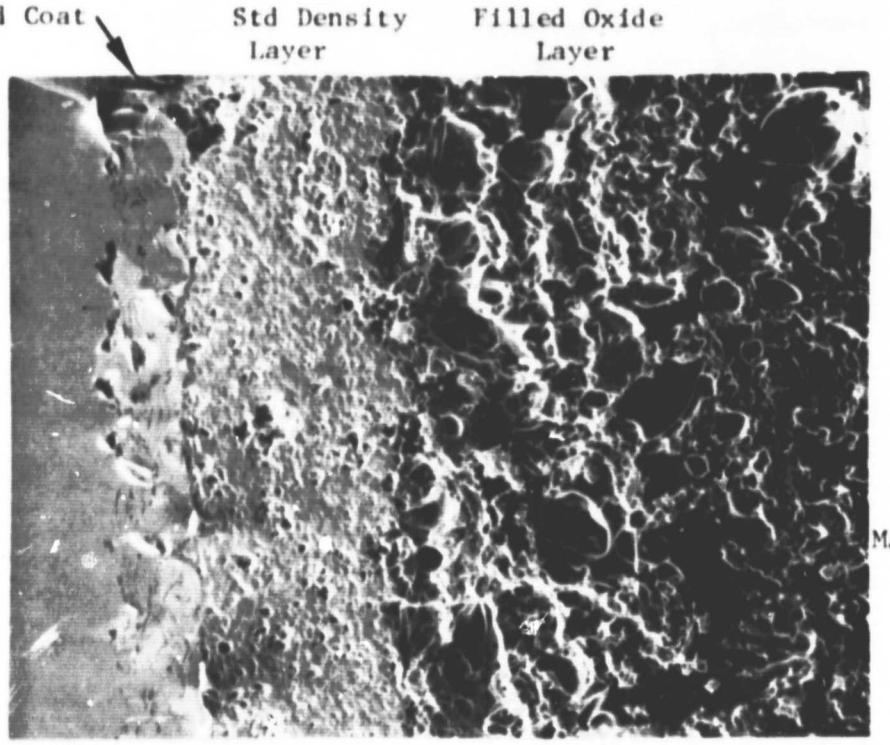

a) Porosity Characteristics

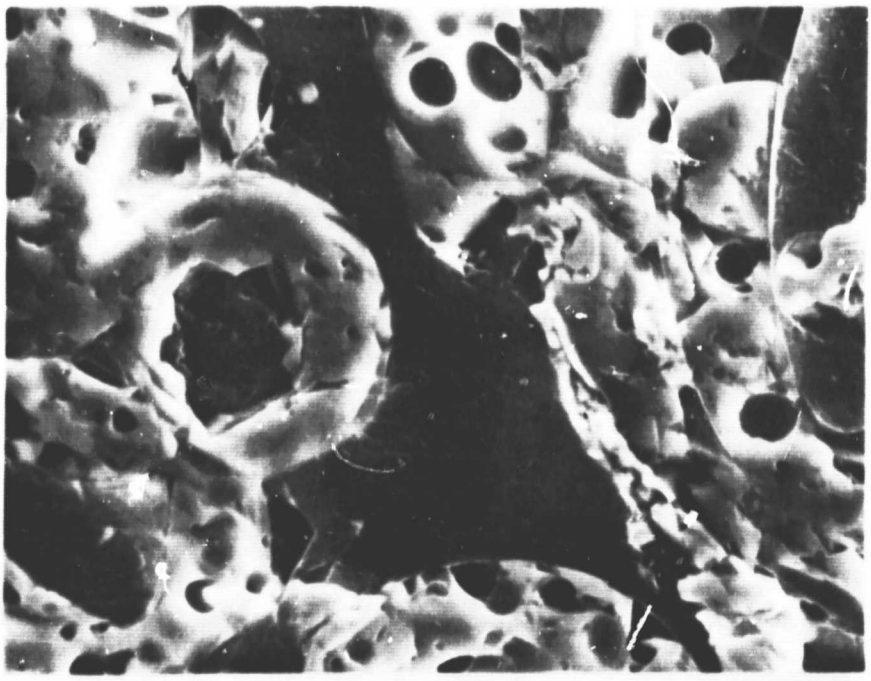

b) Ceramic Particle Morphology (outer layer)

Figure 29 Porosity characteristics and ceramic particle morphology of coating V-F

Magn: 100X

Figure 30 Particle shape of flame-stabilized YSZ plasma-spray grade powder Metco 202 NS

Table III

Composition and Parameter Variations Investigated for Flame-Stabilized YSZ Matrix

YSZ Matrix / Filler Volume Percent Ratio		100/0	80/20	60/40	50/50	40/60	20/80	18/82 (50/50 w/o)	0/100
System		I	J	K	L	M	N	O	P
Spray Parameter Combinations	I	SD 1 (32) PL 2	SD 1 PL 2	SD 1 PL 2	SD 1 PL 2	SD 1 PL 2	SD 1 PL 2		SD 1 PL 2
	II	SD 2 PL 1	SD 2 PL 1	SD 2 PL 1	SD 2 PL 1	SD 2 PL 1	SD 2 PL 1		SD 2 PL 1
	III	SD 1 (33) PL 1	SD 1 (36) PL 1	SD 1 (37) PL 1	SD 1 (38) PL 1	SD 1 (39) PL 1	SD 1 (40) (42) PL 1	SD 1 (43) PL 1	SD 1 (41) PL 1
YSZ Matrix: Metco 202NS	IV	SD 3 (34) PL 1	SD 3 PL 1	SD 3 PL 1	SD 3 PL 1	SD 3 PL 1	SD 3 PL 1		SD 3 PL 1
	V	SD 1 (35) PL 3	SD 1 PL 3	SD 1 PL 3	SD 1 PL 3	SD 1 PL 3	SD 1 PL 3		SD 1 PL 3

SPRAY DISTANCE:
SD 1 = 4.25 in.
SD 2 = 5.25 in.
SD 3 = 3.25 in.

(XX) Figure No. in Text

POWER LEVEL:
PL 1 = 550 amps
PL 2 = 650 amps
PL 3 = 450 amps

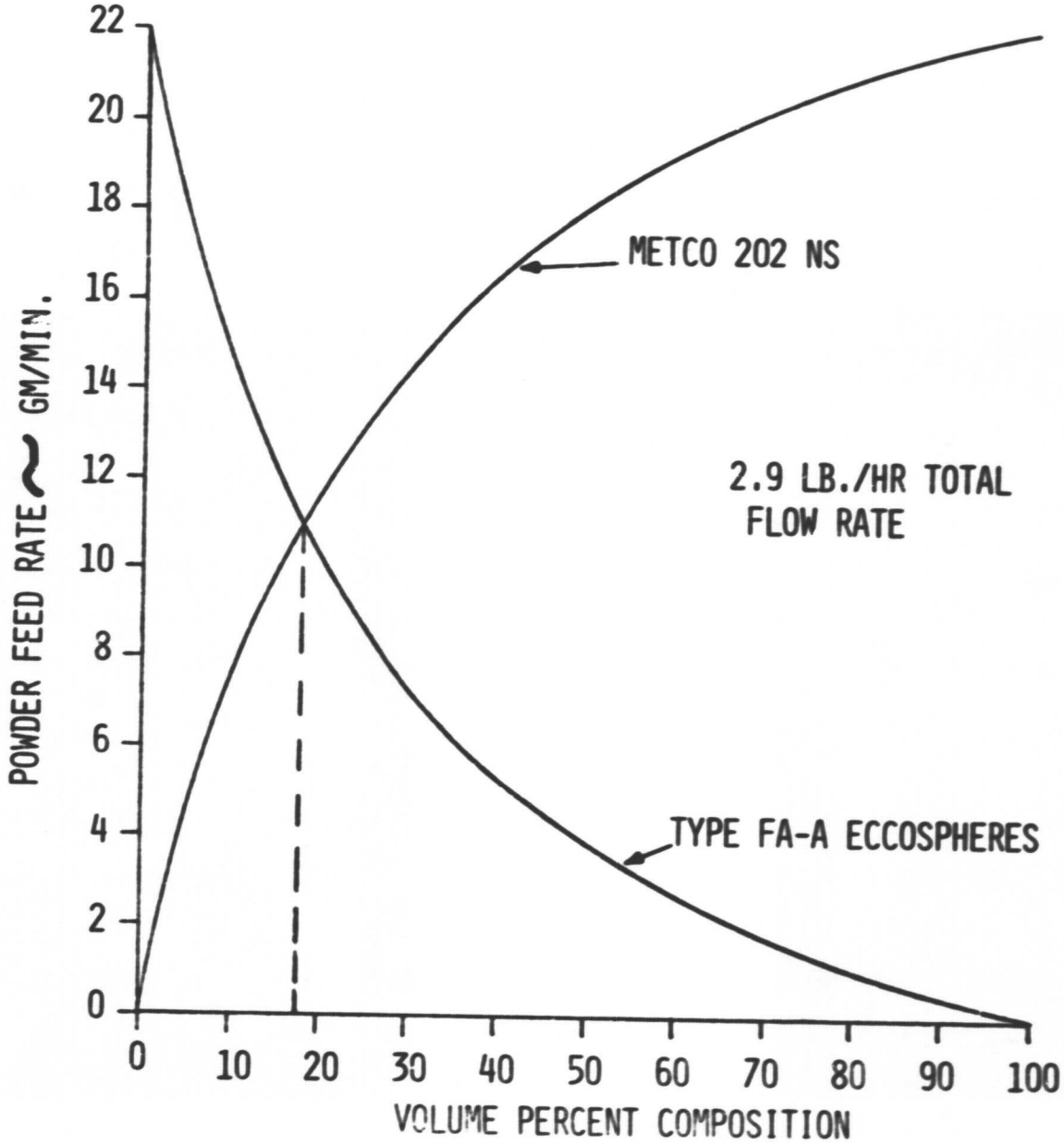

Figure 31 Effect of Volume percent composition on powder feed rate of Metco 202 NS/type FA-A eccosphere coating system

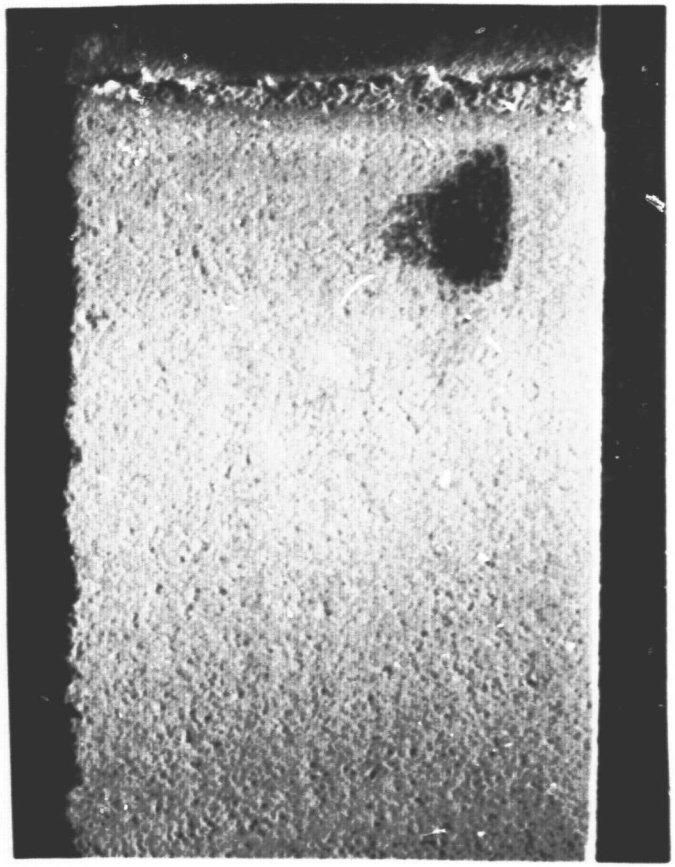

a. Abradability wear scar

(Rub direction ↓)

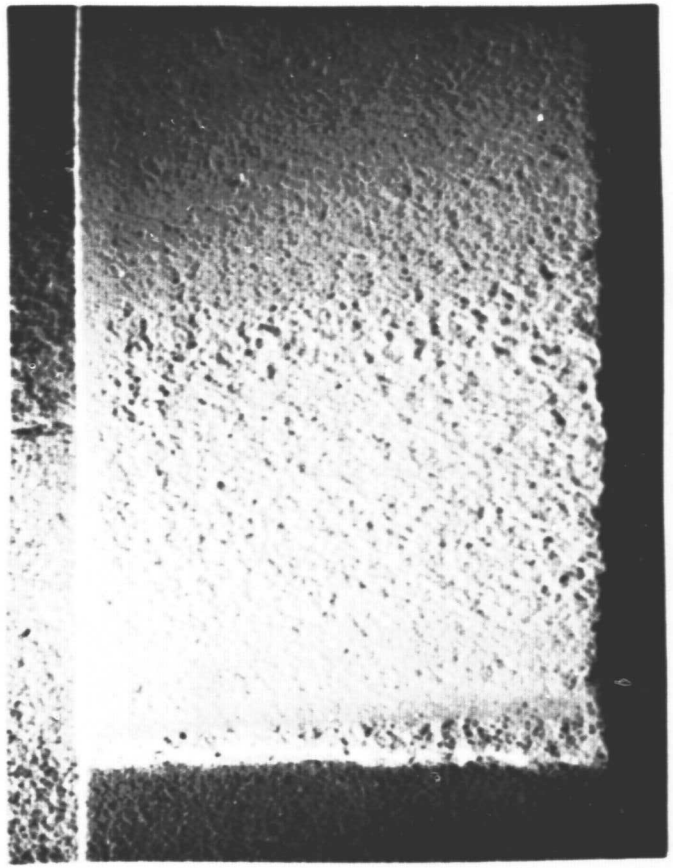

b. Erosion signature (30 min. exposure)

(Flow direction →)

Figure 32 Abradability and initial erosion results for System I-A (Table III) Magn: 3X

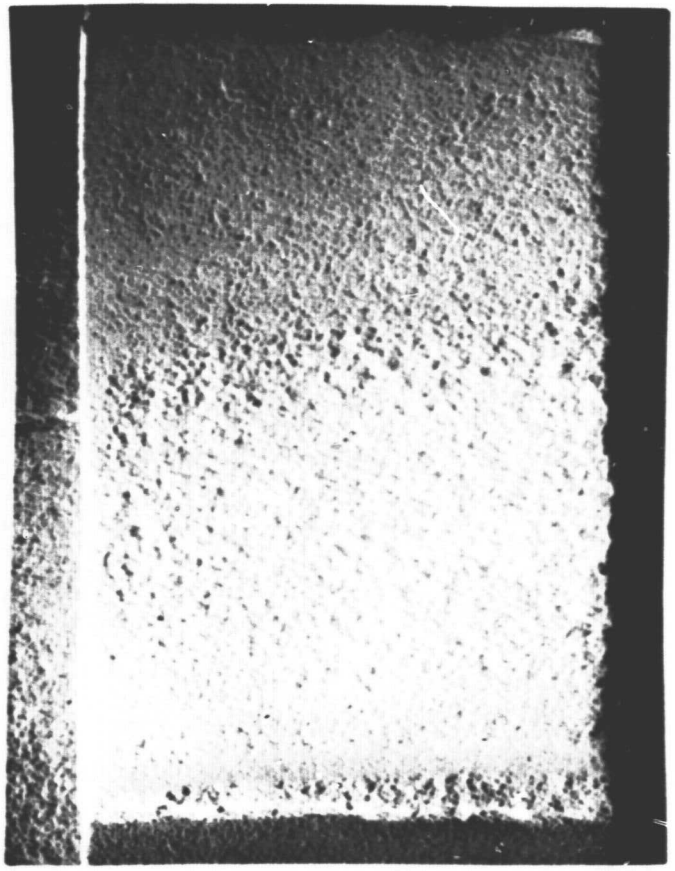

c. Erosion signature (60 min. exposure)

(Flow direction ➡)

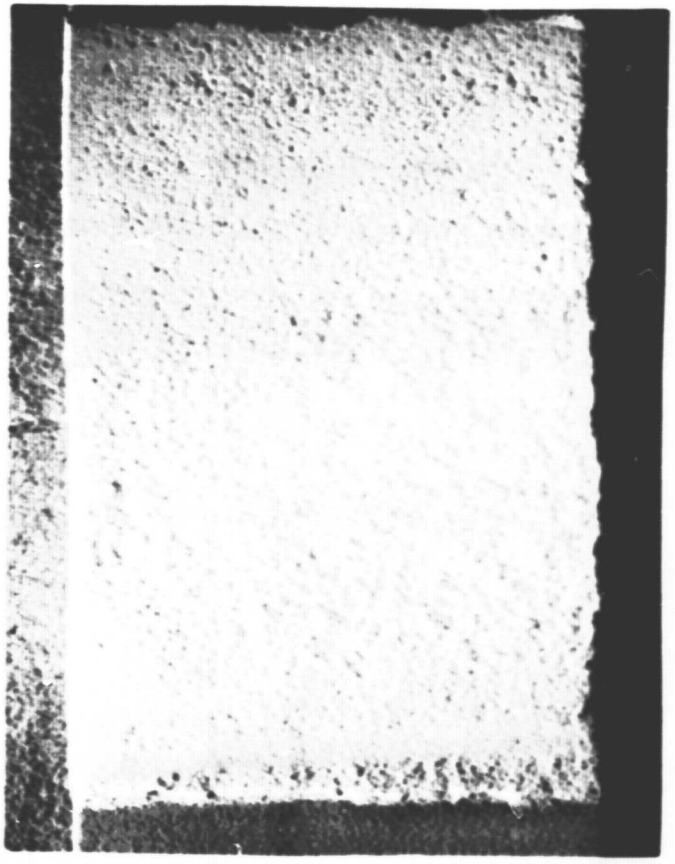

d. Erosion signature (120 min. exposure)

(Flow direction ➡)

Figure 32 Cont'd. Erosion results (continued) for System I-I

(Table III) Magn: 3X

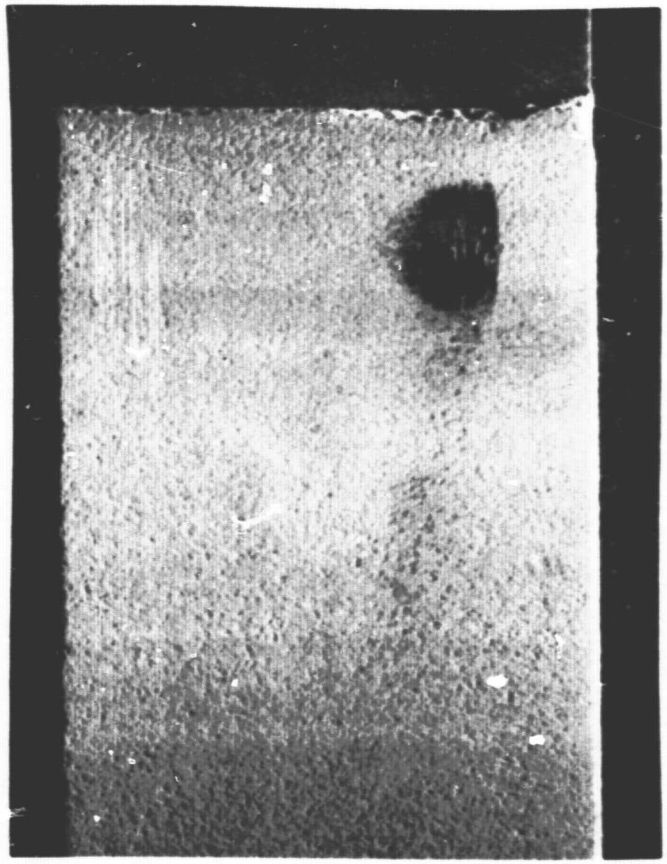

a. Abradability wear scar

(Rub direction ↓)

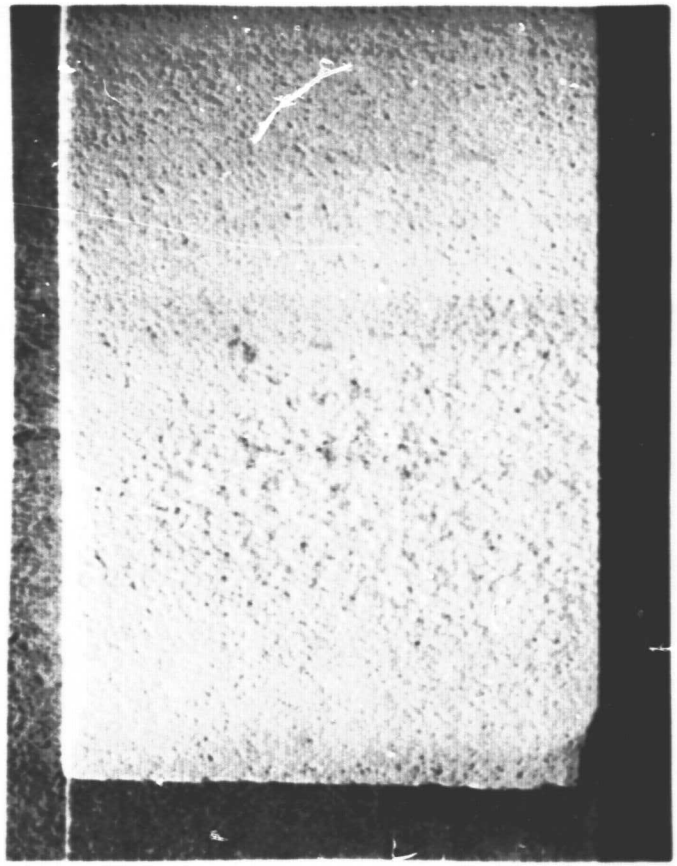

b. Erosion signature (30 min. exposure)

(Flow direction →)

Figure 33 Abradability and initial erosion results for System III-I (Table III) Magn: 3X

c. Erosion signature (60 min. exposure)

(Flow direction ➡)

d. Erosion signature (120 min. exposure)

(Flow direction ➡)

Figure 33 Cont'd. Erosion results (continued) for System III-I
(Table III) Magn: 3X

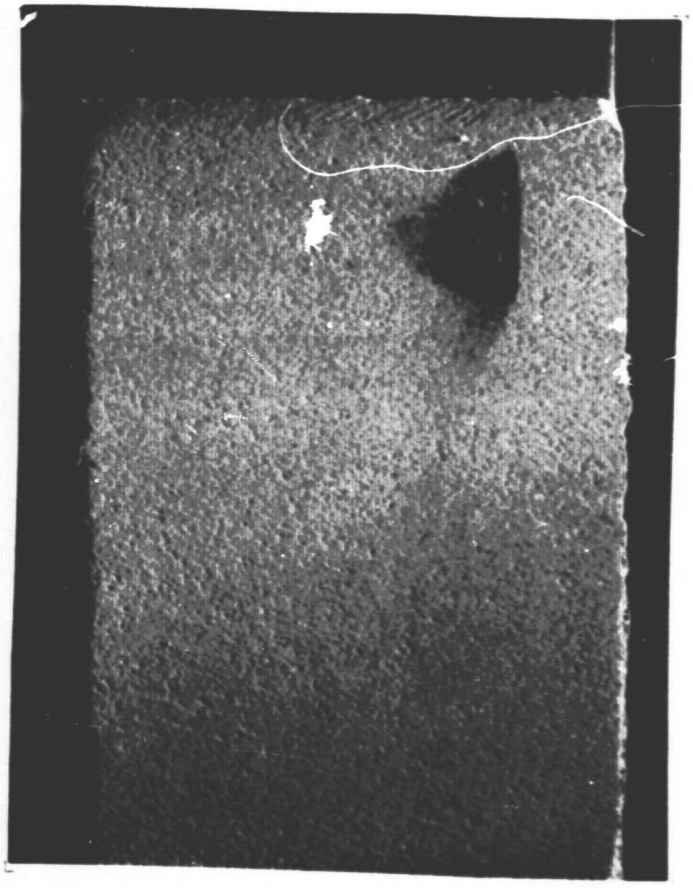

a. Abradability wear scar

(Rub direction ⬇)

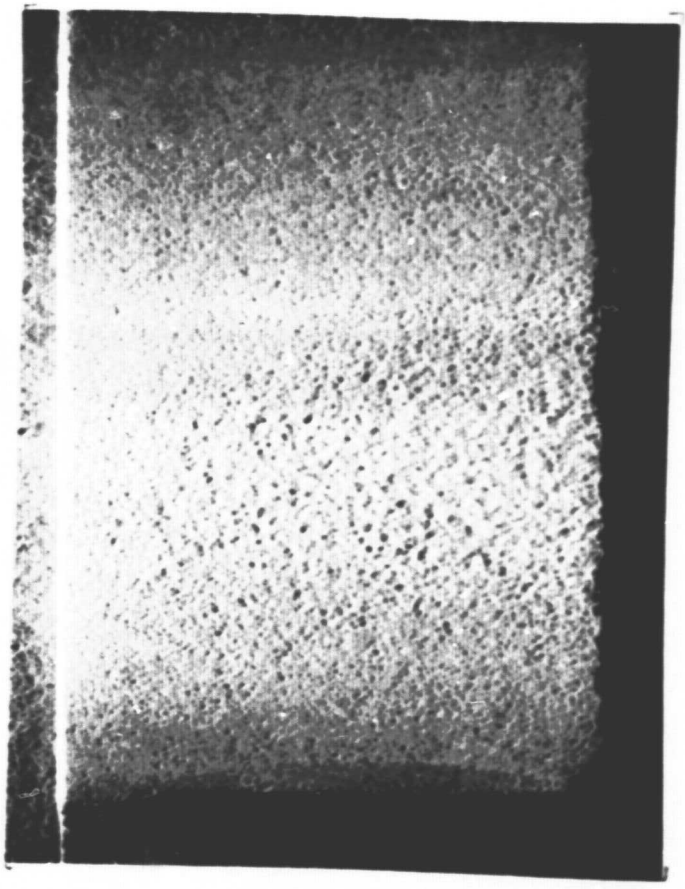

b. Erosion signature (30 min. exposure)

(Flow direction ➡)

Figure 34 Abradability and initial erosion results for System IV-I
(Table III) Magn: 3X

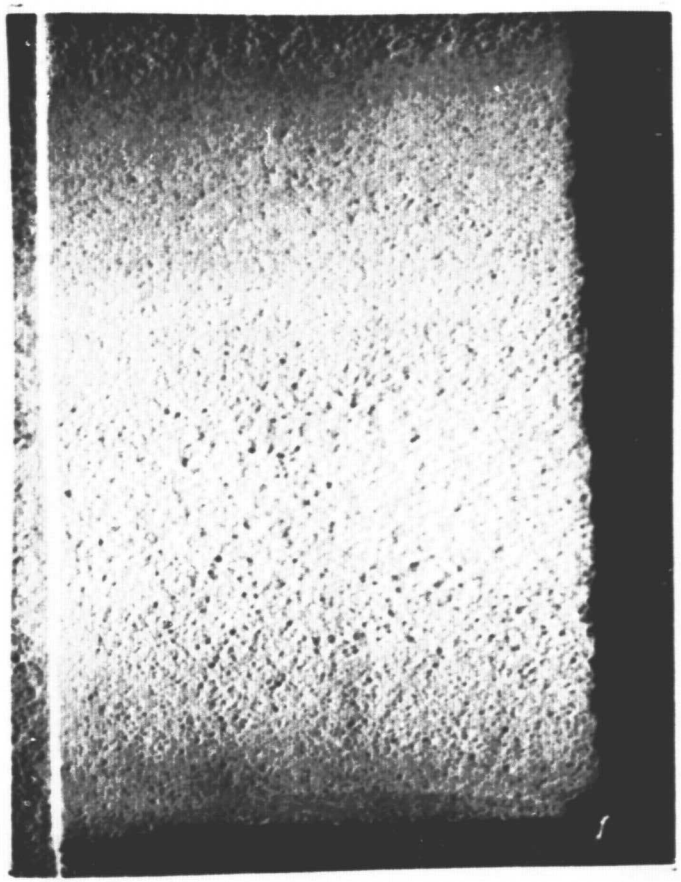

c. Erosion signature (60 min. exposure)

(Flow direction ➡)

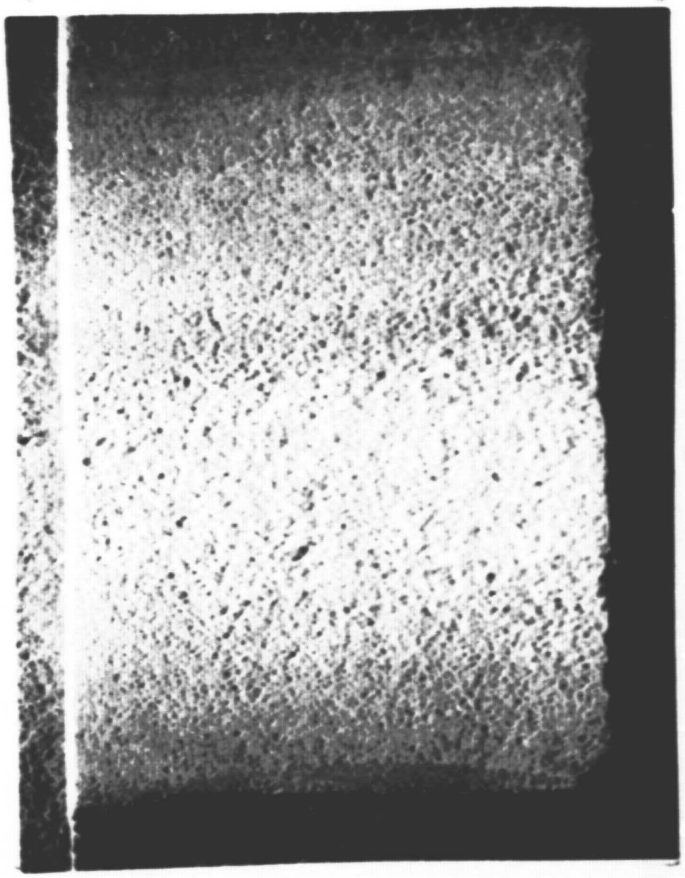

d. Erosion signature (120 min. exposure)

(Flow direction ➡)

Figure 34 Cont'd. Erosion results (continued) for System IV-I

(Table III) Magn: 3X

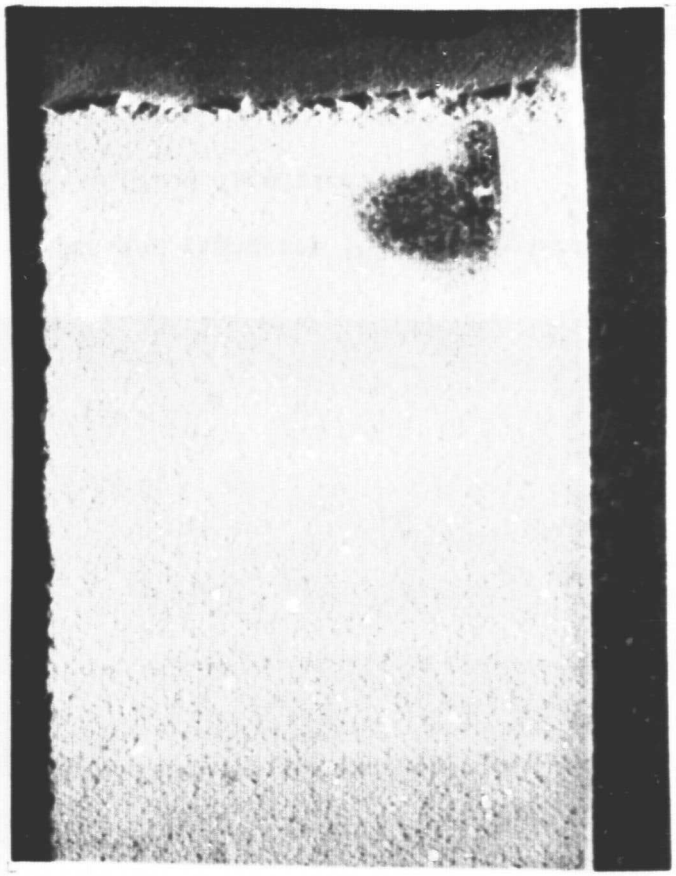

a. Abradability wear scar

(Rub direction ↓)

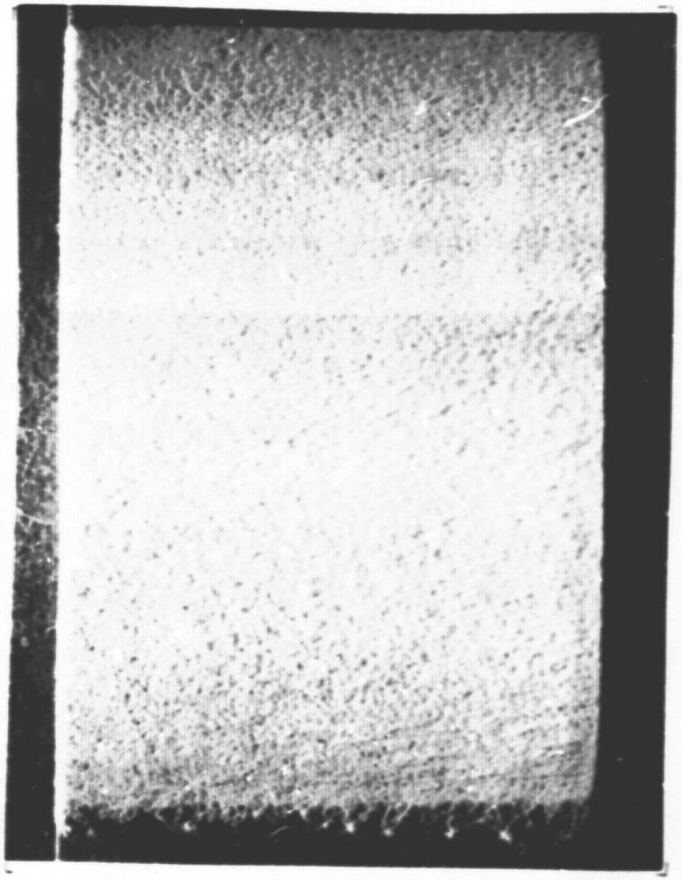

b. Erosion signature (30 min. exposure)

(Flow direction →)

Figure 35 Abradability and initial erosion results for System V-I (Table III) Magn: 3X

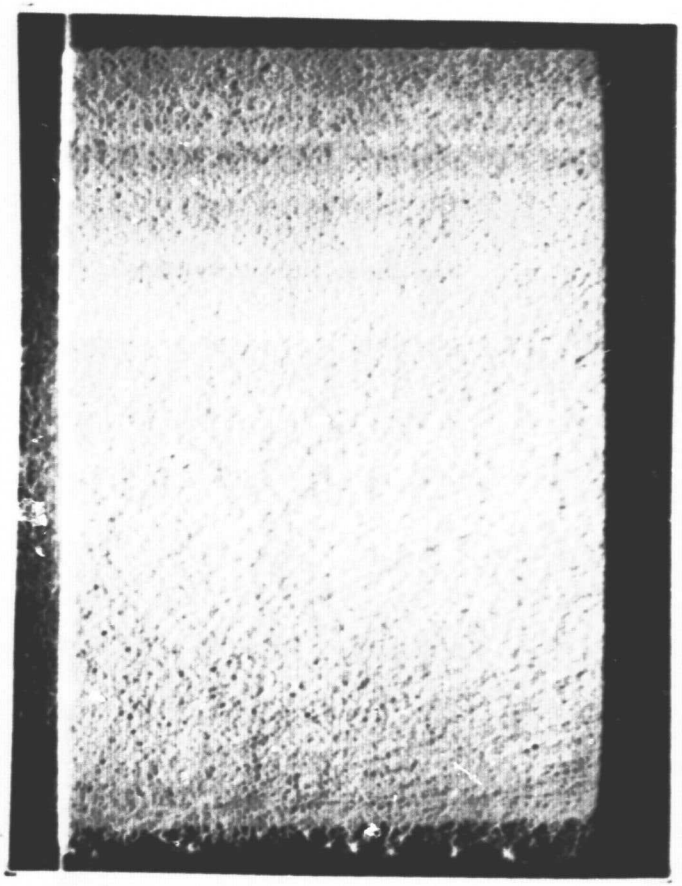

c. Erosion signature (60 min. exposure)

(Flow direction ➡)

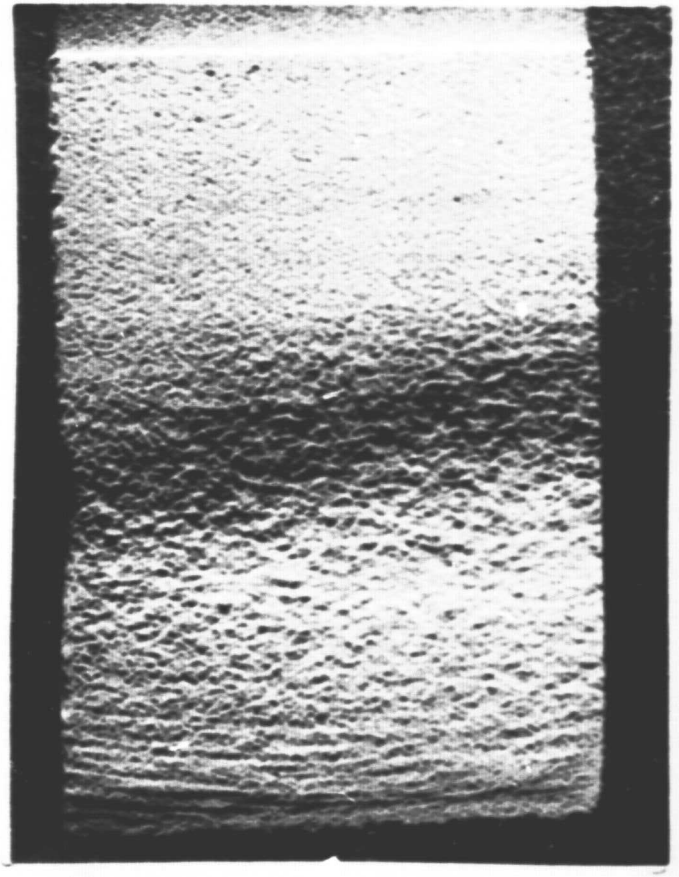

d. Erosion signature (120 min. exposure)

(Flow direction ➡)

Figure 35 Cont'd. Erosion results (continued) for System V-I

(Table III) Magn: 3X

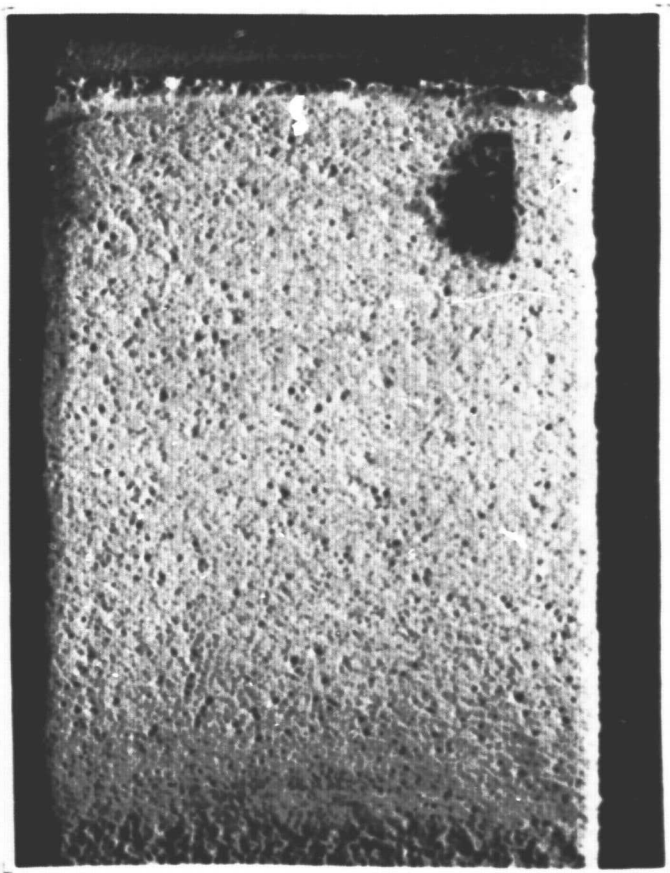

a. Abradability wear scar

(Rub direction ↓)

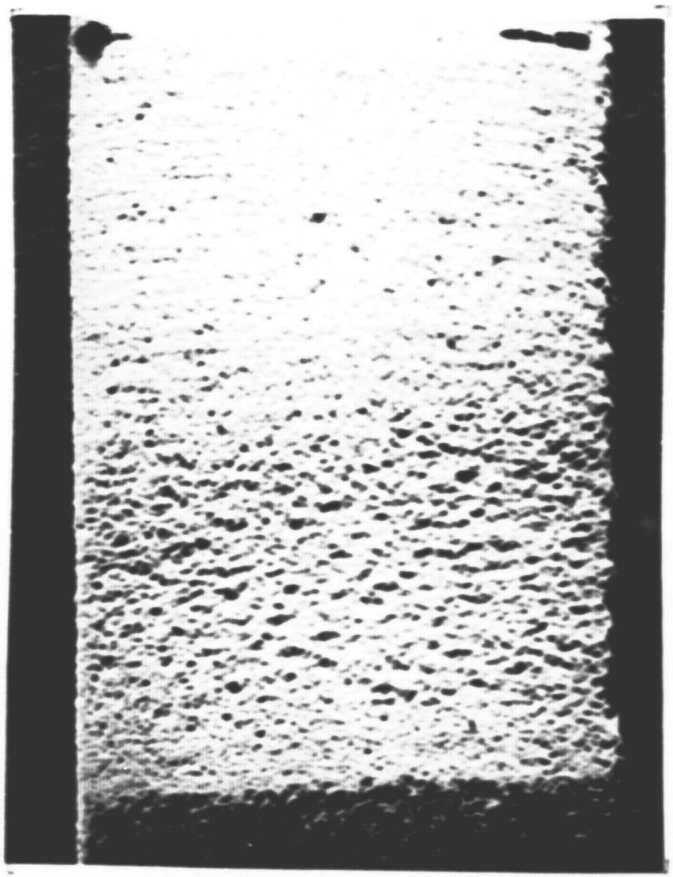

b. Erosion signature (30 min. exposure)

(Flow direction →)

Figure 36 Abradability and initial erosion results for System III-J (Table III) Magn: 3X

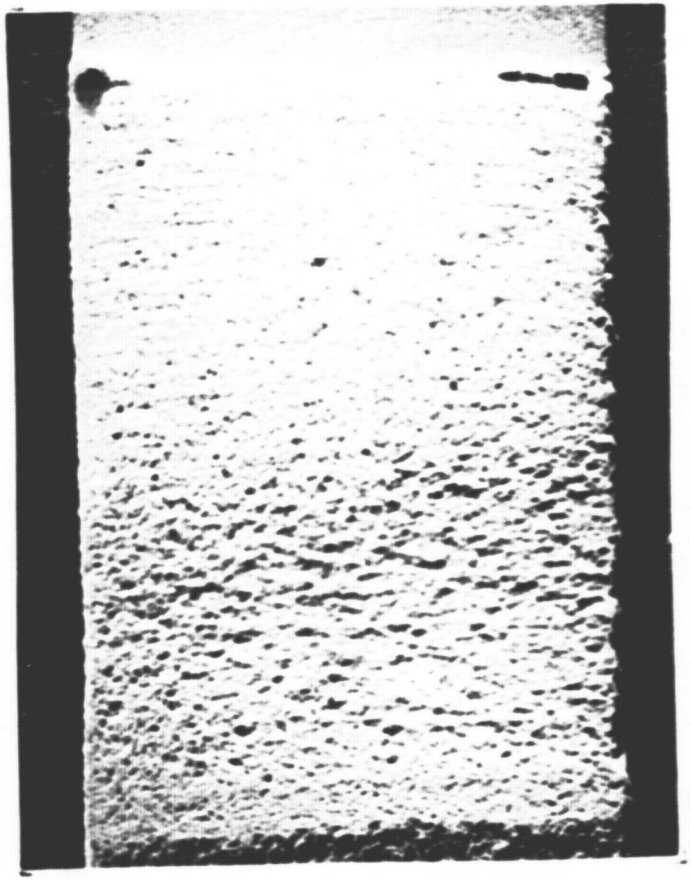

c. Erosion signature (60 min. exposure)

(Flow direction ➡)

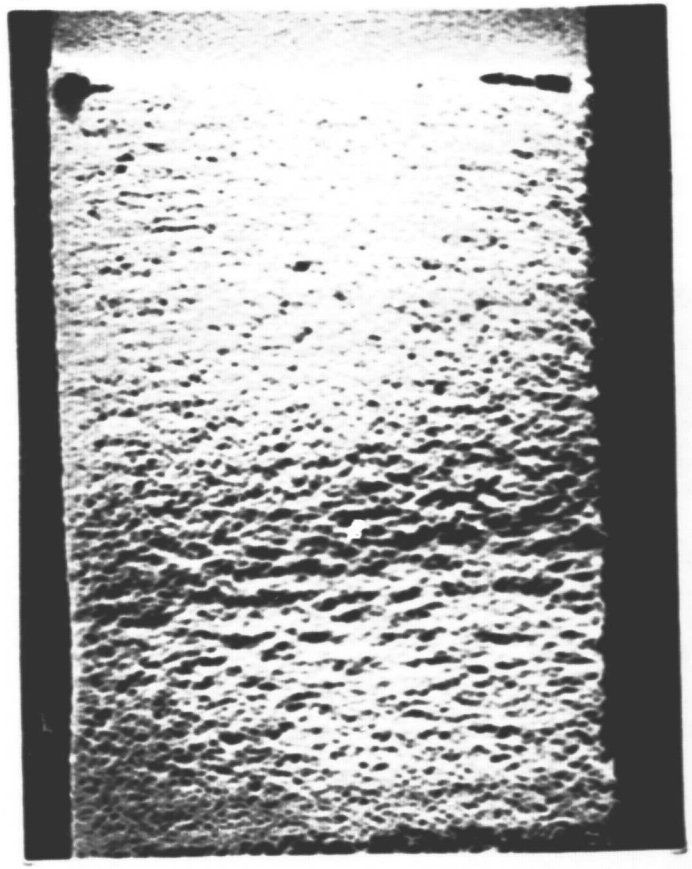

d. Erosion signature (120 min. exposure)

(Flow direction ➡)

Figure 36 Cont'd. Erosion results (continued) for System III-J

(Table III) Magn: 3X

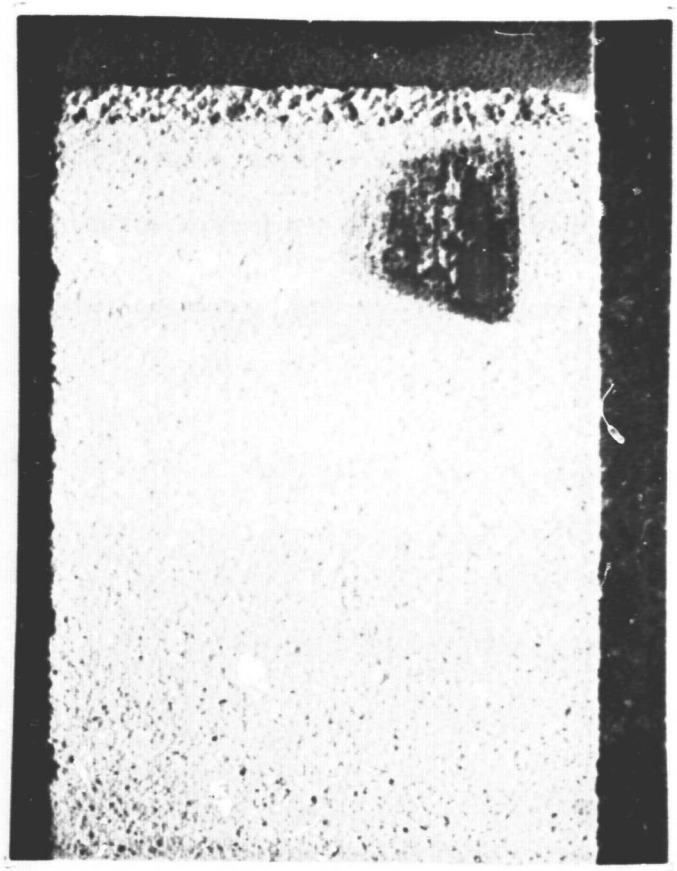

a. Abradability wear scar

(Rub direction ↓)

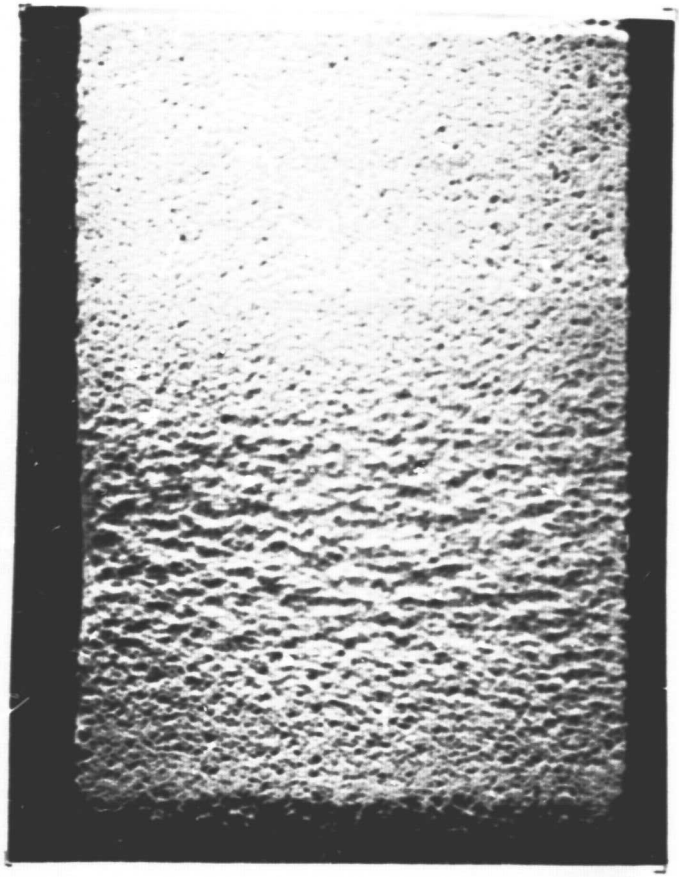

b. Erosion signature (30 min. exposure)

(Flow direction →)

Figure 37 Abradability and initial erosion results for System III-K (Table III) Magn: 3X

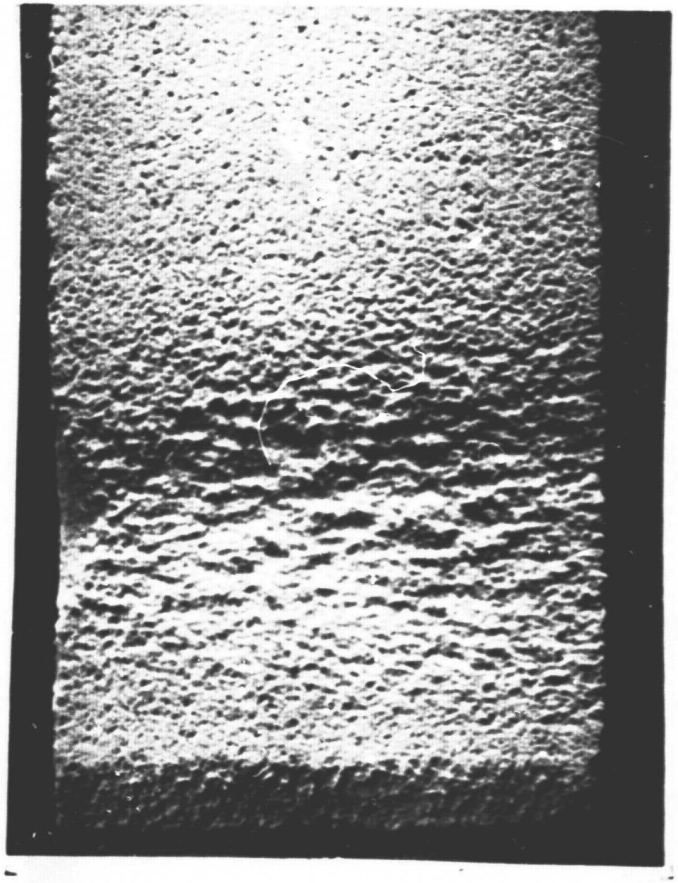

c. Erosion signature (60 min. exposure)

(Flow direction ➡)

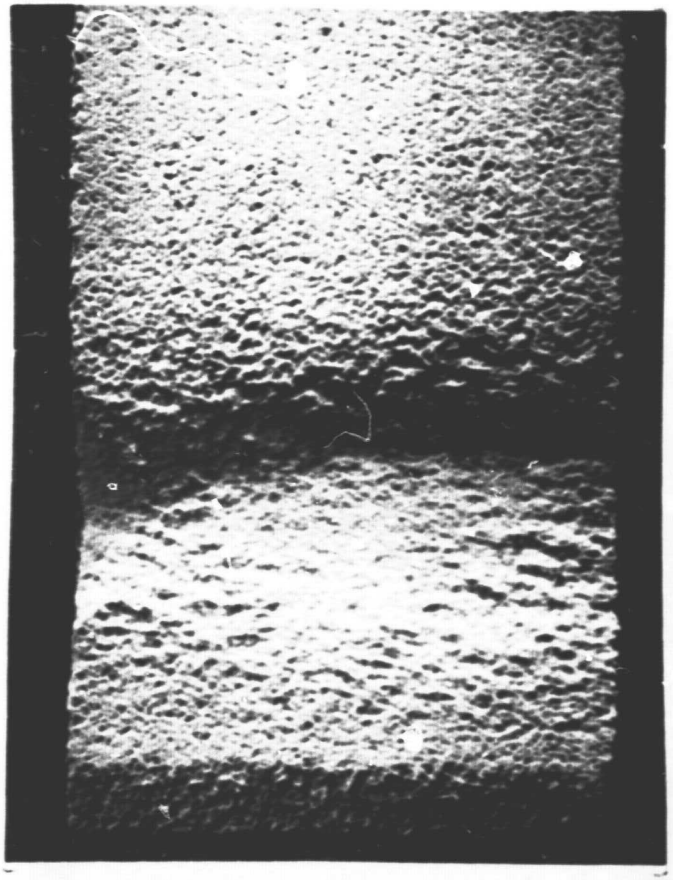

d. Erosion signature (120 min. exposure)

(Flow direction ➡)

Figure 37 Cont'd. Erosion results (continued) for System III-K

(Table III) Magn: 3X

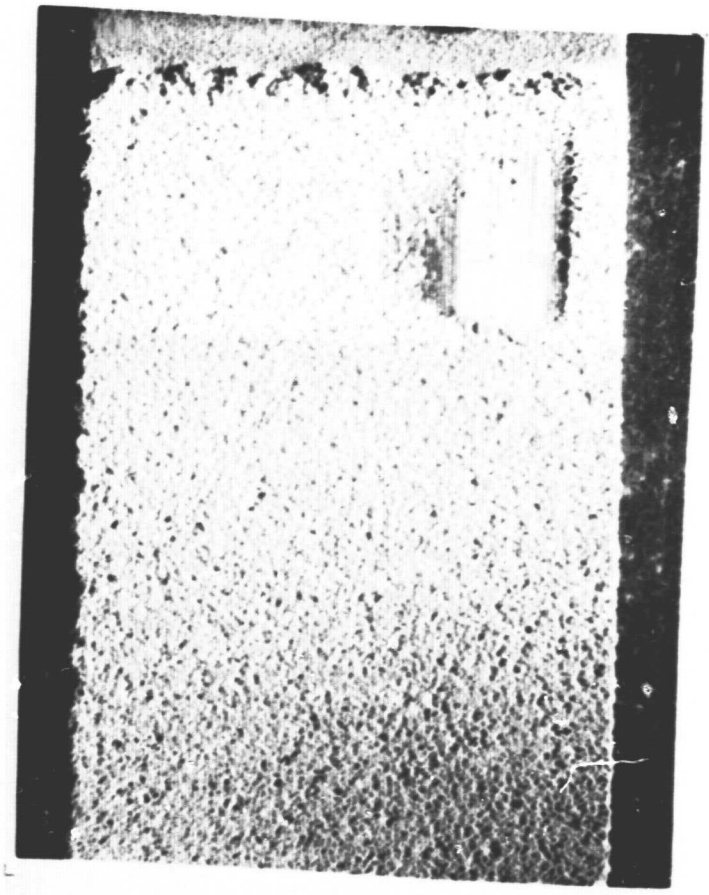

a. Abradability wear scar

(Rub direction ↓)

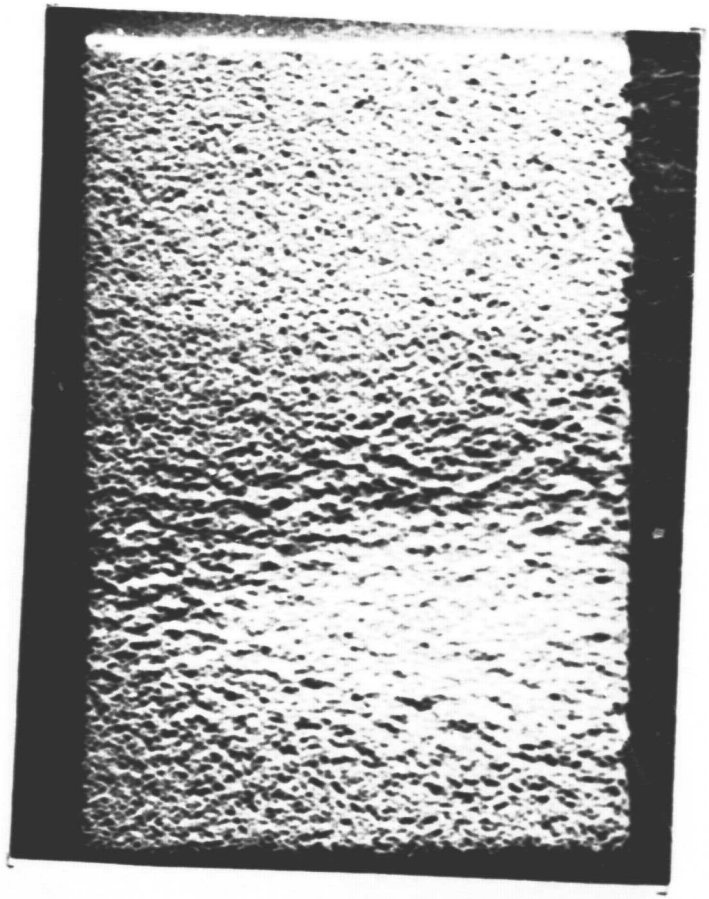

b. Erosion signature (30 min. exposure)

(Flow direction →)

Figure 38 Abradability and initial erosion results for System III-L (Table III) Magn: 3X

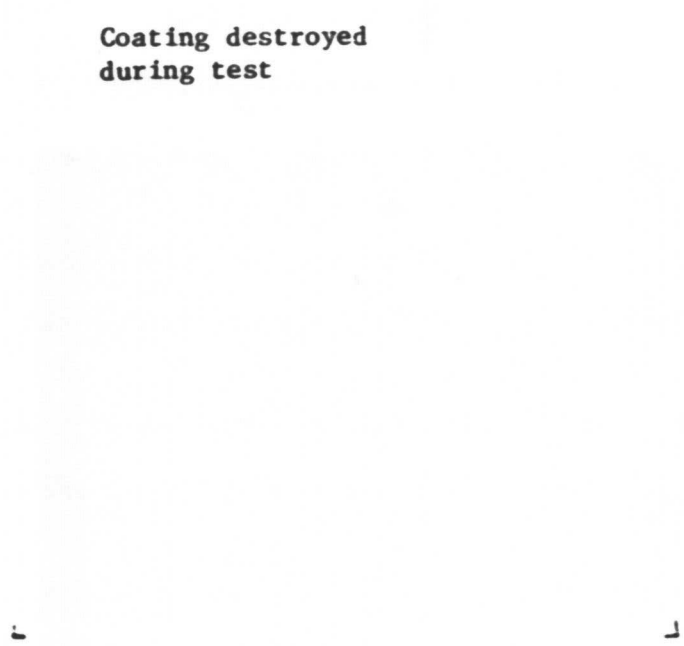

c. Erosion signature (60 min. exposure)

(Flow direction ➡)

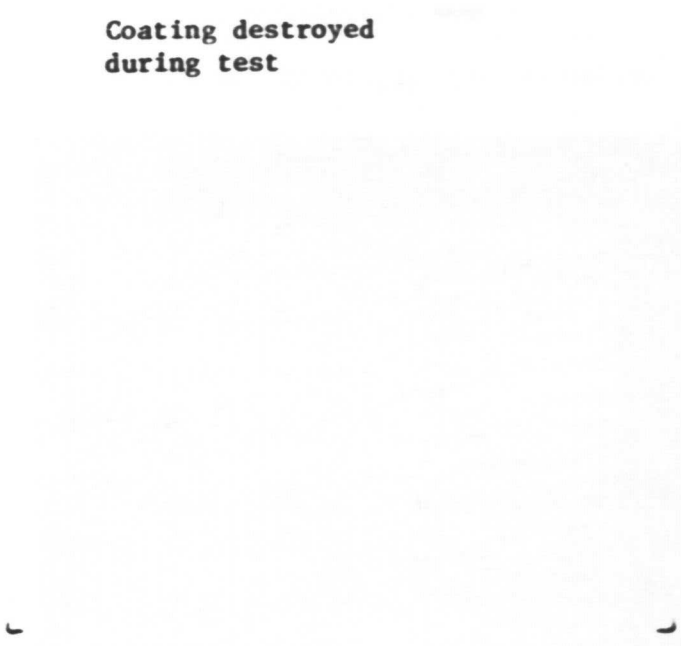

d. Erosion signature (120 min. exposure)

(Flow direction ➡)

Figure 38 Cont'd. Erosion results (continued) for System III-L
(Table III) Magn: 3X

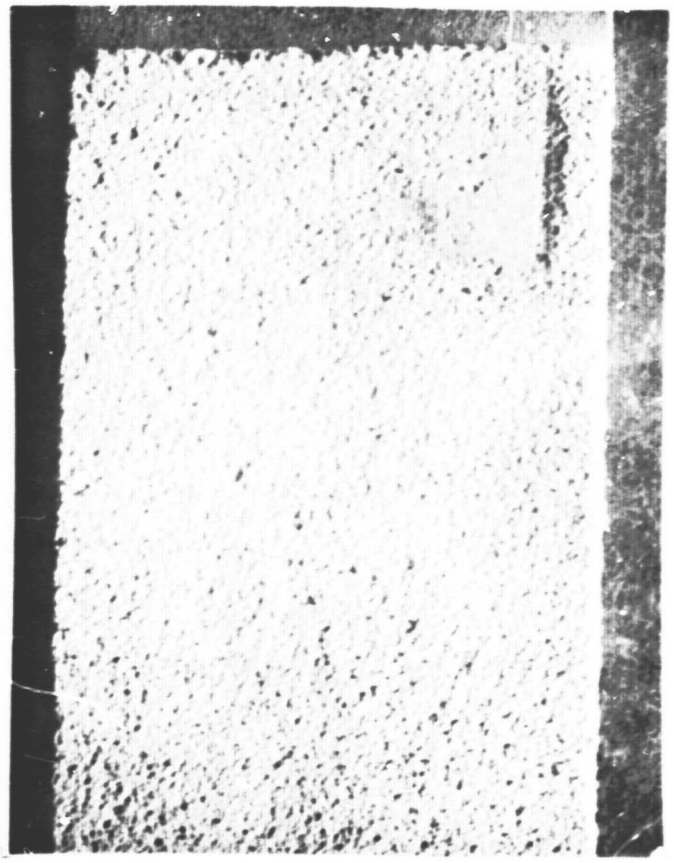

a. Abradability wear scar

(Rub direction ↓)

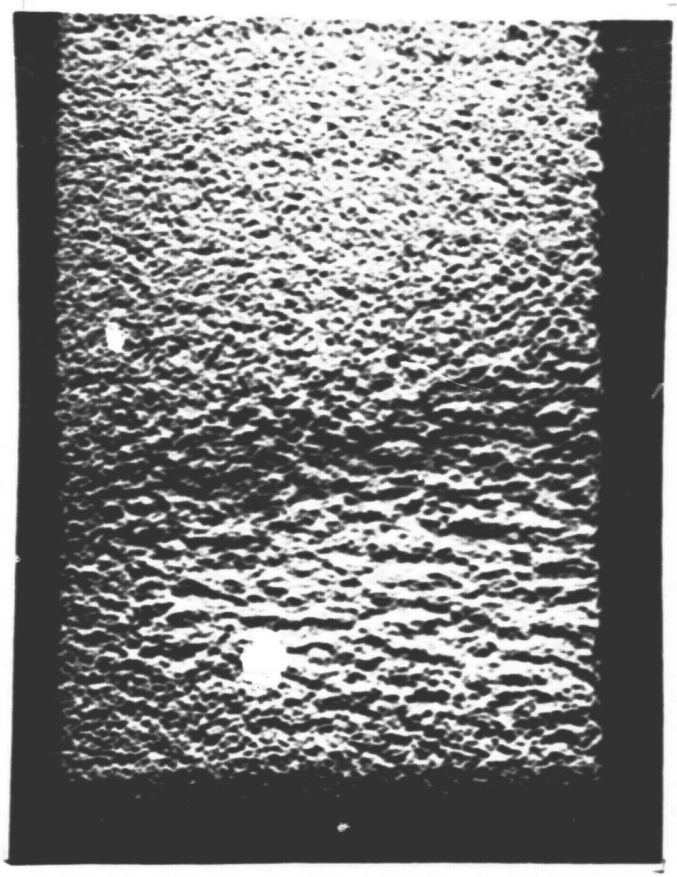

b. Erosion signature (30 min. exposure)

(Flow direction →)

Figure 39 Abradability and initial erosion results for System III-M (Table III) Magn: 3X

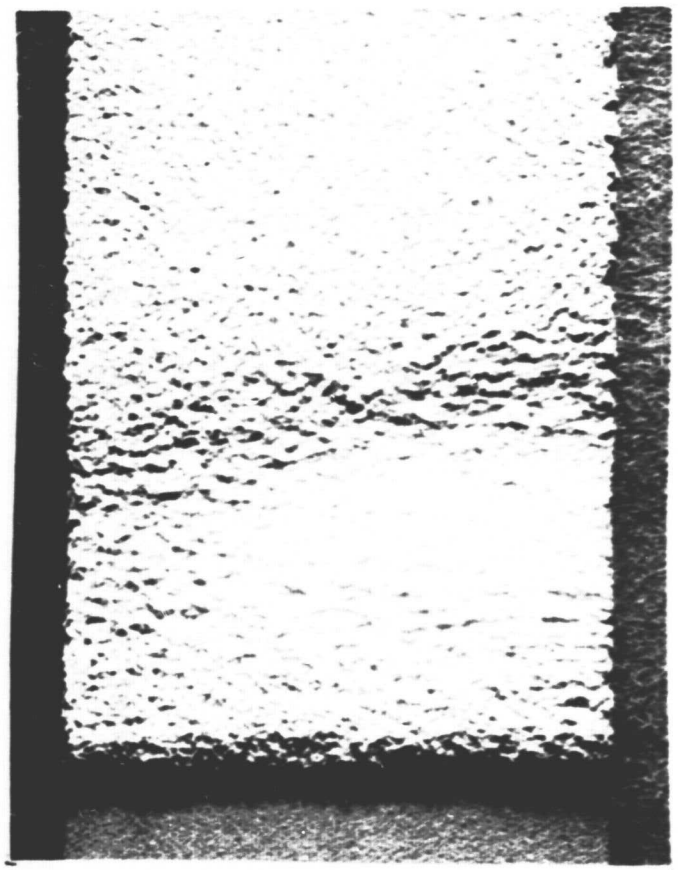

c. Erosion signature (60 min. exposure)

(Flow direction ➡)

Coating destroyed
during test

d. Erosion signature (120 min. exposure)

(Flow direction ➡)

Figure 39 Cont'd. Erosion results (continued) for System III-M
(Table III) Magn: 3X

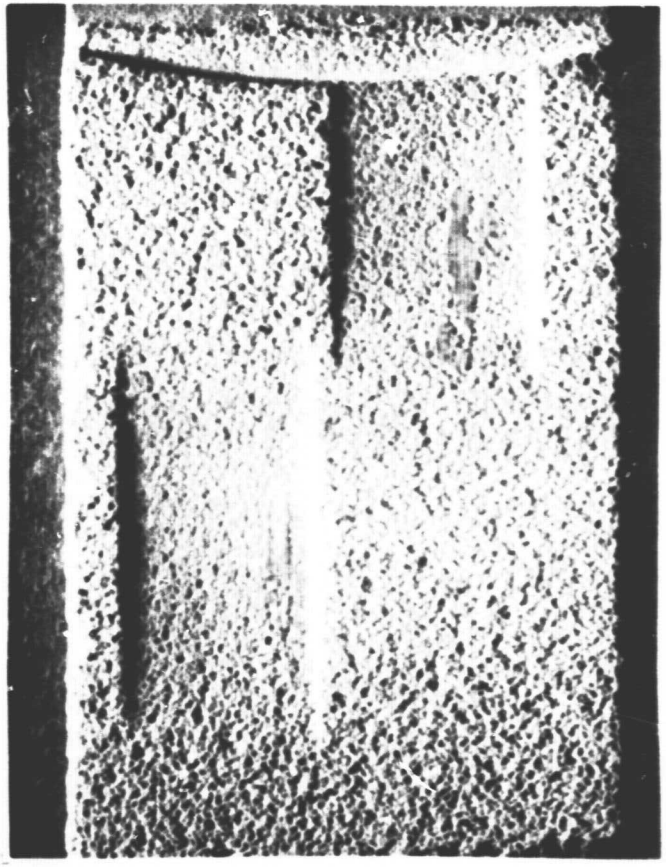

a. Abradability wear scar

(Rub direction ↓)

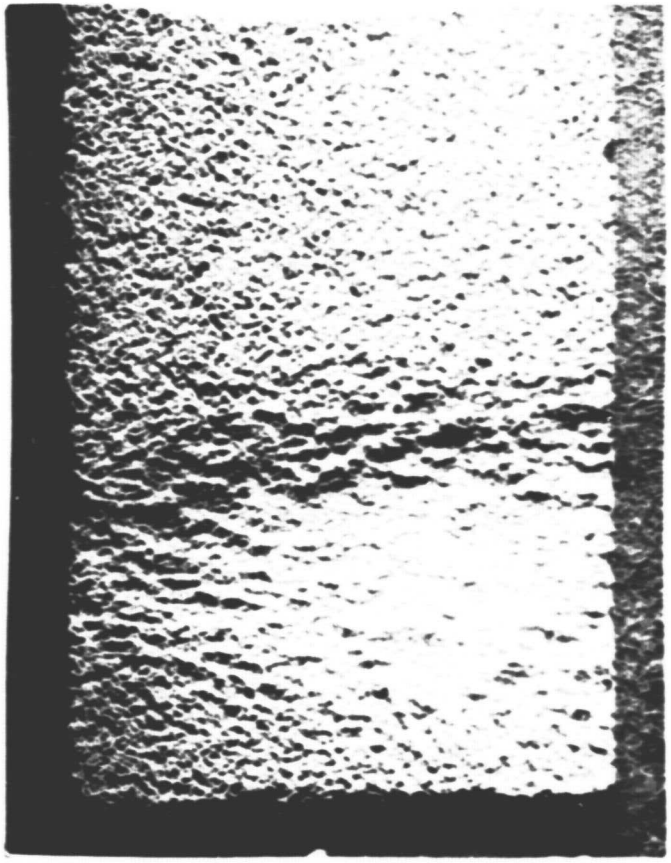

b. Erosion signature (30 min. exposure)

(Flow direction →)

Figure 40 Abradability and initial erosion results for System III-N (Table III) Magn: 3X

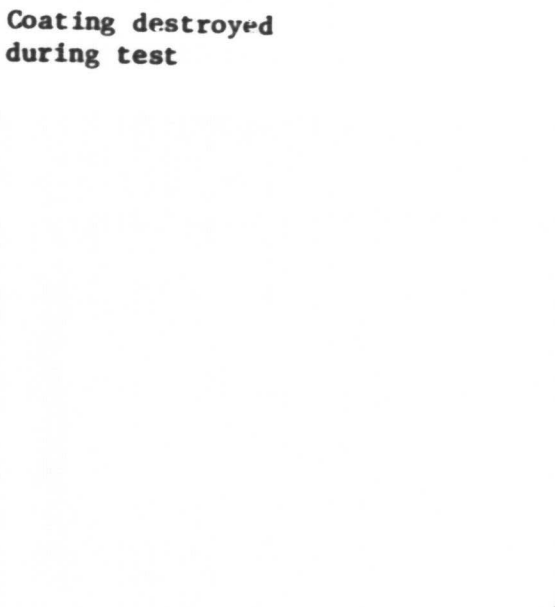

c. Erosion signature (60 min. exposure)

(Flow direction ➡)

d. Erosion signature (120 min. exposure)

(Flow direction ➡)

Figure 40 Cont'd. Erosion results (continued) for System III-N
(Table III) Magn: 3X

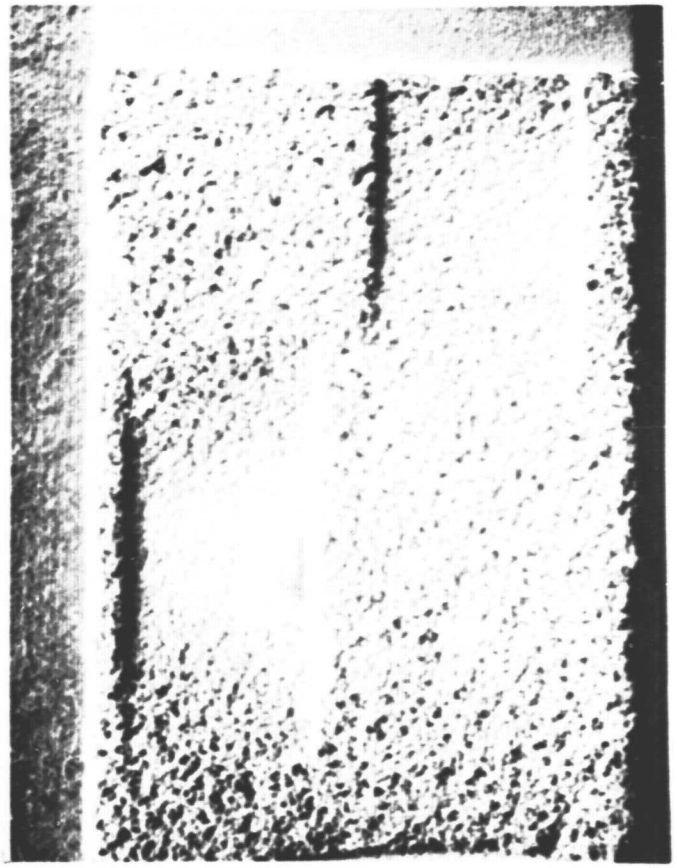

a. Abradability wear scar

(Rub direction ↓)

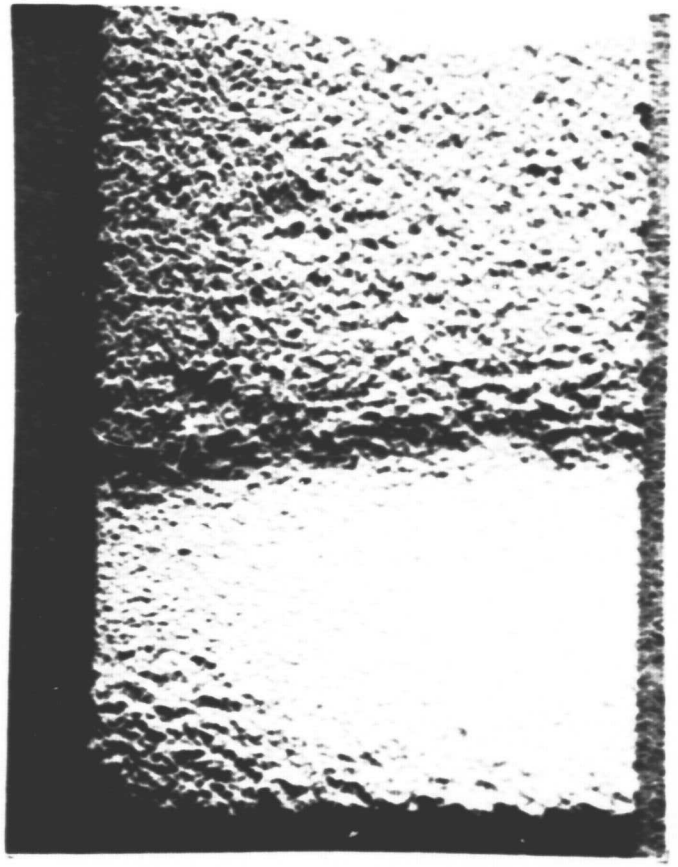

b. Erosion signature (30 min. exposure)

(Flow direction →)

Figure 41 Abradability and initial erosion results for System III-P (Table III) Magn: 3X

Coating destroyed
during test

Coating destroyed
during test

c. Erosion signature (60 min. exposure)

(Flow direction ➡)

d. Erosion signature (120 min. exposure)

(Flow direction ➡)

Figure 41 Cont'd. Erosion results (continued) for System III-P
(Table III) Magn: 3X

Because only the 20/80 and 18/82 ratio systems, prepared by using the mid range parameters (SD 1, PL 1), indicated a reasonable balance between abradability and erosion resistance, high speed rig testing was restricted to these systems. Results of the abradability tests, showing the rub wear scar and blade tip condition for the 20 v/o matrix/80 v/o filler system (System III-N) are presented in Figure 42.

Results obtained for the system comprised of 18 v/o matrix/82 v/o filler (System III-O) are shown in Figure 43 where the rub wear scar and erosion signature following 30 minutes exposure are presented.

Hardness as measured on the R15Y scale as a function of composition was shown previously in Figure 23 for various spray distances and Figure 24 for various power levels.

Photomicrographs of the microstructures corresponding to the spray distance and power level variations of the 80 v/o filler/20 v/o matrix composition are shown in Figures 44-48 inclusive. Both 100X and 1000X magnifications are presented for each of the microstructures.

Permeability

Gas flow permeability for each coating configuration in both the pre-stabilized and flame-stabilized matrix systems was measured using the procedure previously described. Static supply pressures up to 344.5 KPag (50 psig) were applied with zero leakage noted. These results are compared with the results obtained for conventional abradable materials in Figure 49.

The YSZ matrix systems exhibited nearly zero leakage compared to most of the conventional abradable materials. Many of the conventional materials rely on high levels of open porosity to provide abradability, accounting for their high permeability.

a Blade Track Wear Scar

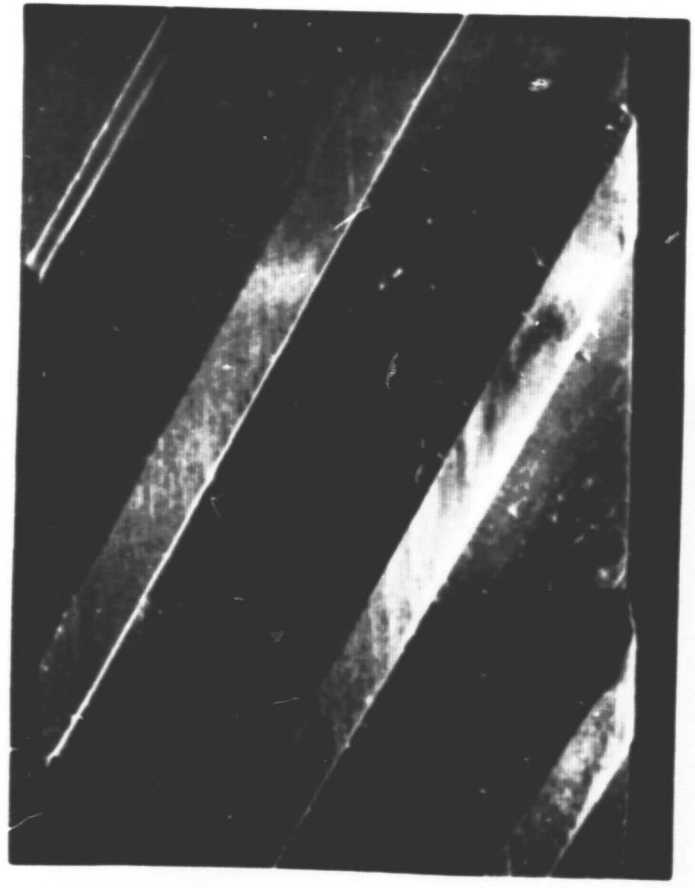

b Blade Tip Condition

Incursion Rate	.0025 cm/sec (.001 in/sec)
Blade Tip Speed	229 m/sec (750 ft/sec)
Depth of Rub	.018 cm (.007 in)

Figure 42 Slow Incursion rate high speed abradability test results for system III N

Magn: 5X

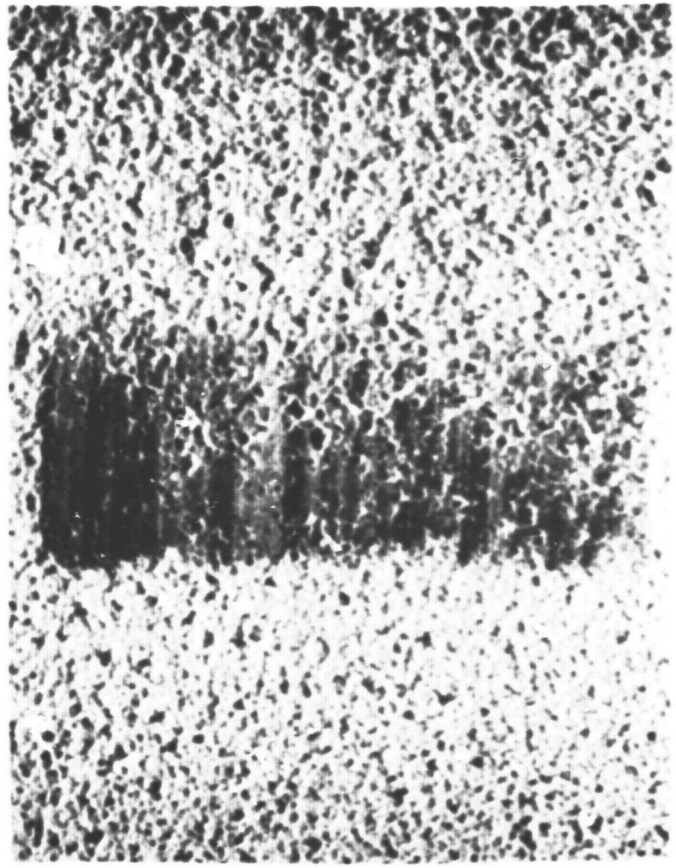

Rub Direction

a Blade Track Wear Scar

b Blade Tip Condition

Incursion Rate	.0025 cm/sec (.001 in/sec)
Blade Tip Speed	229 m/sec (750 ft/sec)
Depth of Rub	.01 cm (.004 in)

Figure 43 Slow incursion rate high speed abradability test results for System III O

Magn: 5X

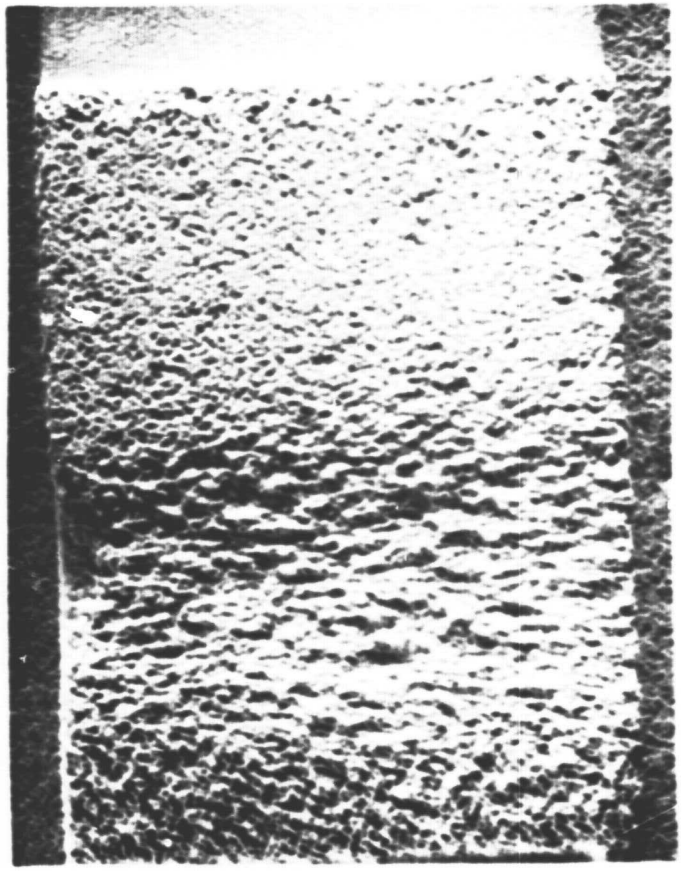

Flow Direction

Figure 43c Erosion test results for System III 0 (30 min. exposure)

Magn: 3X

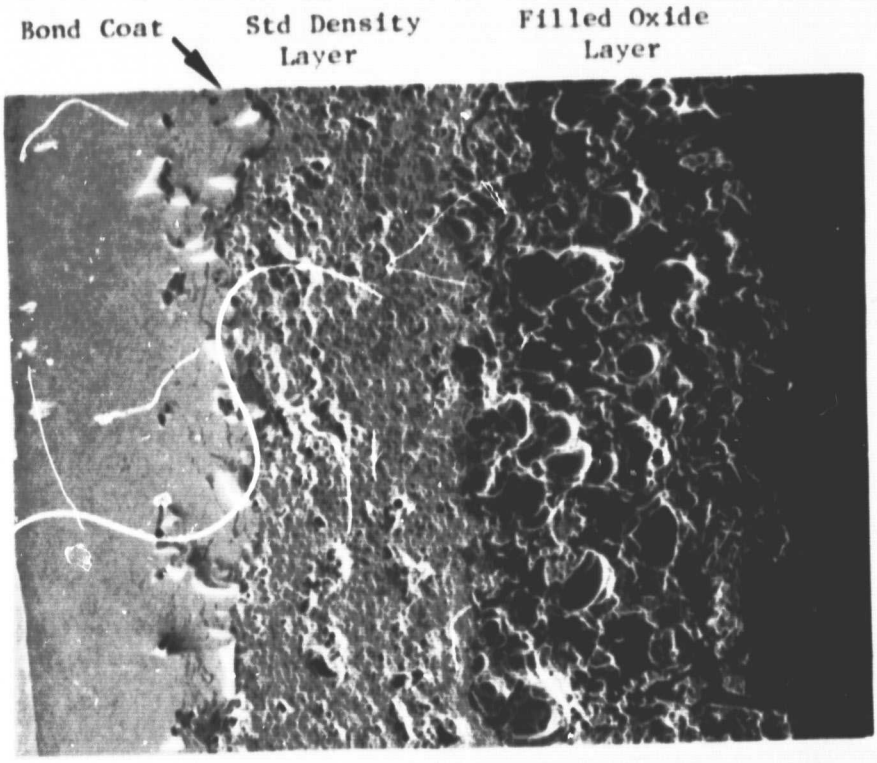

Magn: 100X

a) Porosity Characteristics

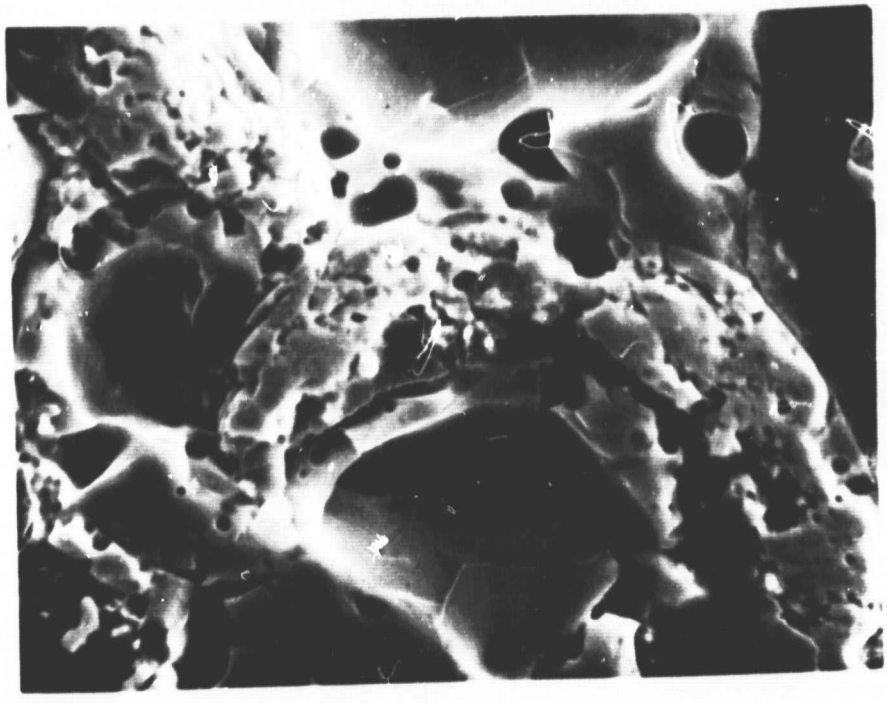

Magn: 1000X

b) Ceramic Particle Morphology (outer layer)

Figure 44 Porosity characteristics and ceramic particle morphology of coating system I-N

C-2

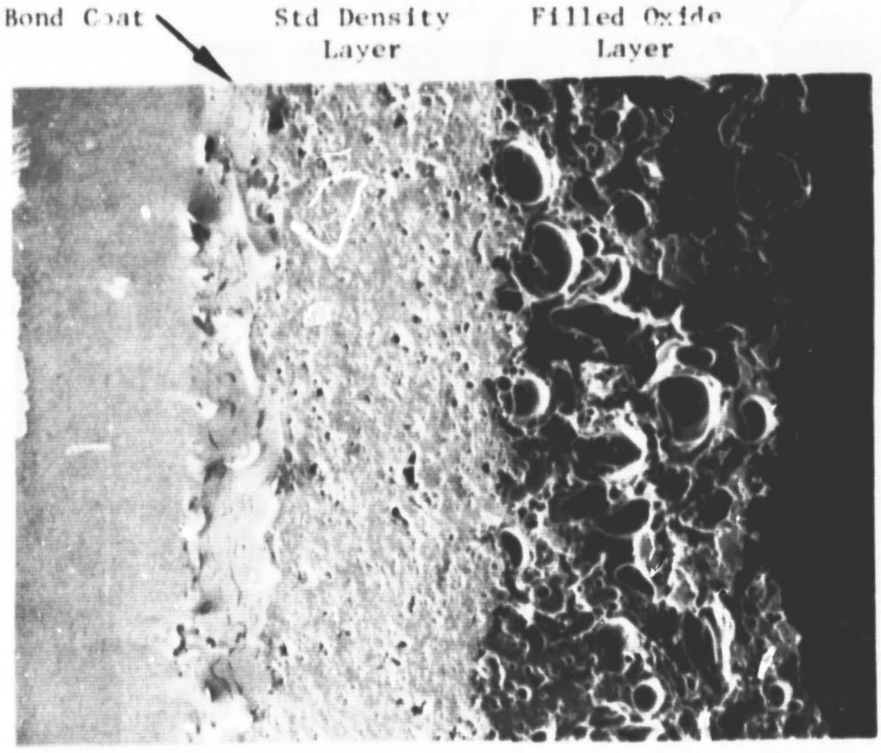

Magn: 100X

a) Porosity Characteristics

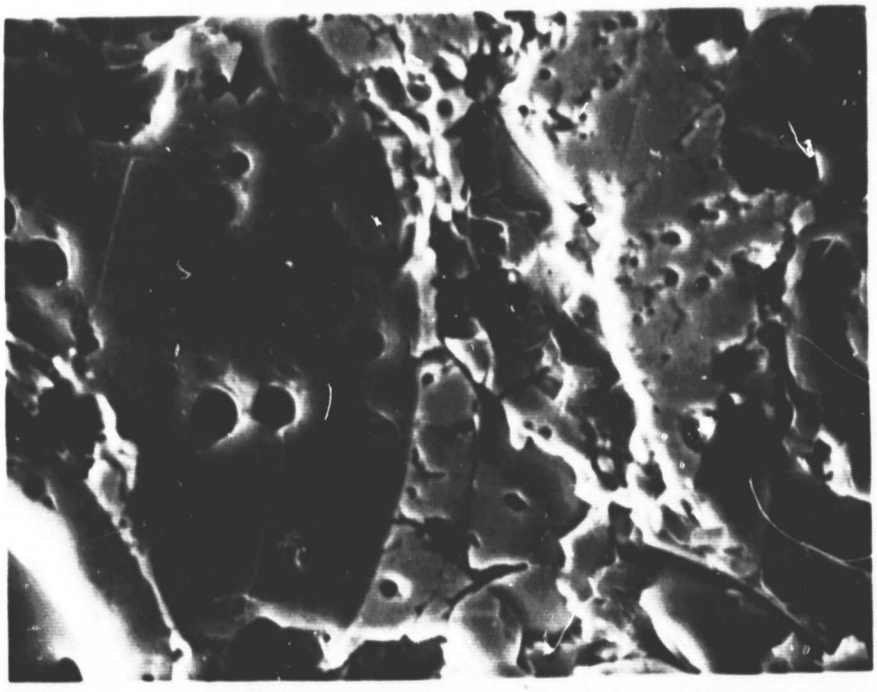

Magn: 1000X

b) Ceramic Particle Morphology (outer layer)

Figure 45 Porosity characteristics and ceramic particle morphology of coating system II-N

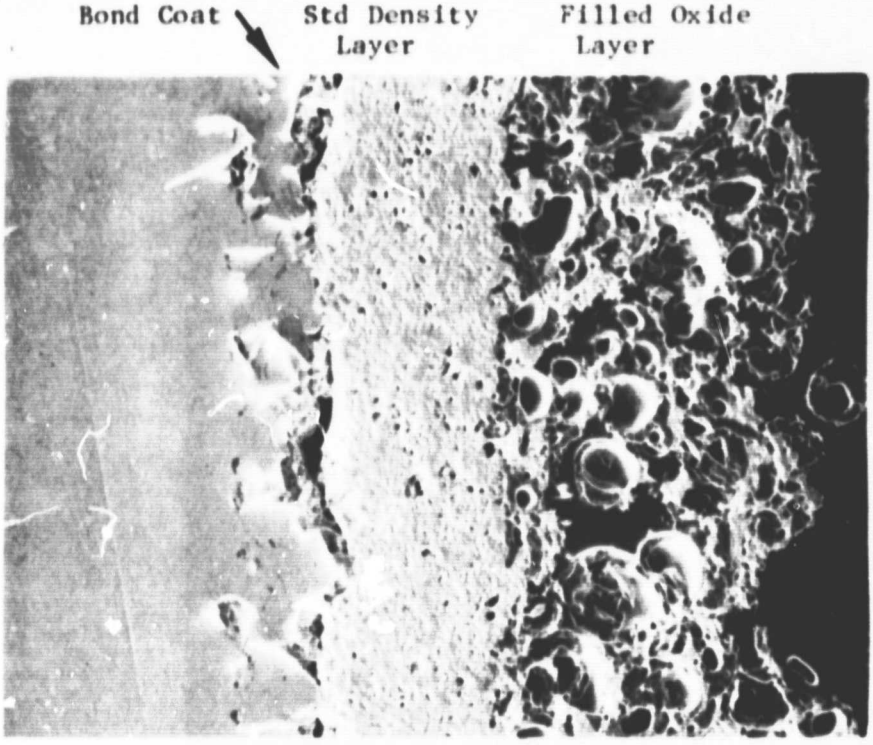

Magn: 100X

a) Porosity Characteristics

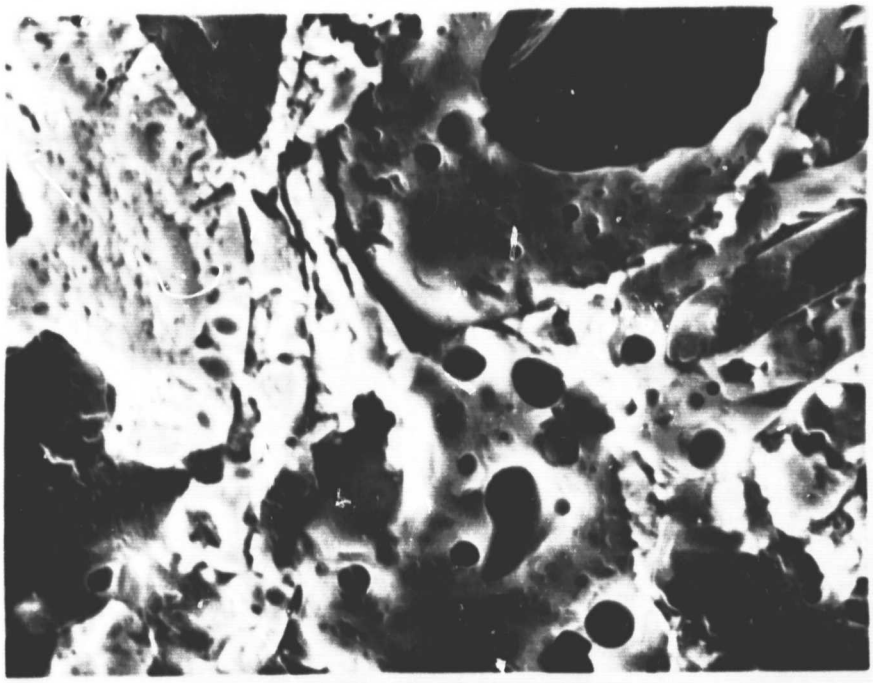

Magn: 1000X

b) Ceramic Particle Morphology (outer layer)

Figure 46 Porosity characteristics and ceramic particle morphology of coating system III-N

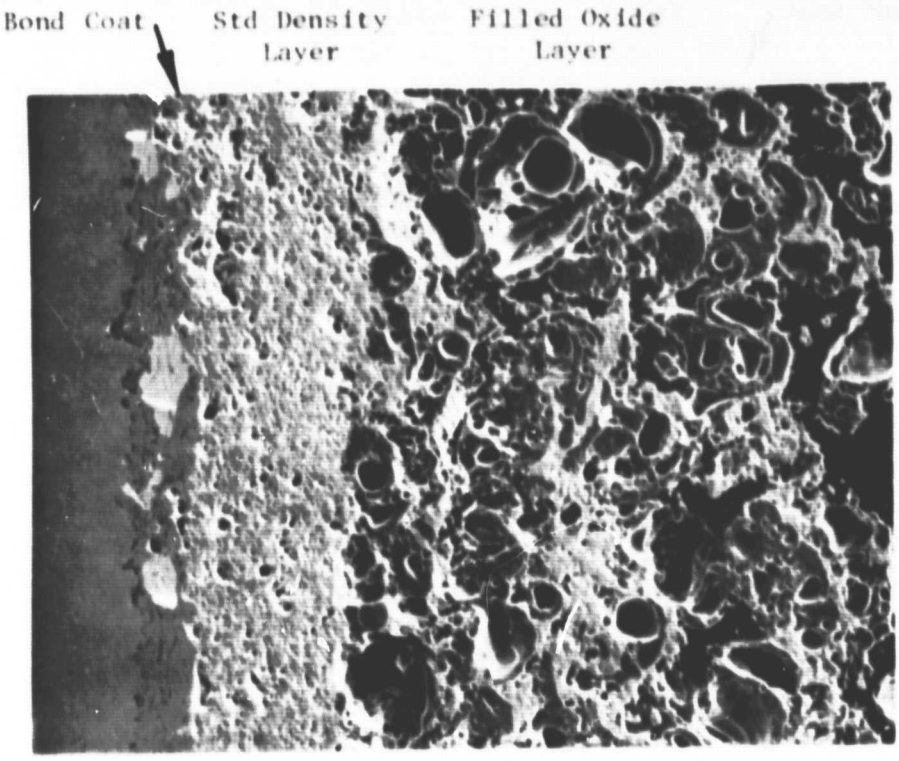

Magn: 100X

a) Porosity Characteristics

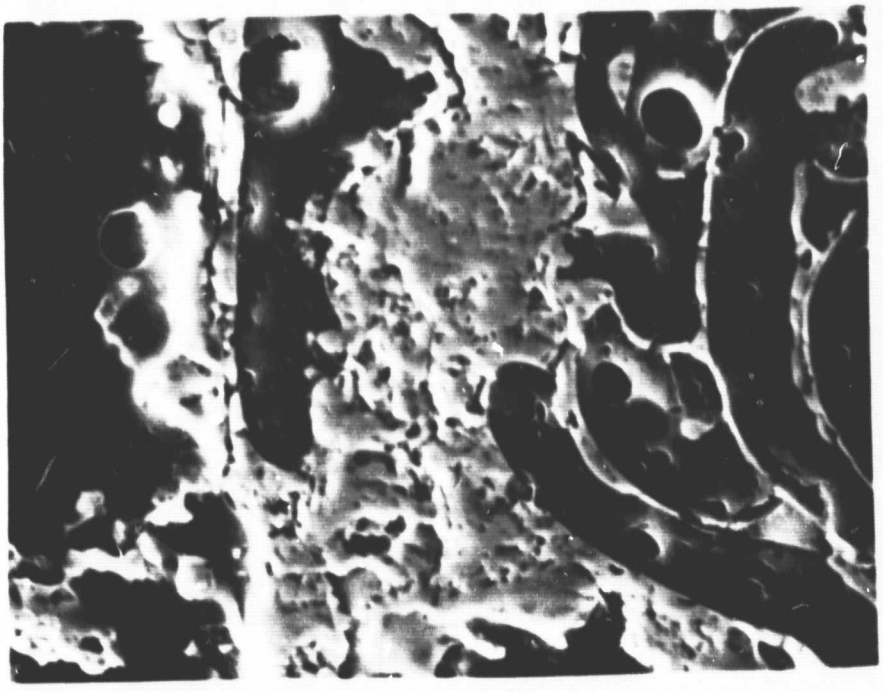

Magn: 1000X

b) Ceramic Particle Morphology (outer layer)

Figure 47 Porosity characteristics and ceramic particle morphology of coating system IV-N

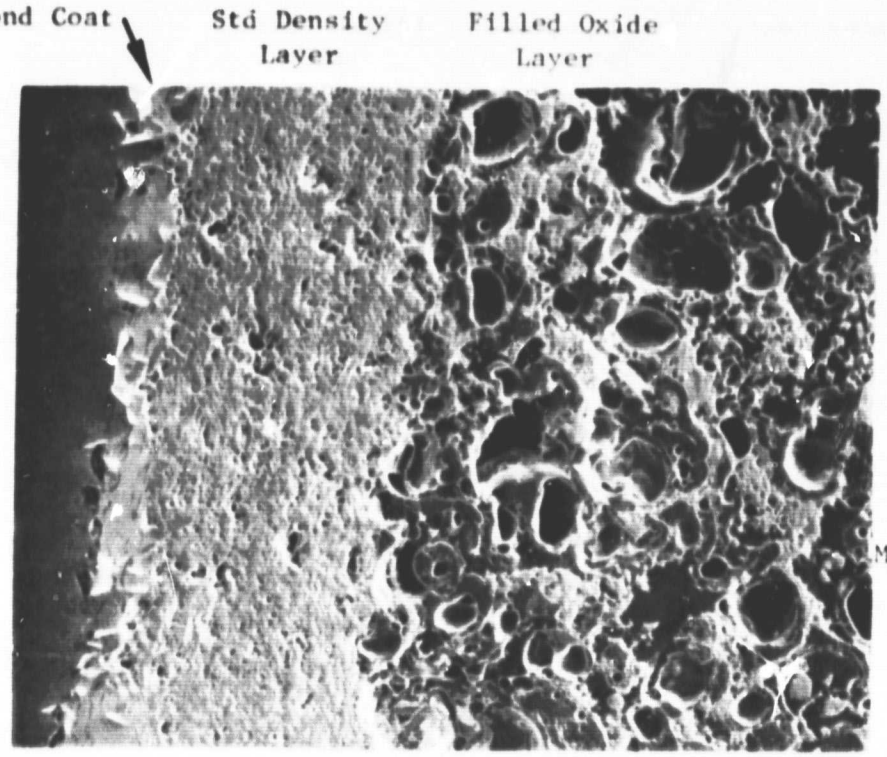

a) Porosity Characteristics

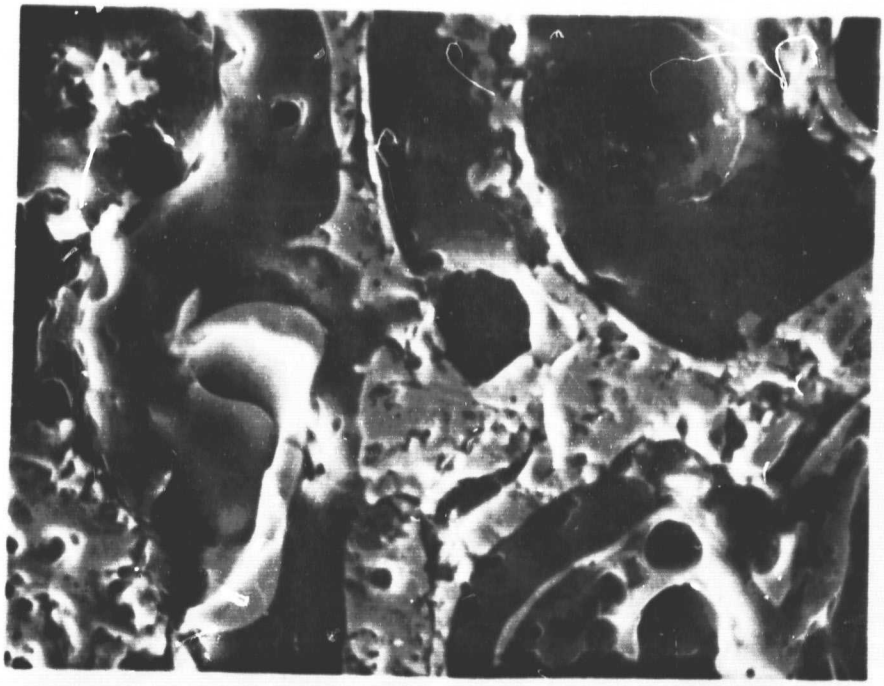

b) Ceramic Particle Morphology (outer layer)

Figure 48 Porosity characteristics and ceramic particle morphology of coating system V-N

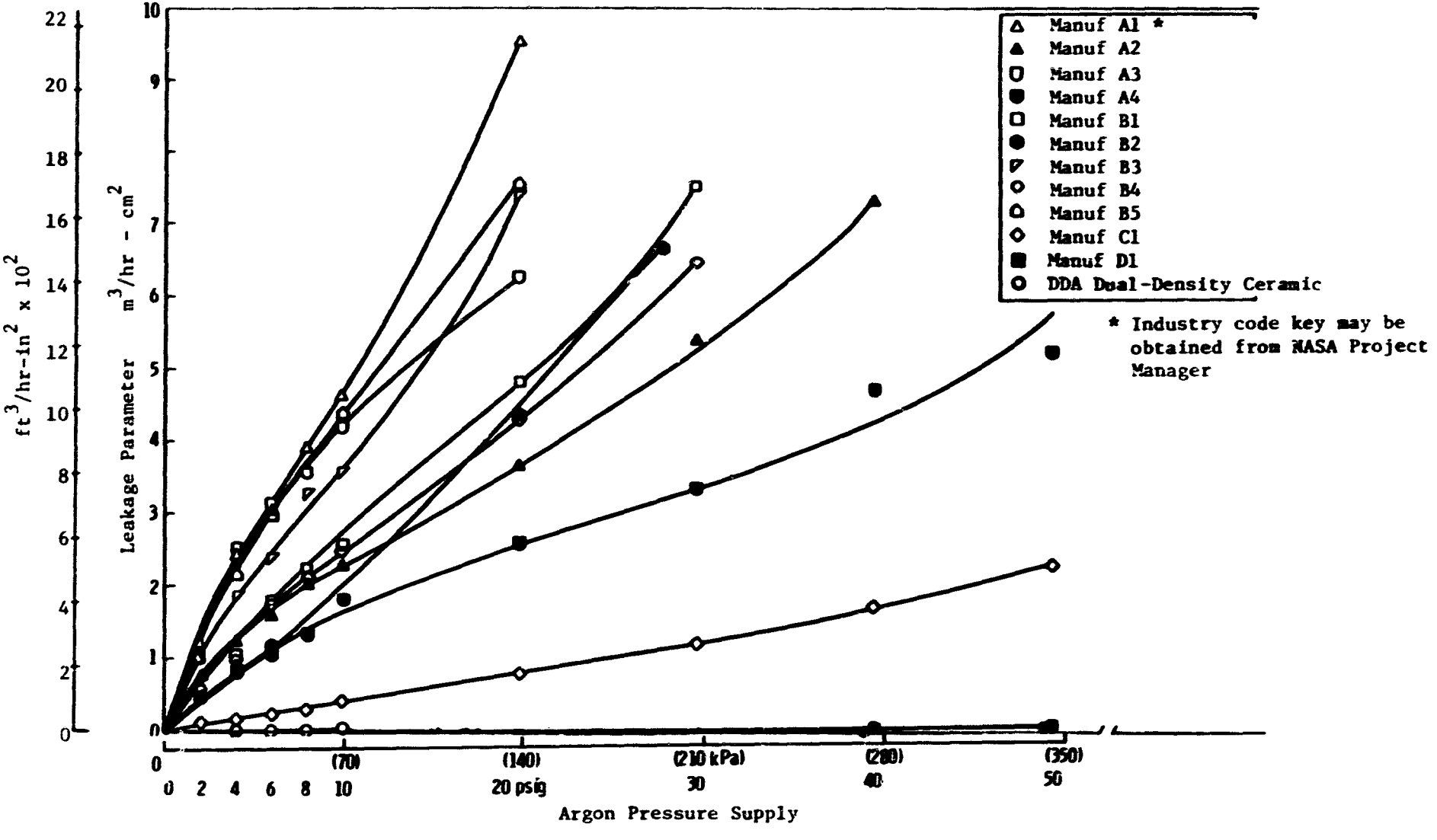

Figure 49 Abradable Seal Material Permeability

Erosion

Material erosion for each coating configuration in both the pre-stabilized (8 w/o) and flame stabilized (M-202) matrix systems was measured using the erosion procedures previously described. These results are shown in Figures 50 through 56.

The 100% YSZ system, which is the standard NASA thermal barrier, is shown in Figure 50 for both the 8 w/o and the M-202 powders. The 8 w/o powder is clearly a more erosion resistant system than the M-202 powder. As the percentage of YSZ is decreased in favor of increasing percentages of eccospheres, the erosion resistance of the M-202 systems decrease more rapidly than the 8 w/o system, as is seen in Figures 52 through 54. In Figure 52, it is seen that the M-202 60/40 system has severely deteriorated in erosion resistance when compared to the 8 w/o system. Similar deteriorated performance is not experienced with the 8 w/o system until a 20/80 composition is tested. This is shown in Figure 55.

ENGINE TEST RESULTS

Abradable turbine tip seal structures resulting from this program were tested in two different engines: the GMA 500/ATDE and a development engine included as part of the CATE (Ceramic Applications in Turbine Engines) program intended to introduce ceramic components into an industrial-type gas turbine. The temperature of the turbine environment in these engines was nominally in the range 1800-2000^{o}F.

Because of the timing of the opportunities for testing, and the subsequent discovery of unsuspected powder feed problems to be discussed later, all seal structures tested in the GMA 500/ATDE were ultimately shown to be of unknown or questionable composition. Early tests conducted in the CATE engine were also subject to these uncertainties.

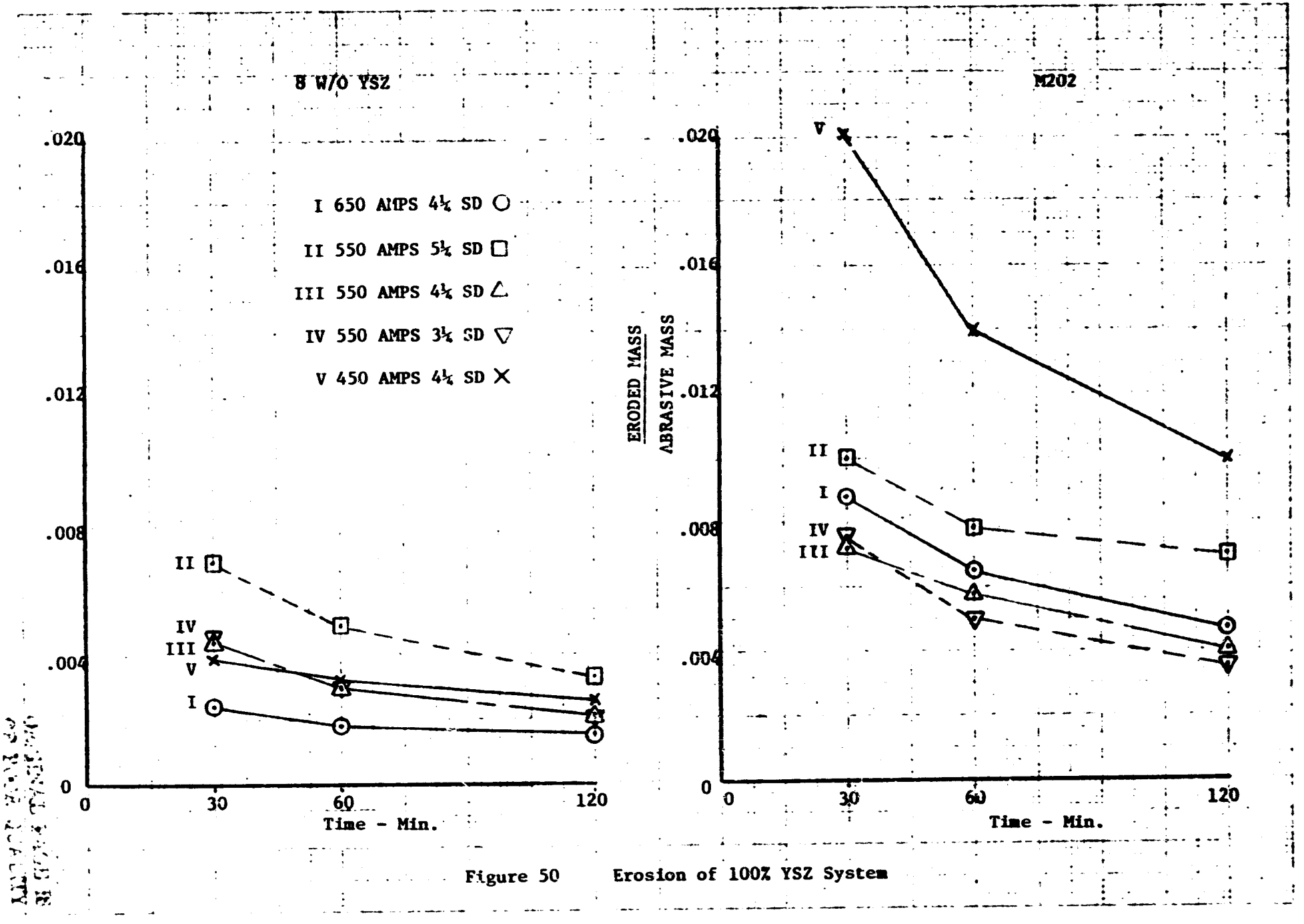

Figure 50 Erosion of 100% YSZ System

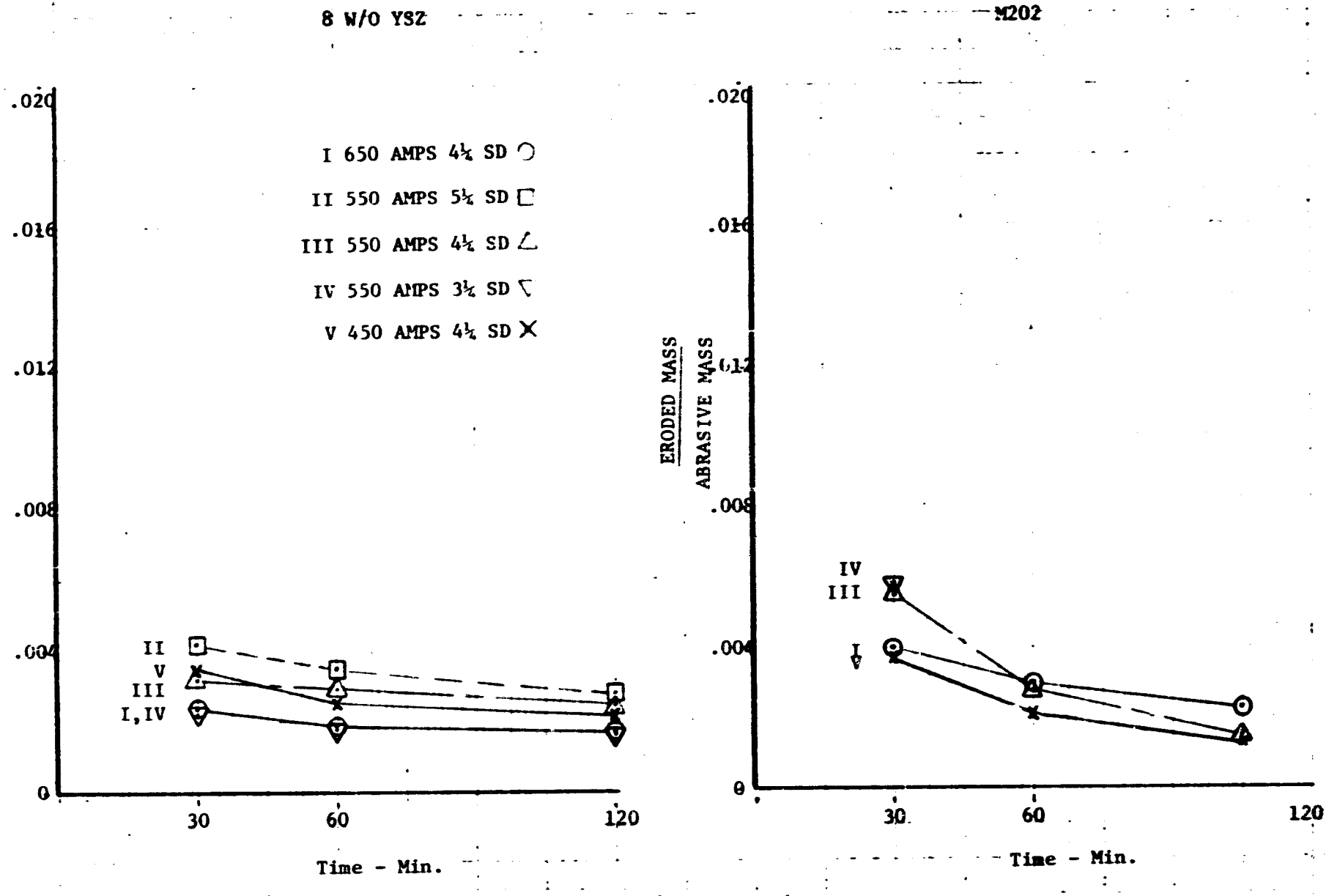

Figure 51 Erosion of 80 v/o YSZ 20 v/o Eccosphere System

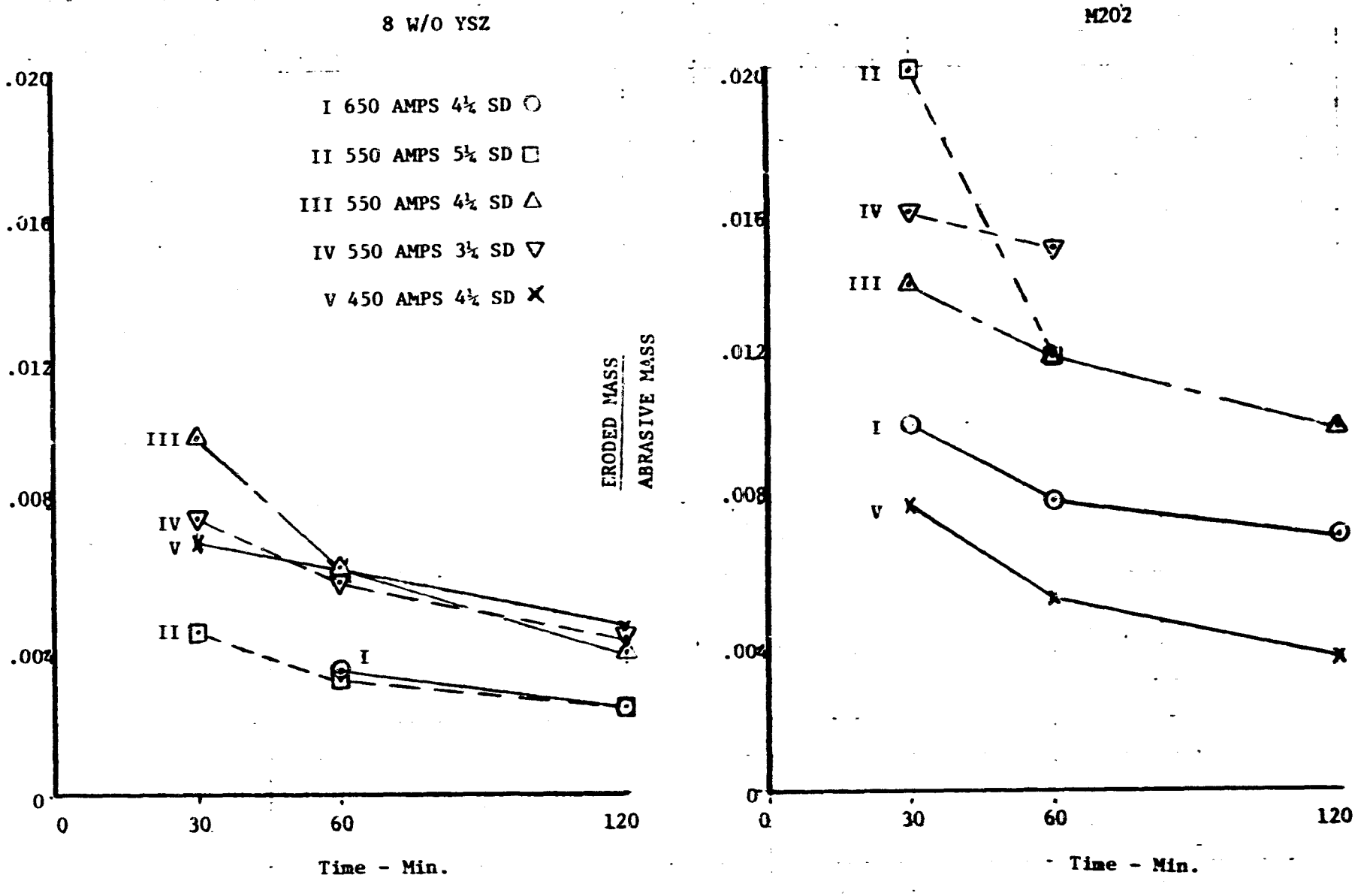

Figure 52 Erosion of 60 v/o YSZ 40 v/o Eccosphere System

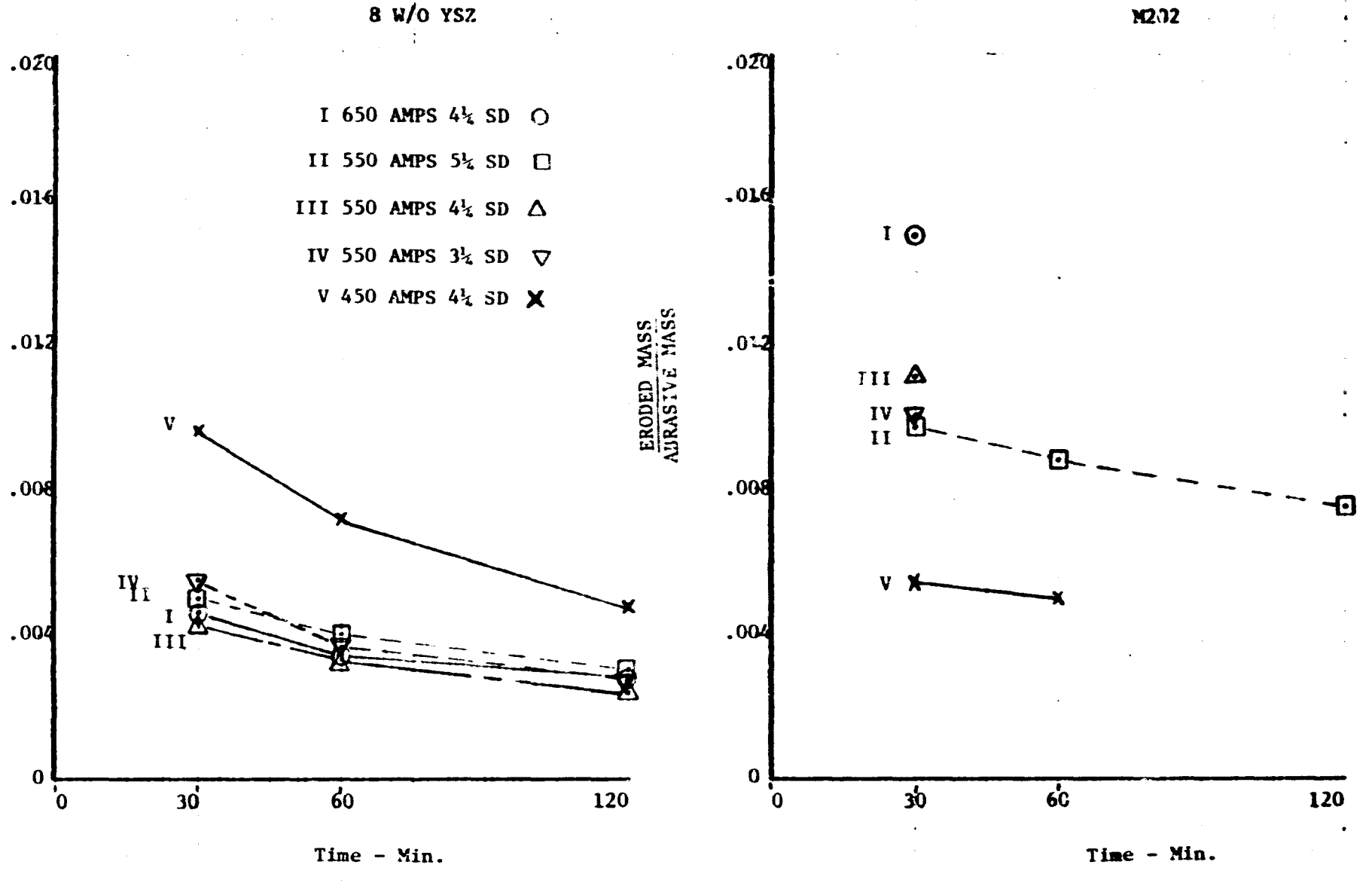

Figure 53 Erosion of 50 v/o YSZ 50 v/o Eccosphere System

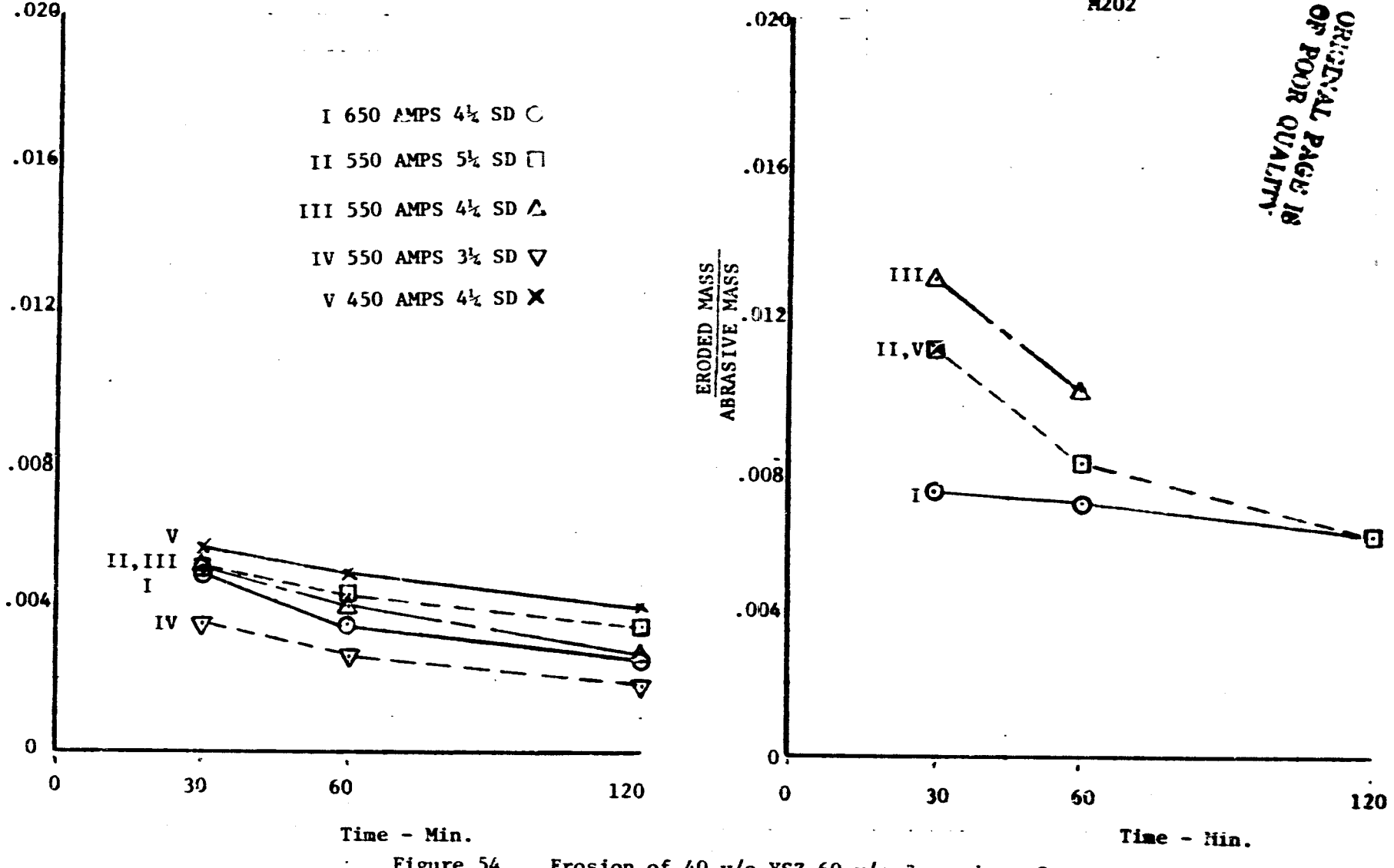

Figure 54 Erosion of 40 v/o YSZ 60 v/o Eccosphere System

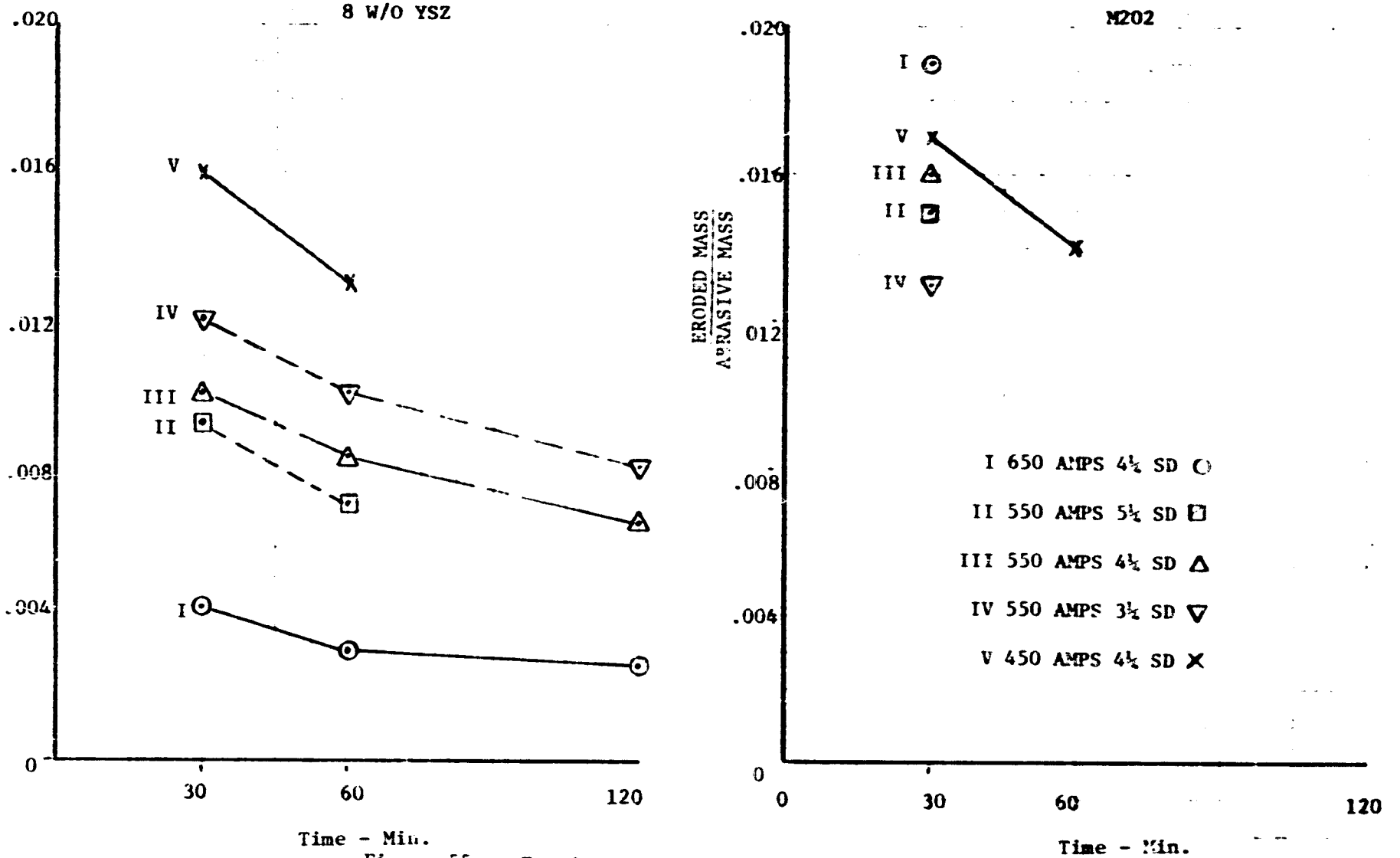

Figure 55 Erosion of 20 v/o YSZ 80 v/o Eccosphere System

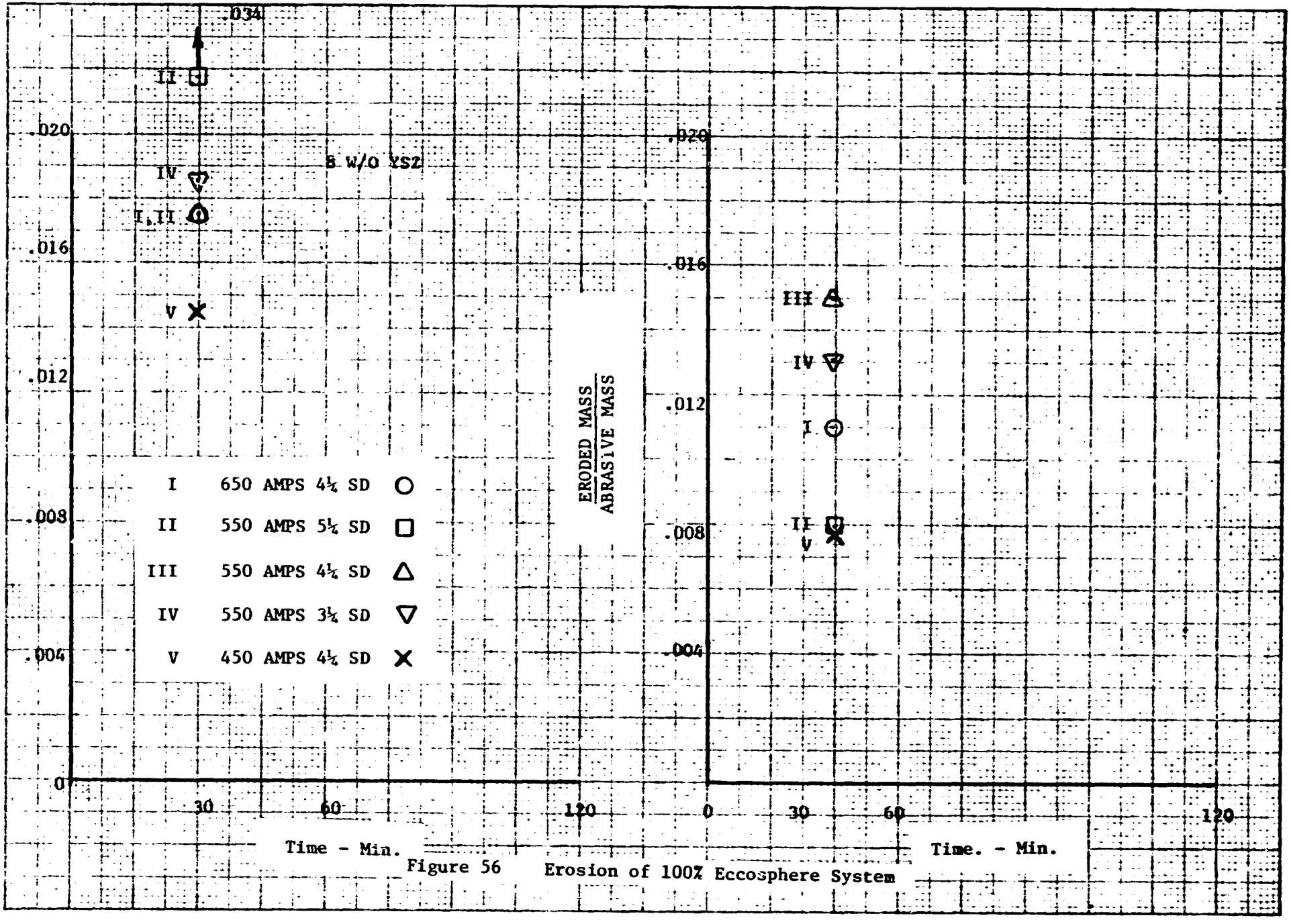

Figure 56 Erosion of 100% Eccosphere System

Following correction of the problem causing the uncertainty in the structures, an opportunity occurred for additional testing in the CATE engine. Results of these tests have become available during the preparation of this report and are significant in that they represent what may be considered as the first qualified success in applying truly abradable seals in a high temperature turbine environment.

Further details of both the GMA 500/ATDE and CATE engine tests are discussed in the following paragraphs.

GMA 500/ATDE Engine Tests

As a direct consequence of the total lack of an effective metal-compatible abradable seal system from other sources, an opportunity for engine testing in the GMA 500/ATDE occurred midway through this program. Because of the timing and the demonstrated critical need for abradable turbine seals (metal-based systems from commercial vendors had produced catastrophic results), a non-optimized dual density ceramic composition was selected as being the best system available at the time.

In order to select the candidate system for engine testing, compositions were examined which covered a wide range of Metco 202 YSZ/Type FA-A Eccosphere ratios. At this time the superiority of the Zircoa material had not yet been fully established and the Metco material was selected strictly on the basis of cost. The ratios were defined by potentiometer control settings of the Plasmadyne Model 1000A powder feeders subsequent to determining the measured flow rates. The initial set of specimens, identified as A, B and C had powder feeder control ratios and hardness values as shown in Table IV.

Low speed abradability tests at room temperature on the sofest specimen (A) resulted in virtually no perceptible penetration and produced significant adhesive transfer in the rub zone. Conversely, little distress was observed to result from erosion tests. Both results led to the conclusion that specimen A, and consequently the rest of this series, were too hard and another set of specimens, identified as D-K, plus 100% FA-A Eccospheres, was prepared. The corresponding powder feeder control setting ratios and the respective hardness values are shown below the dashed line in Table IV, arranged in order of apparent increasing Eccosphere content.

Table IV

YSZ/FA-A Spray Combinations and R15Y Hardness Levels

Specimen	YSZ/FA-A Potentiometer Ratios	Hardness-R15Y	
A	35/35	89-92	Sprayed as
B	35/25	91-94	one batch
C	35/15	93-94	↓
D	35/50	61-66	Sprayed as
H	35/60	48-61	one batch
I	35/70	54-59	↓
J	35/75	70-77	Anomalous
E	35/80	65-67	hardness
K	35/85	58-74	values
F	25/90	4-24	
G	15/100	-14-7	
100% FA-A	0/100	-18	

The expected trend of decreasing hardness with increasing Eccosphere content was observed with the exception of specimens E, J and K which constituted one-third of the specimen population. No explanation for this anomolous behavior was found at the time and was consequently attributed to the vagaries which can be present in the hand-held application of plasma sprayed coatings. The source of the problem was ultimately found to be related to the particular model powder feeders used throughout much of the program and is discussed more fully later in this section.

The composition selected for engine testing in the 4th stage turbine location of the GMA 500/ATDE was the 35/70 mixture corresponding to specimen "I". Two additional specimens were prepared with the hardness again ranging in the mid-50"s on the R15Y scale. Low-speed room-temperature abradability was checked to a depth of 0.016 in. with no distress to the labyrinth knives; erosion resistance was good, if not outstanding. The abradability test wear scar is shown in Figure 57 in which some glazing of the seal material has occurred at the bottom of the grooves formed by the labyrinth knives.

An opportunity to also test seals in the 1st and 2nd stage turbine blade tip locations in the GMA 500/ATDE was created when a commercially obtained blade tip seal material was rubbed by the rotor blade tips, resulting in extensive adhesive transfer of blade tip material to the stationary seals. The extent of the damage required replacement of the seal segments and a composition of 35/60 was selected to withstand the more highly erosive environment of the unshrouded early turbine stages. This composition should have corresponded to that of specimen "H" discussed earlier, but specimen coupons sprayed simultaneously with the engine parts exhibited R15Y hardness levels in the range from 36-50, which is appreciably softer than the 48-61 exhibited by the "H" specimen.

The difference in hardness values between coupons sprayed individually and those sprayed in conjunction with the preparation of engine parts provided a clue to why coatings on parts for engine service often performed far differently than expected. It was subsequently observed that the spray equipment appeared to perform unpredictably on occasion, apparently depending upon the amount of spray material in the powder feeder hoppers. To confirm the supposition that the hopper fill level was influencing the resulting coatings, both powder feeders were calibrated for three different fill levels. The results of these calibrations are shown in Figure 58 where it can be readily seen that for a constant powder feeder control setting, the actual powder output can vary by as much as 100 percent, depending on the amount of material in the hopper.

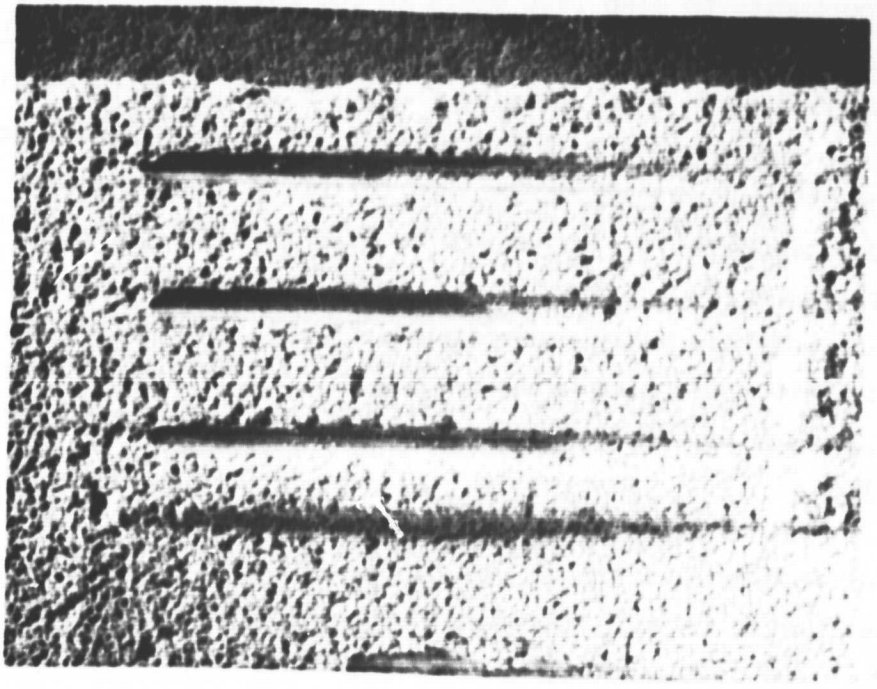

Magn: 5X

Figure 57 Labyrinth seal abradability test results IN 713 knives vs 35/70 M 202 YSZ/FA-A 0.016 in deep

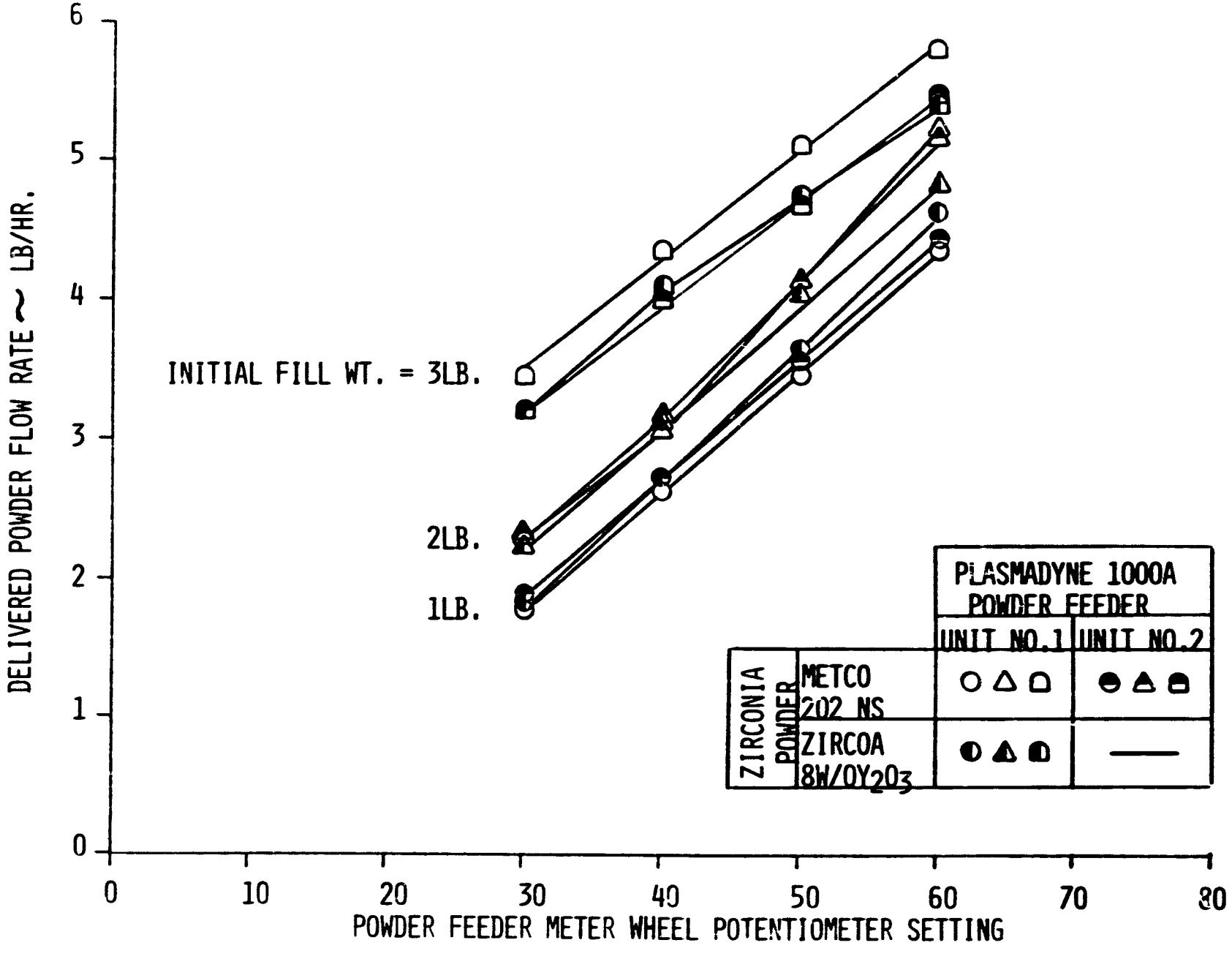

Figure 58 Dependence of zirconia powder flow rate on powder feeder fill weight

The implications of this discovery are obvious. The usual laboratory technique employed in preparing small numbers of specimens during coating development has been to use a small amount of powder in the feeders. This reduces the risk of contamination of unused material and simplifies the changing from one powder to another. Conversely, when engine parts are sprayed the hopper is filled to near capacity so that the powder supply will not be exhausted prior to completion of the coating. Thus, because of the proven fill-level dependency, coatings on engine parts sprayed with parameters established on the basis of development coupons can have characteristics vastly different from those expected.

The solution to the problem of achieving the desired composition on a predictable and repetitive basis has been to replace the suspect powder feeders with models representing the latest state of the art. Plasmadyne Model 1250A units have been recently acquired and shown to deliver powder to the spray gun at rates which are virtually independent of the hopper fill level as shown by the calibration data in Figure 59.

The turbine tip seals tested in the 1st, 2nd and 4th stages of the GMA 500/ATDE were prepared prior to the discovery and subsequent correction of the powder feeder problem. Consequently, the compositions actually tested in the engine were probably not those intended; no pre-test measurements are available.

Although no valid conclusions can be drawn regarding the performance of the dual density ceramic seals tested in the GMA 500/ATDE, it may be of interest to observe the types of distress experienced by the components.

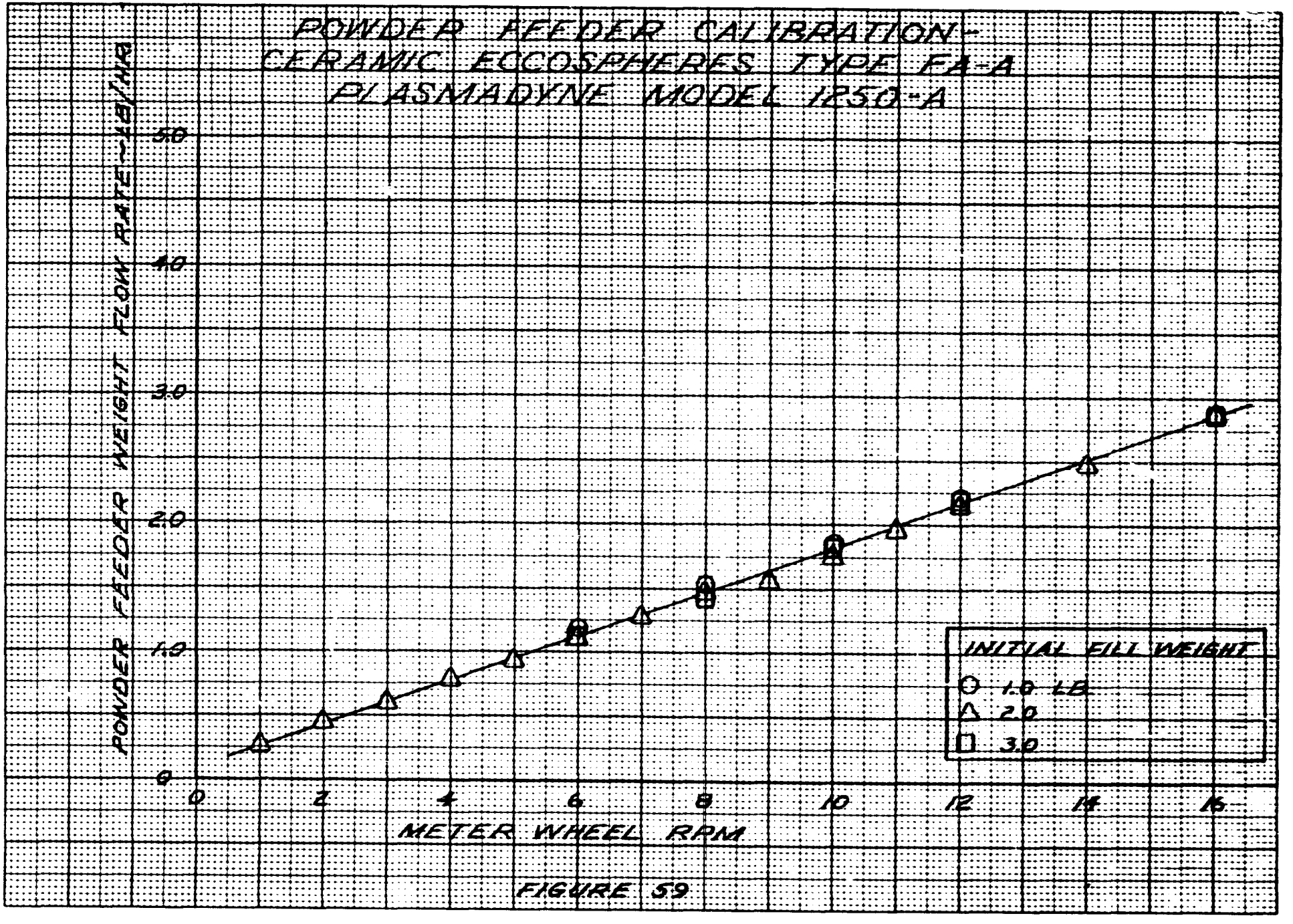
POWDER FEEDER CALIBRATION-
CERAMIC ECCOSPHERES TYPE FA-A
PLASMADYNE MODEL 1250-A
POWDER FEEDER WEIGHT FLOW RATE-LB/HR
5.0
4.0
3.0
2.0
1.0
0
0
2
4
6
8
10
12
14
16
METER WHEEL RPM
INITIAL FILL WEIGHT
1.0 LB
2.0
3.0

FIGURE 59

Because of exceptionally tight clearances selected for the particular build in which the dual density ceramic seals were incorporated, an extremely heavy rub occurred within the first minute of operation which resulted in an immediate shut-down. The condition of the first stage turbine tip seals following the heavy rub (one minute of operation) is shown in Figures 60 and 61. Metallic deposits resulting from the adhesive transfer of blade tip material to the seal surfaces are evident in Figure 60. Evidence of an even harder rub is shown in Figure 61, where a massive section of the ceramic has been plowed away by the penetrating blade tip.

During the tear-down following the hard rub, the clearances were increased by removing stock from the seal surfaces. The engine was re-assembled and returned to the stand to resume testing. Following 68:12 hours of additional testing, the engine was again disassembled for inspection. The condition of the first and second stage turbine seals was as shown in Figures 62 and 63, respectively. The severe erosion evidenced in these photographs may have been triggered by the scrubbing action of particles initially removed from the damaged area of the first stage seal, resulting in a type of avalanche effect in removing further material. It appears that the erosion of the second stage seal material has been accelerated as a consequence of the bombardment by erosive wear debris from the first stage seal. Regardless of the erosion mechanism that was active, the seal structure has been found to be appreciably softer than intended and probably lacked any significant amount of erosion resistance even under ideal circumstances. Erosion was not limited to the abradable layer; material loss in both the first and second stages also included the standard density intermediate layer.

The condition of the seal installed in the 4th stage turbine seal location following 35:29 hours of testing is shown in Figure 64. It can be seen from this photograph that the knives on the shroud have rubbed the seal over the entire circumference. Some slight evidence of erosion at the aft edge of the seal is also present.

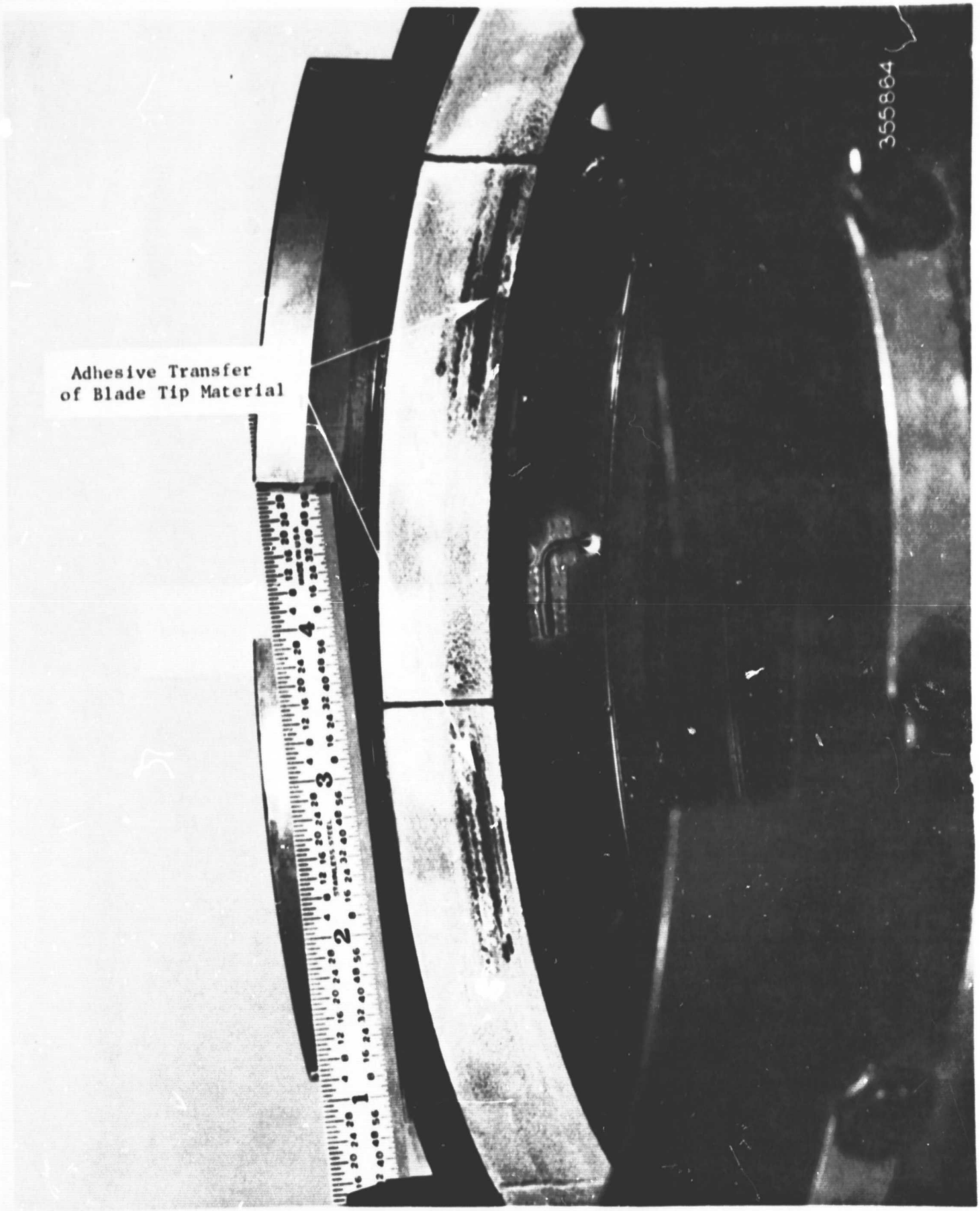

Figure 60 Adhesive transfer to GMA 500/ATDE first-stage turbine tip seal following heavy rub during first minute of operation.

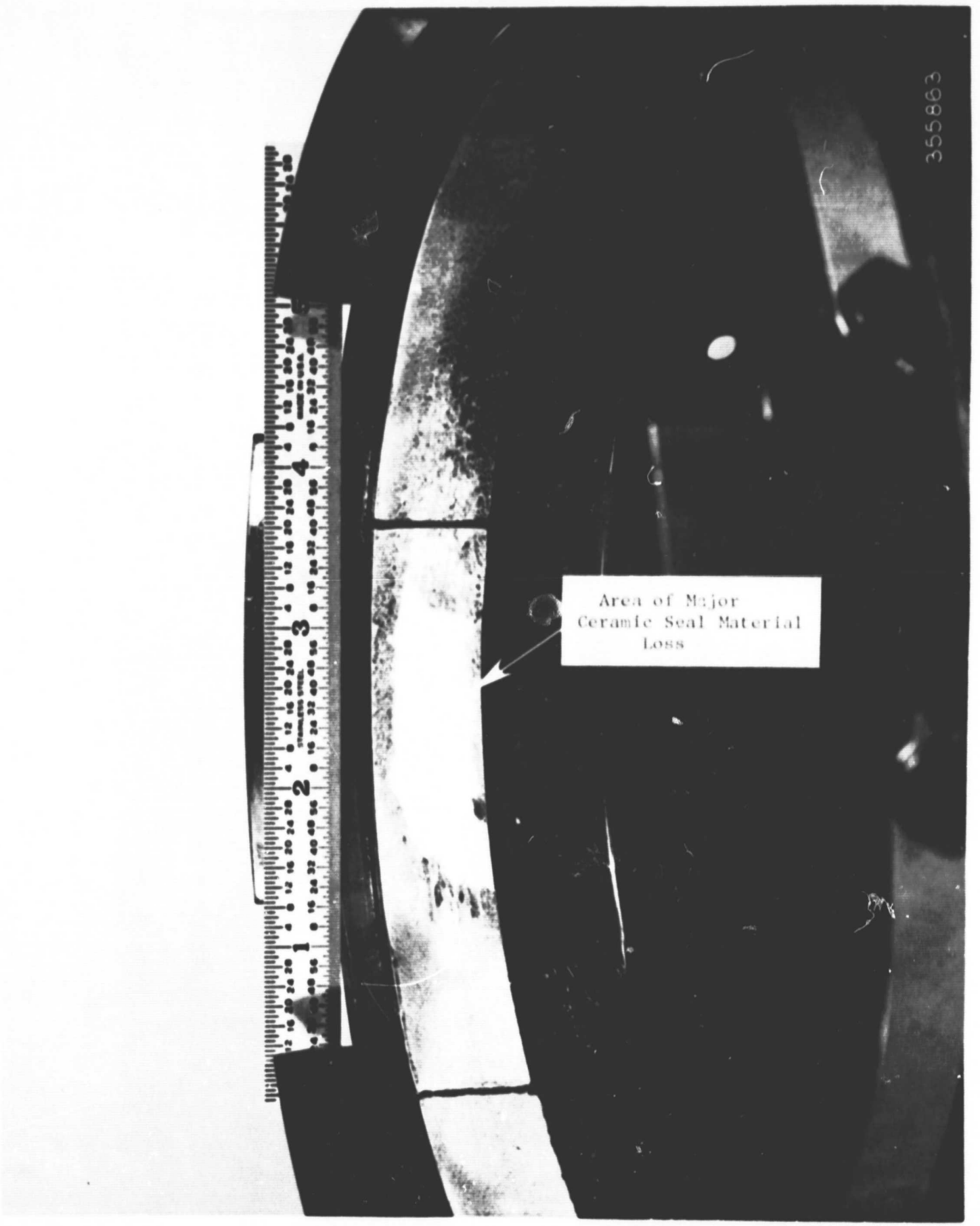

Figure 61 Material removed from GMA 500/ATDE first-stage turbine tip seal following heavy rub during first minute of operation.

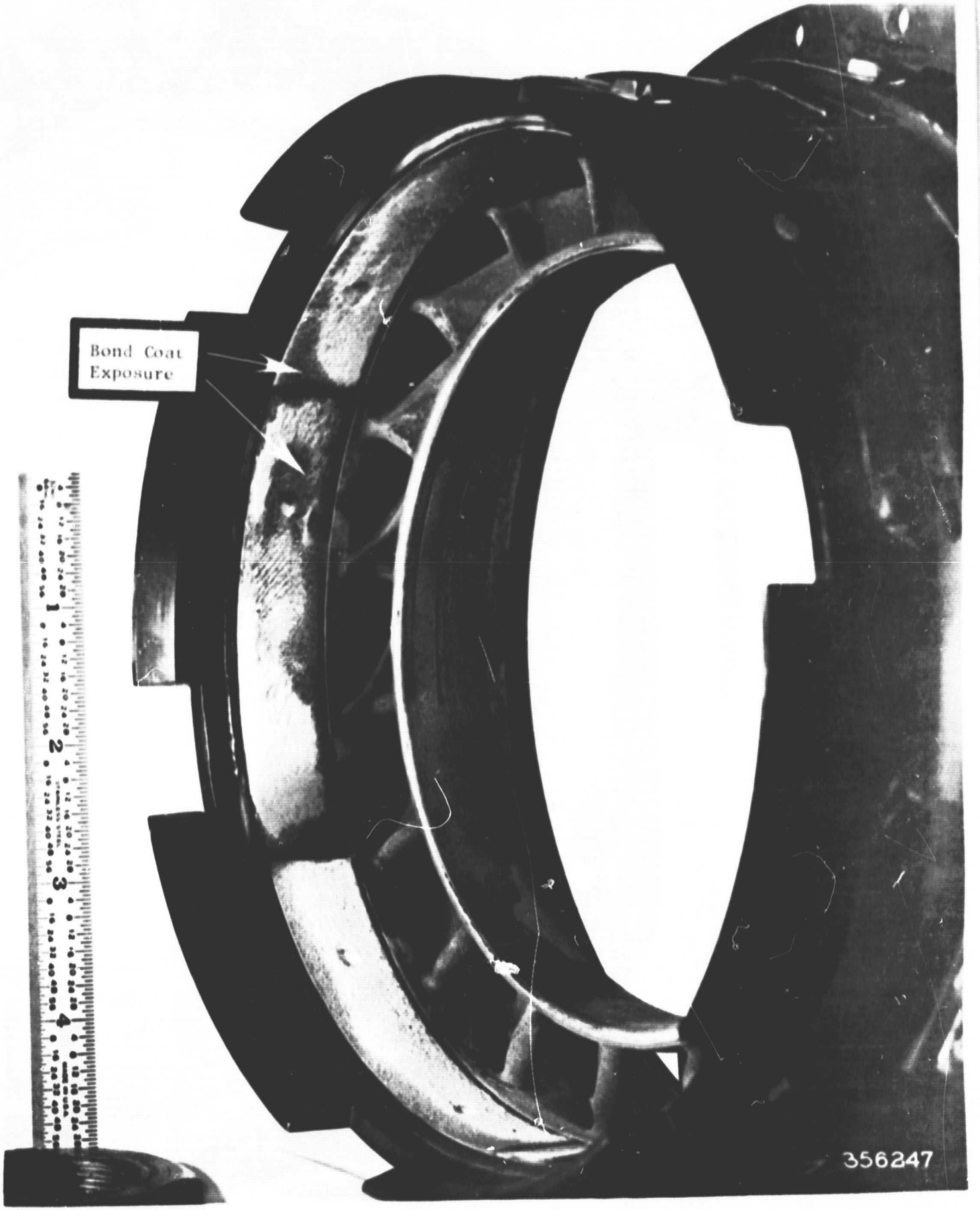

Figure 62 Condition of GMA 500/ATDE first-stage turbine tip seal following 68:13 hours total test time.

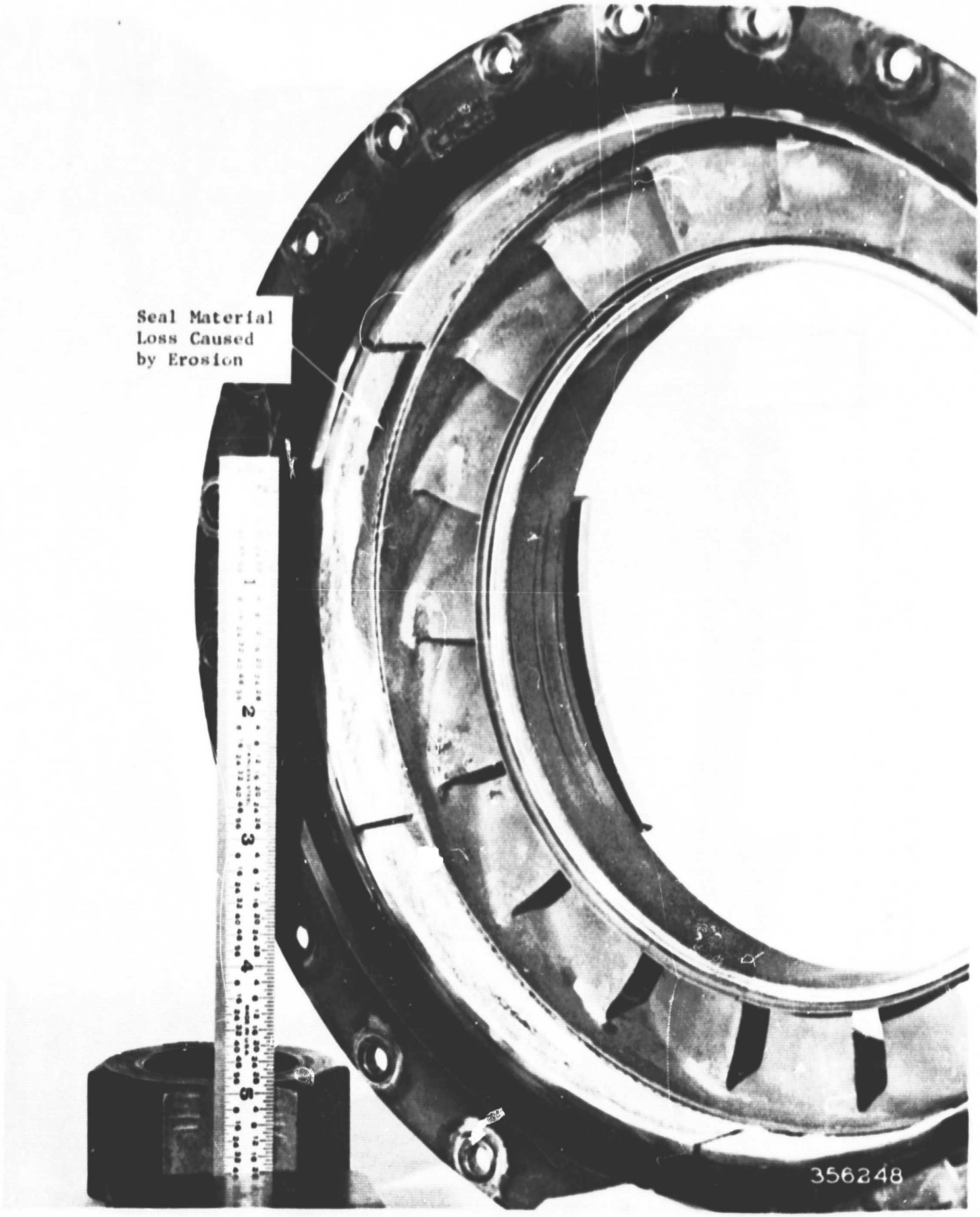

Figure 63 Condition of GMA 500/ATDE second-stage turbine tip seal following 68:13 hours total test time.

Figure 64 Condition of GMA 500/ATDE fourth-stage turbine tip seal following 35:29 hours total test time.

Since the time that the photograph of the seal was made, the seal has been installed in two additional builds with test times of 68:12 and 3:25 hours, respectively. This seal has now accumulated 107:06 hours of test time and is still considered to be serviceable. Although the unit is not accessible for preparation of a photograph showing its present condition, visual observation has shown no appreciable change in its condition during the last 71:37 hours of testing.

In comparing the 4th stage seal test results with those of the 1st and 2nd stages, it should be noted that not only are the temperatures significantly different at each of these locations but also the erosive environment is significantly less severe for the shrouded 4th stage. Further, the rub mechanisms are different, in that the knives of a shrouded stage do not tend to generate loose wear debris to the extent that is typical of seals abraded by discrete blade tips.

CATE Engine Tests

Two additional opportunities to engine test dual density ceramic seals were made available as part of the CATE (Ceramic Applications in Turbine Engine) program sponsored by the Department of Energy and administered by NASA. The location selected for evaluation was the gasifier turbine tip seal and since the testing opportunities preceded the availability of ceramic blading specified for this program, MAR M246 turbine blades were employed in the turbine. Thus, the rub situation was similar to that found in the GMA 500/ATDE 1st and 2nd turbine stages with respect to both materials and temperatures.

The first dual-density ceramic seal for the CATE application was fabricated prior to resolution of the previously described powder feeder problem. Because of the poor erosion resistance experienced in the GMA 500/ATDE tests, it was arbitrarily decided to increase the hardness of the structure by a modest amount. Because of the unsuspected uncertainty associated with the

powder feeders, the hardness was over-corrected with an R15Y range of 74-80. Post-test semi-quantitative X-ray energy dispersion analysis (XEDA) results indicated that the actual composition of the seal material was 75 percent zirconia and 25 percent eccospheres, by weight.

Adhesive transfer of blade tip material to the stationary seal surface resulted in the wear scar shown in Figure 65a. The corresponding distress to the blade tips is shown in Figure 65b, where the maximum depth of material removed was observed to be approximately .020 in. (.051 cm). Damage of this magnitude resulted in severe performance degradation requiring removal of the engine from the test stand.

The second (and latest) opportunity to evaluate the dual density ceramic seal concept in a CATE engine has resulted in the preparation and installation of a gasifier turbine seal that was still undergoing testing at the time of this writing. The composition selected for this seal consisted of equal weight percentages of pre-stabilized ZrO_2 · 8 w/o Y_2O_3 and Type FA-A Eccospheres, sprayed at a total weight flow rate of 2.90 lb/hr (1.32 kg/hr). Because of the significant difference in density of the YSZ and filler materials, the volume percentages were 14 and 86, respectively. This seal was sprayed with newly acquired, state of the art powder feeders which have been shown to be free from the previously described powder feed-rate uncertainties.

The CATE engine in which the latest seal configuration has been installed is being used primarily to develop a microprocessor for its electronic fuel control. Consequently, the engine has experienced numerous starts and stops but has logged relatively few hours of running time. Although the dual density ceramic turbine seal in this installation has accumulated only a few tens of hours of actual test time, it has experienced considerable thermal

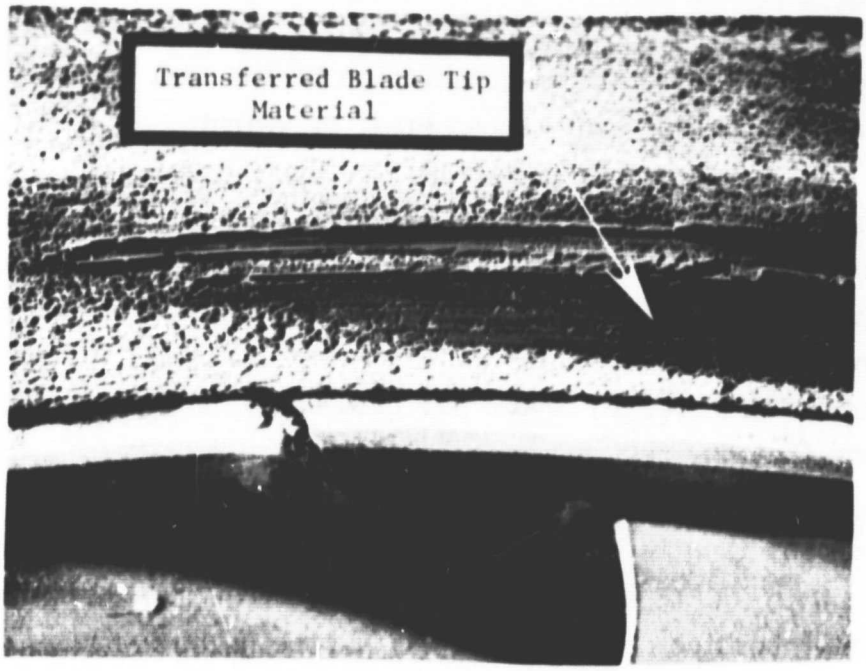

a. Adhesive transfer of blade tip material to seal following rub Magn: 3X

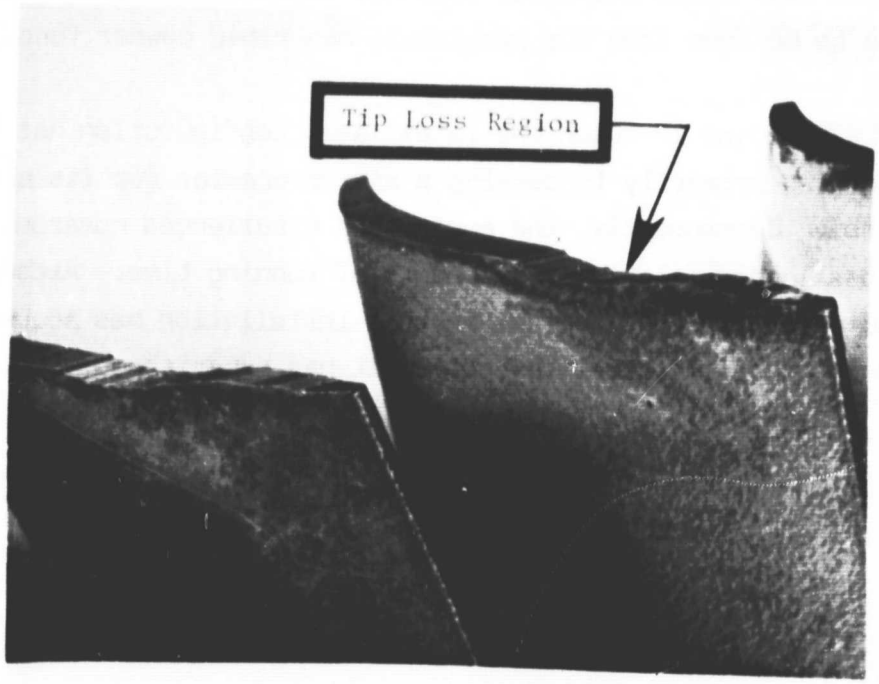

b. Resulting blade tip distress Magn: 5X

Figure 65 CATE gasifier turbine tip seal rub results

cycling, apparently without incident. The exceptionally fine performance of the engine has been attributed by the test engineers to significant improvement in the gasifier turbine seal. It is perhaps significant to note that no deterioration in performance with time has been observed, indicating that erosion is not yet a serious concern.

The condition of the seal following 41:00+ hours of testing is shown in Figure 66. Although it is apparent that some adhesive transfer of blade material to the seal has occurred, the seal has been abraded to a net depth of 0.010 in. (0.025 cm). Measured removal of blade tip material is also approximately 0.010 in (0.025 cm). Both material removal from the blade tip and deposition on the seal appeared to be uniform over the entire width of the rub path, with no localized build-up on either member. The post test condition of the blade tips is shown in Figure 67.

The rubbed blade track surface appears to contain a glassy phase of the seal material and exhibited extensive mud-flat cracking of the glazed surface, as shown in Figure 66. The damage appears to be superficial and has not seriously affected the ability of the coating to withstand the engine environment.

The circumferential extent of the rub interaction experienced during the 41+ hours of testing is shown in Figure 68. Following photographic documentation this seal was re-installed in the engine for additional service.

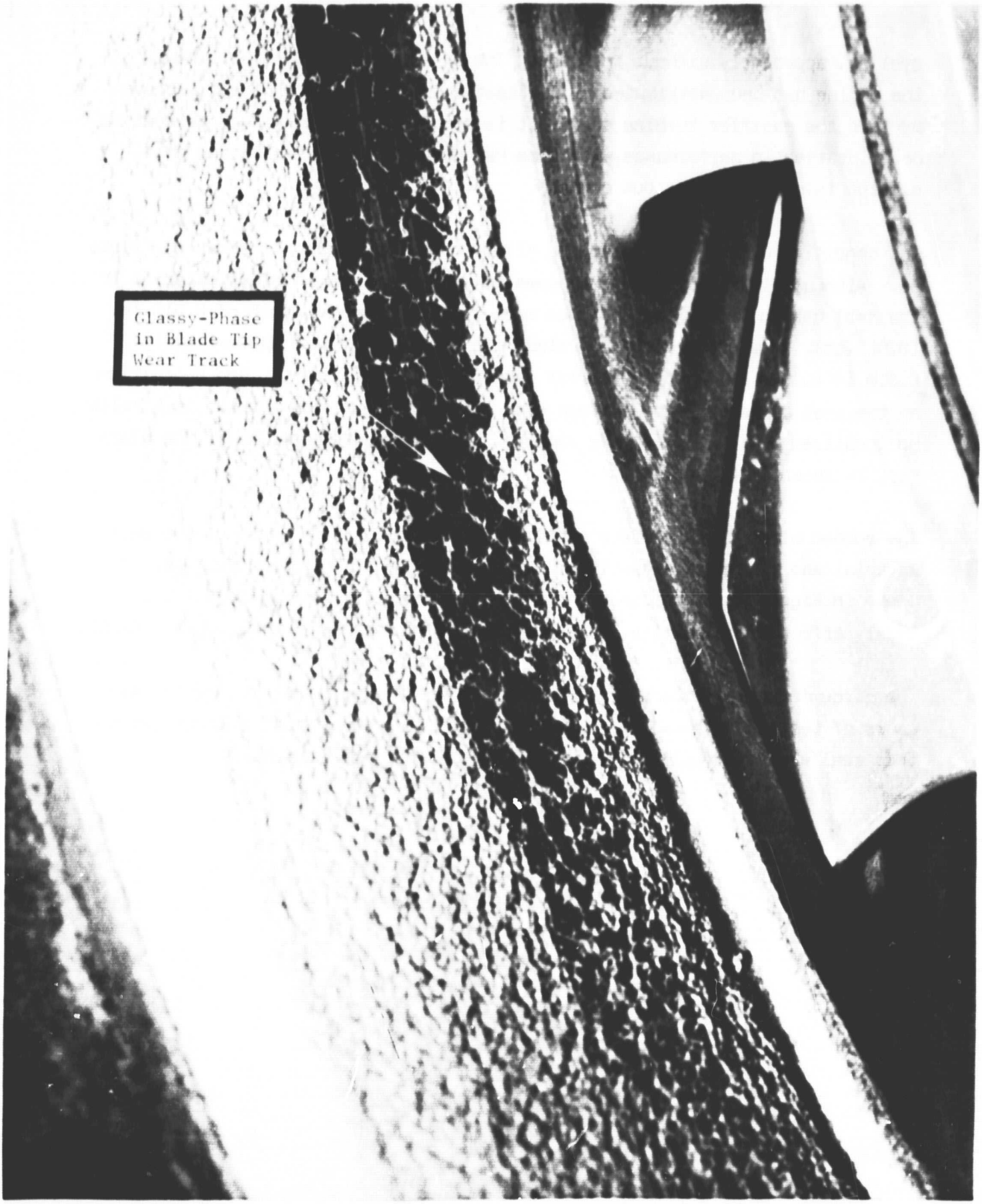

Figure 66 Condition of successful CATE gasifier turbine seal following 41:00+ hours total test time.

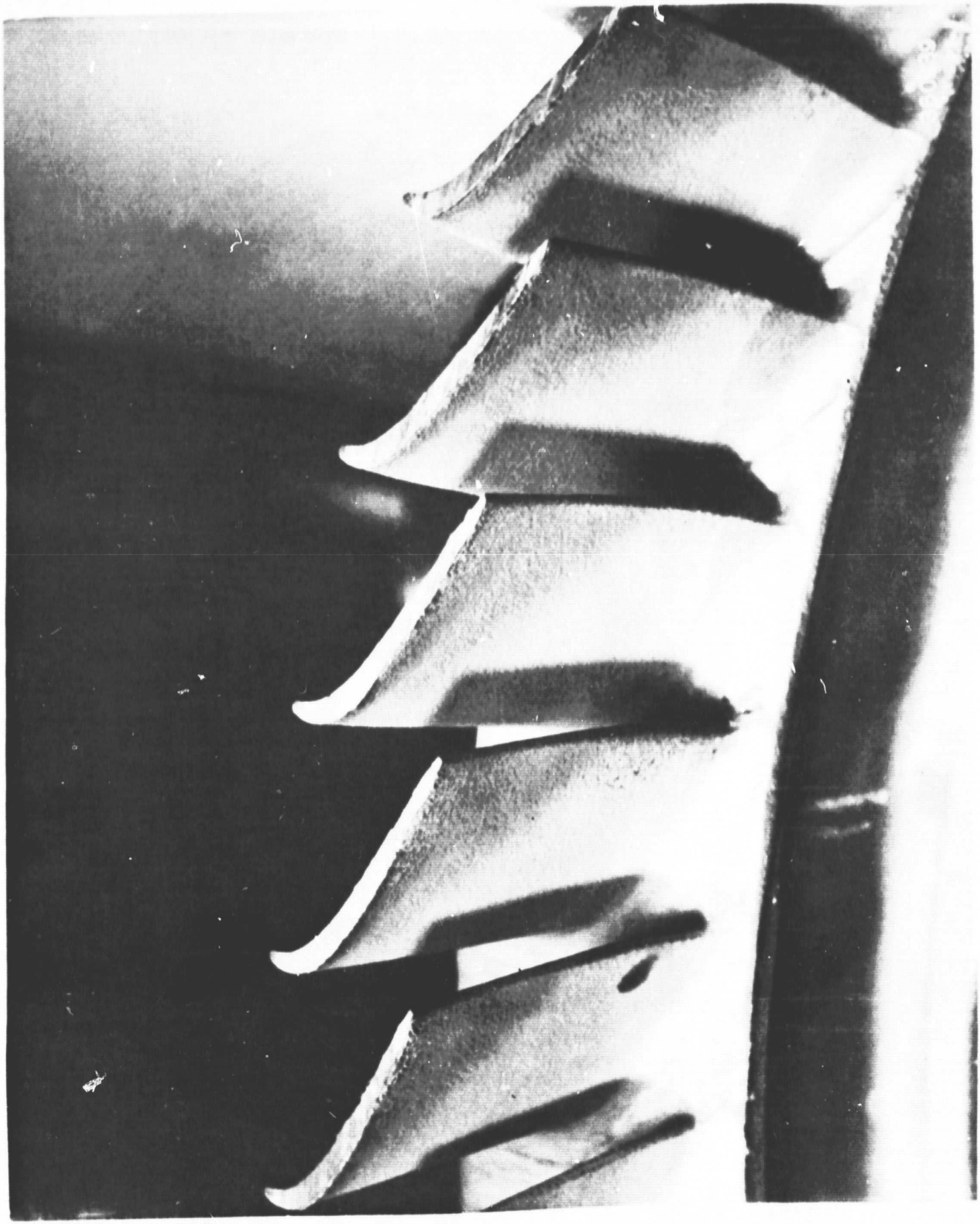

Figure 67 Condition of CATE gasifier turbine blades following 41:00+ hours total test time.

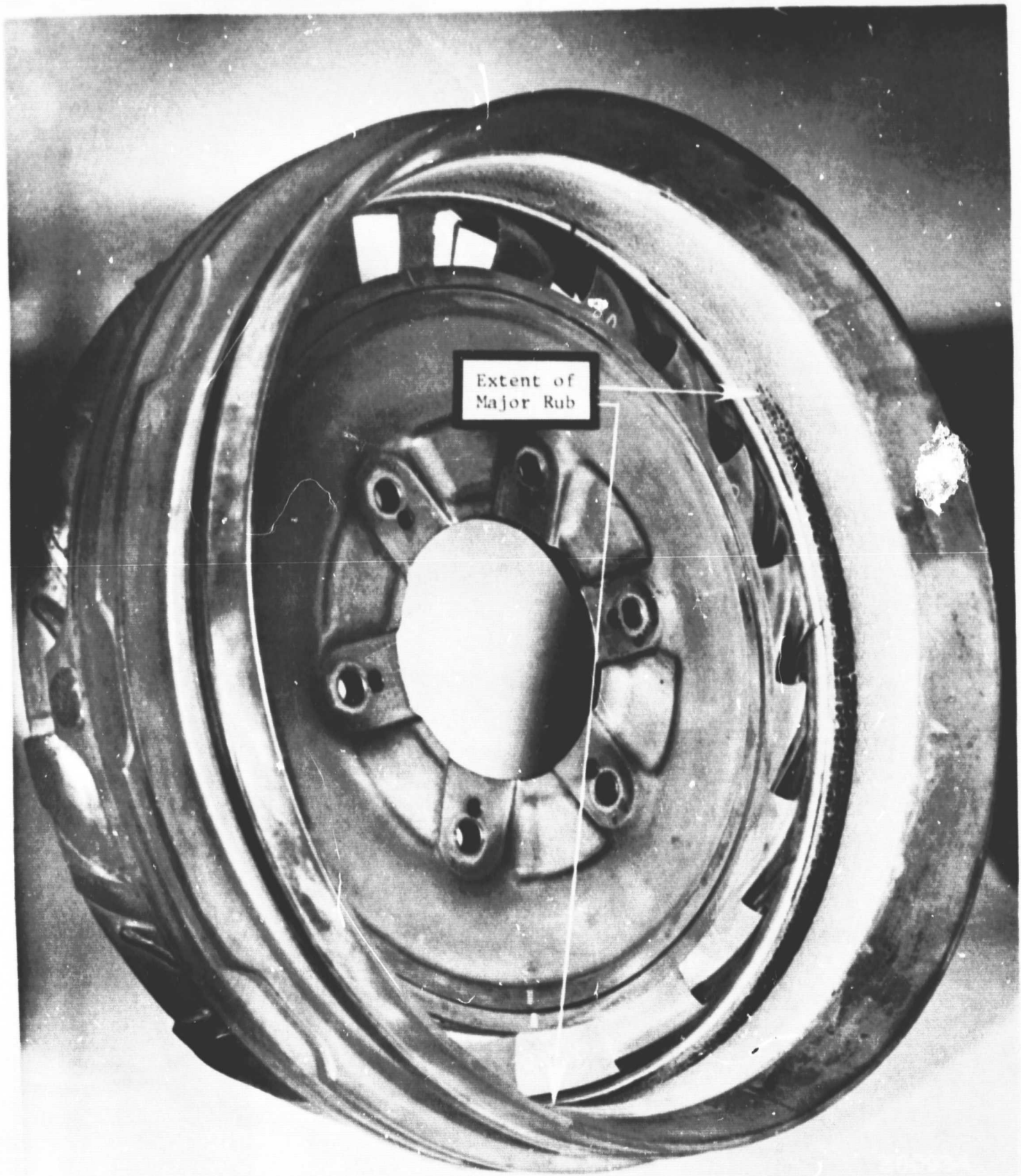

Figure 68 Circumferential extent of rub interaction experienced during 41:00+ hours total test time.

DISCUSSION OF RESULTS

A numerical argument for the observed behavior of the various seal systems can be obtained from order-of-magnitude standard machining considerations. If each blade is assumed to be analogous to a cutting tool, then the incursion depth per blade encountering the seal material is given by the simple relationship:

$$D_B = \frac{\dot{r}}{N \cdot n}$$

where:

D_B = incursion depth per blade (in/blade)
$\dot{r}$ = radial rotor axis displacement (incursion) rate (in/sec)
N = rotational speed (rev/sec)
n = number of blades on disk

For the observed test conditions,

$$D_B = \frac{.001 \text{ in/sec}}{\frac{34200}{60} \text{ rev/sec} \times 38 \text{ blades}}$$

$$= 4.6 \times 10^{-8} \text{ in/blade}$$

For a chip to be produced, the radius of curvature of the cutting "tool" (R_c, blade tip edge) must be less than the incursion (depth of cut) per blade. This is readily seen from Figure 69, in which the depth of cut is shown to be less than the tool cutting edge radius. It is obvious from this figure that the local tangent to the blade at or below the seal material surface will always indicate a resultant force (acting normal to the tangent) directed downward into the seal material with a forward component in the direction of engagement. Standard manufacturing techniques and materials are incapable of producing blades with edges sufficiently sharp to machine freely at the incursions encountered in actual rub situations. The end result is the smearing of the seal and adhesive transfer of the blade material to the seal structure frequently observed in practice.

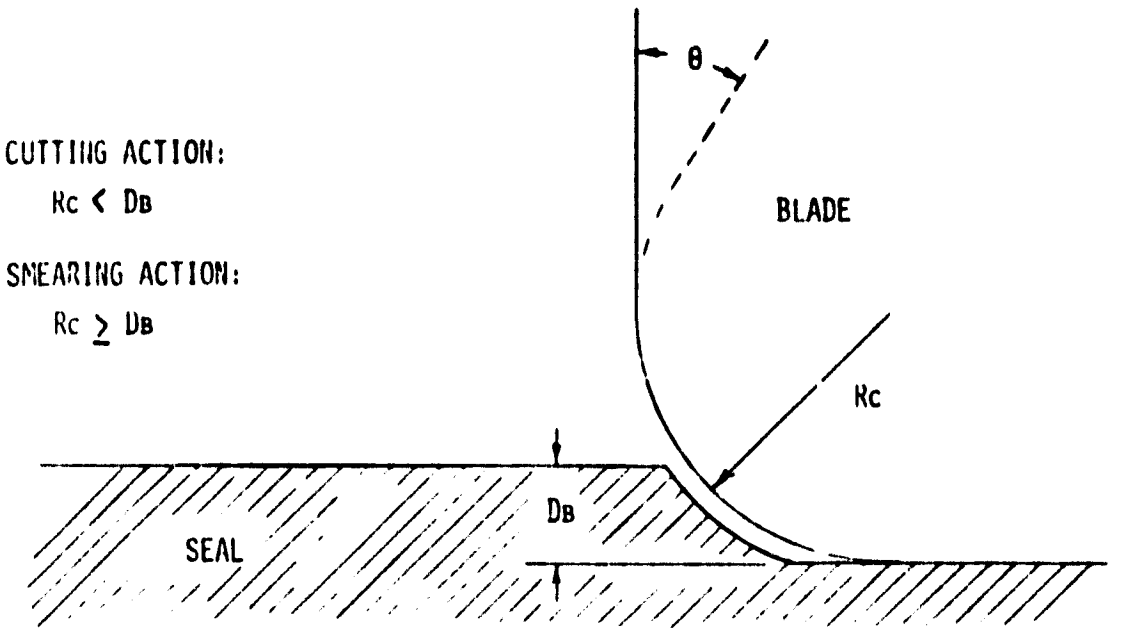

Figure 69 Material Removal Considerations

Thus, for producible blades, movement of the blade into the seal will always tend to cause densification or compaction of the seal material. This explanation is compatible with the fact that no satisfactory turbine seal has yet been developed in spite of widespread industry attention.

The apparent abradability demonstrated by some of the dual density ceramic seal system compositions investigated in this program likewise does not contradict the foregoing argument. The brittle nature of the ceramic matrix, particularly with high concentrations of porosity, results in failure by crushing during an encounter with a blade. When the structures are sufficiently porous and weak, the wear debris is flushed from the rub zone by turbulence in the gas path and insufficient heat is generated to cause further distress to the wear scar.

For structures with higher densities, considerable heat is generated during the rub which causes melting and smearing of the wear debris in the rub zone. Ultimately, the local density in the wear scar can become sufficiently high to cause adhesive transfer of blade material to the seal structure.

The brittle nature of the porous ceramic structures that contributes to the abradability is also manifested in reduced erosion resistance. Bombardment of the seal surface by incident particles entrained in the working fluid results in the brittle fracture of the target and the formation of additional wear debris that can be erosive to downstream components. It is probable, however, that the total material available from this mechanism is insufficient to create significant damage.

FINAL COATING SYSTEM EVALUATION AND SELECTION

The two coating systems selected for a complete evaluation analysis are 20/80 v/o and 50/50 w/o YSZ/FA-A compositions. A 50/50 w/o composition corresponds to a 14/86 v/o for the 8% YSZ coating and an 18/82 v/o mixture for the M-202 YSZ coating. These coatings are referred to in Table II and III as systems III-F, III-G, III-N and III-O respectively. The high speed abradability test results for these systems are shown in Figures 21, 22, 42 and 43.

For evaluation purposes, the systems were presumed to have operating temperature requirements no higher than 2100°F. The systems were subjected to the criteria as listed in Table I within the constraints described below. The ratings are based upon a score of zero to ten, with ten being equivalent to a perfect material, and are listed in Table V.

Abradability was judged on the formation and condition of the wear scar and the condition of the blade tip after a high speed rub. The basis for a score of 10 is a rub in 100% FA-A, as shown in Figures 20 and 41.

Thermal shock resistance scoring is based on in-house DDA evaluation of normal density 12 w/o and M-202 YSZ material. A 10 rating is given to the 12 w/o YSZ which was tested at 1950°F for 6000 cycles without failure. The M202 coating failed at 4000 cycles. The composite systems investigated here were 8% YSZ, contained eccospheres in the final coating and were not thermally cycled; thus, their specific performance is unknown. It has been speculated that the presence of the eccospheres may degrade the thermal shock resistance. There is no difference in performance between the 20/80 v/o and 50/50 w/o systems.

Erosion resistance scoring is based on a 30 minute erosion test of each of the samples, which is then compared to the 30 minute erosion of a normally dense 8 w/o YSZ system.

Stability with time at temperature is based upon in-house DDA studies of normally dense 8 w/o YSZ and M-202. For purposes of this investigation, it has been assumed that the inclusion of an eccosphere filler will not degrade the stability characteristics of the system.

Fabrication repeatability scoring is based upon the spread of Superficial Rockwell Hardness readings taken on each of the coating systems.

Chemical stability with respect to turbine environment has not been judged due to insufficient experience with these systems in this particular area.

Cost scoring is based upon the price of raw materials for each of the coating systems.

Permeability scoring is based on through-flow leakage tests conducted on each of the systems.

Risk of mechanical damage to downstream components is scored on the basis of possible erosion damage to components subjected to the displaced abradable material. The total amount of YSZ material available to affect downstream components is small and the resultant possible damage is minimal.

Chemical and metallurgical compatibility with downstream components is scored on the basis of interaction of the YZS with engine components. This effect is considered negligible.

Surface roughness is scored on the basis of comparing the machined surfaces of the system with that of a 100% YSZ system.

Multiplying each of the scores by the appropriate weighting factors results in the scores shown in Table VI. System F, the 20/80 v/o 8 w/o YSZ system out-performs the other coating systems. If the cost criterion is removed from consideration, the M-202 systems are removed completely from consideration in favor of the 8% system.

Table V

Coating System Ratings

	Weighting Factor	System Scores Sys F 20/80-8%	Sys G 14/86-8%	Sys N 20/80-202	Sys O 18/82-202
Abradability	4.8	3	4	5	6
Thermal Shock Resistance	4.3	8	8	3	3
Erosion Resistance	4.?	5	3	1	2
Stability with Time (at Temperature)	3.9	10	10	5	5
Fabrication Repeatability	3.8	5	4	6	7
Chemical Stability (wrt Turbine Environment)	3.5	--	--	--	--
Cost	3.3	2	2	10	10
Permeability	3.2	10	10	10	10
Risk of Mechanical Damage to Downstream Components	2.9	8	8	8	8
Chemical & Metallurgical Compatibility w/ Downstream Components	2.8	9	9	9	9
Surface Roughness	2.6	6	6	7	7

TABLE VI

Weighted Scores of Four Final Coating Systems

	System Scores			
	Sys F 20/80-8%	Sys G 14/86-8%	Sys N 20/80-202	Sys O 18/82-202
Abradability	14.4	19.2	24.0	28.8
Thermal Shock Resistance	34.4	34.4	12.9	12.9
Erosion Resistance	21.0	12.6	4.2	8.4
Stability w/Time (at Temp)	39.0	39.0	19.5	19.5
Fabrication Repeatability	19.0	15.2	22.8	26.6
Chemical Stability (wrt Turbine Environment)	--	--	--	--
Cost	6.6	6.6	33.0	33.0
Permeability	32.0	32.0	32.0	32.0
Risk of Mechanical Damage to Downstream Components	23.2	23.2	23.2	23.2
Chemical & Metallurgical Compatibility w/Downstream Components	25.2	25.2	25.2	25.2
Surface Roughness	15.6	15.6	18.2	18.2
Σ	230.4	222.0	215.0	227.8
Σ w/o Cost	223.8	215.4	186.8	195.2

CONCLUSION:

Results of engine tests conducted early in the program were misleading because of unsuspected difficulties with the powder feeders supplying the plasma spray unit. Correction of the problem by replacement of the suspect powder feeders with models representing the current state of the art led to a demonstrated ability to create structures of known composition on a repeatable basis.

Engine testing of a gasifier turbine seal of known composition was accomplished successfully in a CATE test engine for a period exceeding 41 hours. The condition of the seal upon removal for inspection was such that it was re-installed in a subsequent build for additional testing which is still in progress.

Although some blade tip material was lost during the rub process, the depth of the wear scar in the seal was of comparable dimension, indicative of the abradable qualities of the material.

The extent of the engine testing was insufficient to fully assess the erosion resistance of the seal material. However, it is expected that the long term erosion resistance will be inadequate to satisfy the durability requirements for applications beyond limited duty test vehicles.

A wide range of possible structures with greater hardness (and consequently improved erosion resistance) exists between the engine-tested structures and 100% YSZ. Thus, considerable latitude is available for improving erosion resistance if some assistance is given to the blade tips. This is most likely to occur in the form of an abrasive material applied to the blade tips to convert the seal material removal process from one analogous to milling to another more representative of grinding. The latter should benefit from the high speeds and light feeds exhibited by the rotor during an incursion.

It is strongly recommended, therefore, that future evaluations of turbine abradable seal materials be conducted with blades (real or stylized) which incorporate a fully developed abrasive tip treatment.